NASA CR-135393
R78AEG444

PROGRAM FOR IMPACT TESTING OF SPAR-SHELL FAN BLADES

TEST REPORT

by

R. Ravenhall
and
C.T. Salemme

GENERAL ELECTRIC COMPANY

Prepared For

National Aeronautics and Space Administration

NASA-Lewis Research Center
NAS3-20801

TABLE OF CONTENTS

LIST OF ILLUSTRATIONS

LIST OF ILLUSTRATIONS (Continued)

LIST OF ILLUSTRATIONS (Continued)

LIST OF ILLUSTRATIONS (Concluded)

LIST OF TABLES

1.0 SUMMARY

This report describes the results of a program to foreign object impact test six NASA-supplied, filament-wound, composite SPAR-SHELL fan blades, drawing number 920-010 (Figure 1). Six of the eight QCSEE-type blades, manufactured by the Fiber Science Corporation, were whirligig impact tested in the General Electric whirligig facility. The test conditions were selected to assess the capability of these blades relative to foreign object damage resulting from ingestion of birds into the fan blades of a QCSEE-type engine.

As shown in Figure 1, the blades are of an integral airfoil and hub design with the airfoil formed from a longitudinal bundle of graphite fibers that wrap around a metal pin at the root and are splayed out to the full chord at the tip. A shell of oriented graphite filament is wound around the entire blade. The filament-wound assembly is pressed and cured to final configuration. The leading edge protection on the blades is stainless steel, either cocured with the composite or secondarily bonded to the composite. The selected six blades included different fiber and leading edge bonding combinations.

Eight blades were supplied by NASA for use in selecting six blades for whirligig impact testing. The selection process was based on GE/NASA reviews of the frequency and ultrasonic C-scans. The first four blades were tested by injecting 12.7 cm (5 in.) diameter RTV "birds" into the path of the blades, rotating at 3255 rpm, and the last two were tested by injecting 0.113 kg (4 oz) starlings into the path of the blade.

All of the four blades, tested with RTV birds, lost the stainless steel leading edge and suffered severe breakage and delamination of the airfoil. In these tests, the bird slice size ranged from 0.391 kg (13.8 oz) to 0.482 kg (17.0 oz). Test Numbers 1, 2, and 3 had the blade angle set at 33° at the 80% span impact location, while Test Number 4 had the blade angle set at 23°. Material loss varied from 0.463 kg (1.2 lb) to 0.703 kg (1.55 lb), generally in proportion to the slice weight. For the starling impact of Test Number 5, the blade angle was set at 33° at the 80% span impact location, and damage consisted of the loss of the leading edge protection plus fiber breakage and delamination. This damage differed only slightly from that on the other blades impacted by larger RTV bird slices. The airfoil material loss was 0.299 kg (0.66 lb) for this test.

In Test No. 6, the second starling test, the blade angle was reduced to 23°. Damage from this test consisted of bending of the stainless steel leading edge protection and delamination in the airfoil outer span but no weight loss.

The results of the testing are compared with the results for earlier impact testing of QCSEE blades. These results show that the SPAR-SHELL

Figure 1. NASA/Fiber Science, Inc. Composite Blade.

blades had levels of damage less than the original QCSEE design and generally greater than obtained from the blades designed and tested in the NASA-sponsored (NAS3-17836) impact improvement program. A positive result of the testing was that none of the blades failed at the root, and a new type blade attachment technique was demonstrated.

All eight blades were frequency and ultrasonically inspected in the as-received condition. Following test, all of the impacted blades were ultrasonically inspected, and the blade from Test No. 6 again was frequency inspected.

High speed movies were taken of each test.

2.0 BLADE INFORMATION

2.1 INTRODUCTION

Development of a flight-worthy, variable-pitch fan for the QCSEE engine hinged on attaining a lightweight composite material fan blade. Design goals for this blade included foreign object damage resistance consistent with FAA requirements. A number of composite blade development efforts, both in General Electric and other organizations, are leading to technical advances that should satisfy the FOD requirements for intermediate-tip-speed, variable-pitch fan blades. Early efforts on the QCSEE program provided a lightweight composite fan blade suitable for variable-pitch demonstrator engine operations, but with inadequate foreign object damage resistance. A development effort under NASA program NAS3-17836 provided data for modified composite material systems that appear to offer considerable improvement in capability.

NASA/Fiber Science Composite QCSEE blades, tested in this program, offer innovations in composite blade design and processing techniques which warranted FOD resistance evaluation. The program consisted of whirligig impact testing the NASA/Fiber Science blades at simulated bird impact conditions similar to those use to test the QCSEE UTW blades, namely a two-pound bird encounter at take-off conditions, as well as at other conditions of interest.

2.2 TEST BLADE DESCRIPTION

The blades used for this testing were QCSEE-type, filament-wound, SPAR-SHELL composite blades manufactured by the Fiber Science Corporation and supplied to GE for testing by NASA. These blades included different fiber materials and two variations in the leading edge bonding method.

The blade configuration is shown in Figure 1. The outer 38 cm (15 in.) of the blade airfoil span were formed to the QCSEE blade configuration. The remaining lower airfoil span of approximately 11.4 cm (4.5 in.) at the leading edge and approximately 8.3 cm (3.25 in.) at the trailing edge deviated from the QCSEE airfoil configuration to permit transitioning to the circular integral attachment configuration employed. Figure 2 shows the test blade as seen from the convex side, and Figures 3 and 4 show two concave side views of the blade as well as a QCSEE blade mounted in a QCSEE test trunnion viewed from approximately the same angle. The similarities and differences in configuration can be seen from the photographs.

The blade construction is made up of a core of longitudinal filaments that are wrapped around and attached to a steel pin at the root and are splayed out to the full chord width at the tip. An overwound shell of helical (angle plies) windings wraps around the longitudinal filament forming the blade aerodynamic contour. The steel pin in the root is retained by a clevis which is integral with a trunnion post.

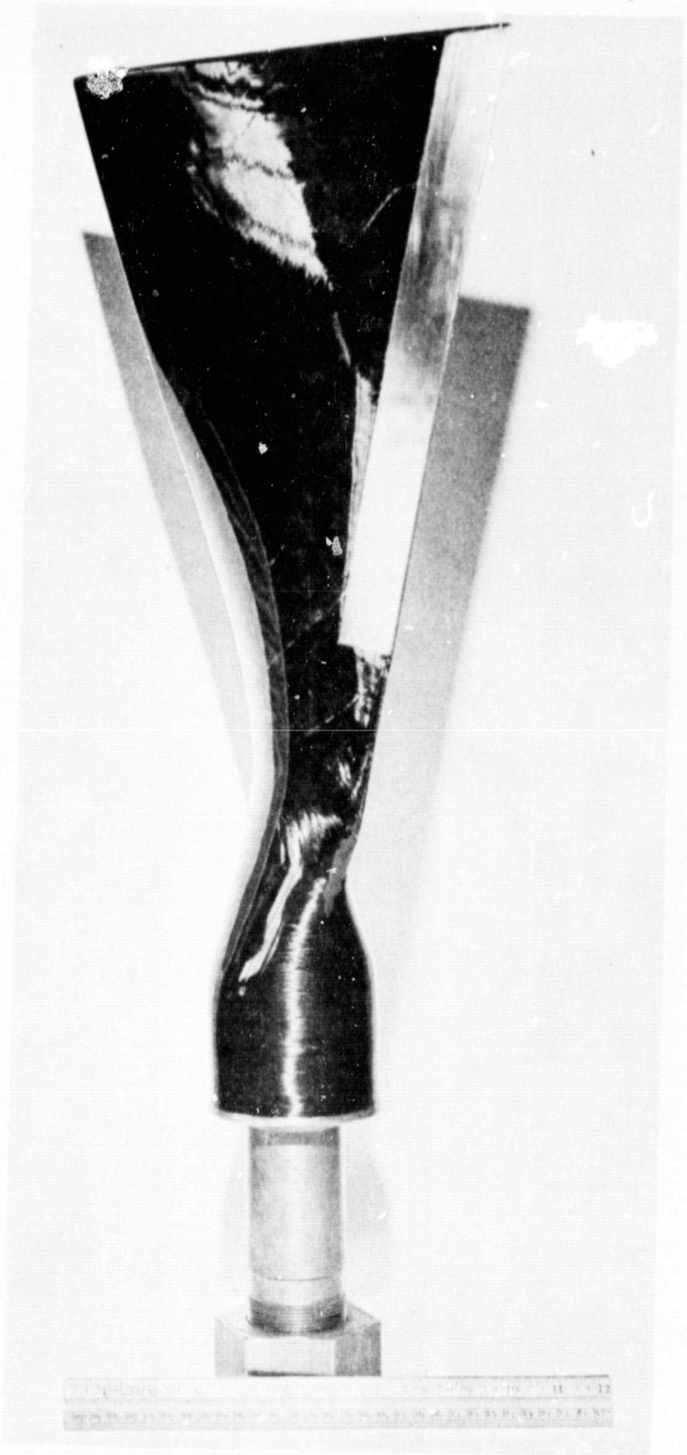

Figure 2. Test Blade Viewed from Convex Side.

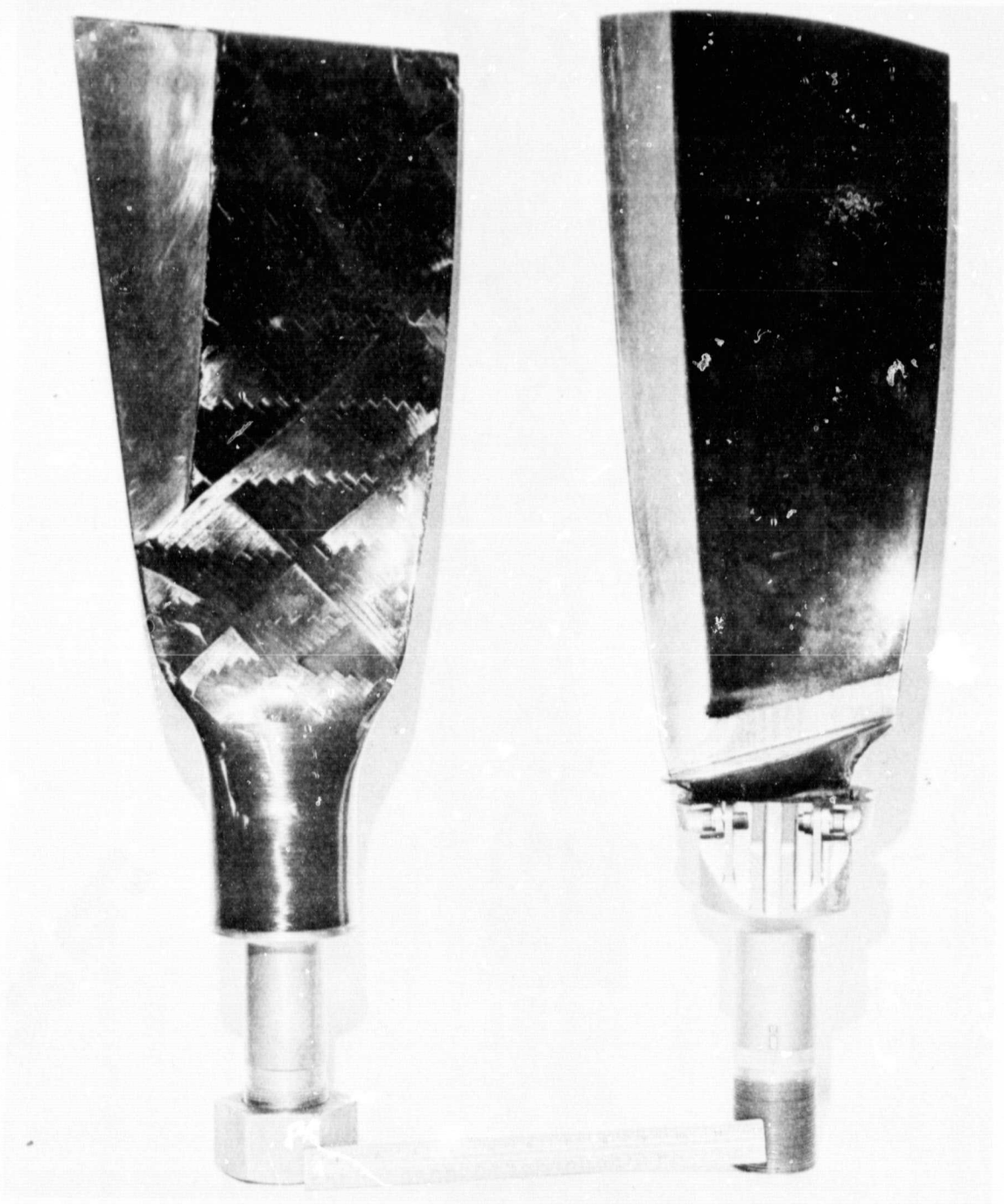

Figure 3. Test Blade and QCSEE Blade Viewed from Concave Side.

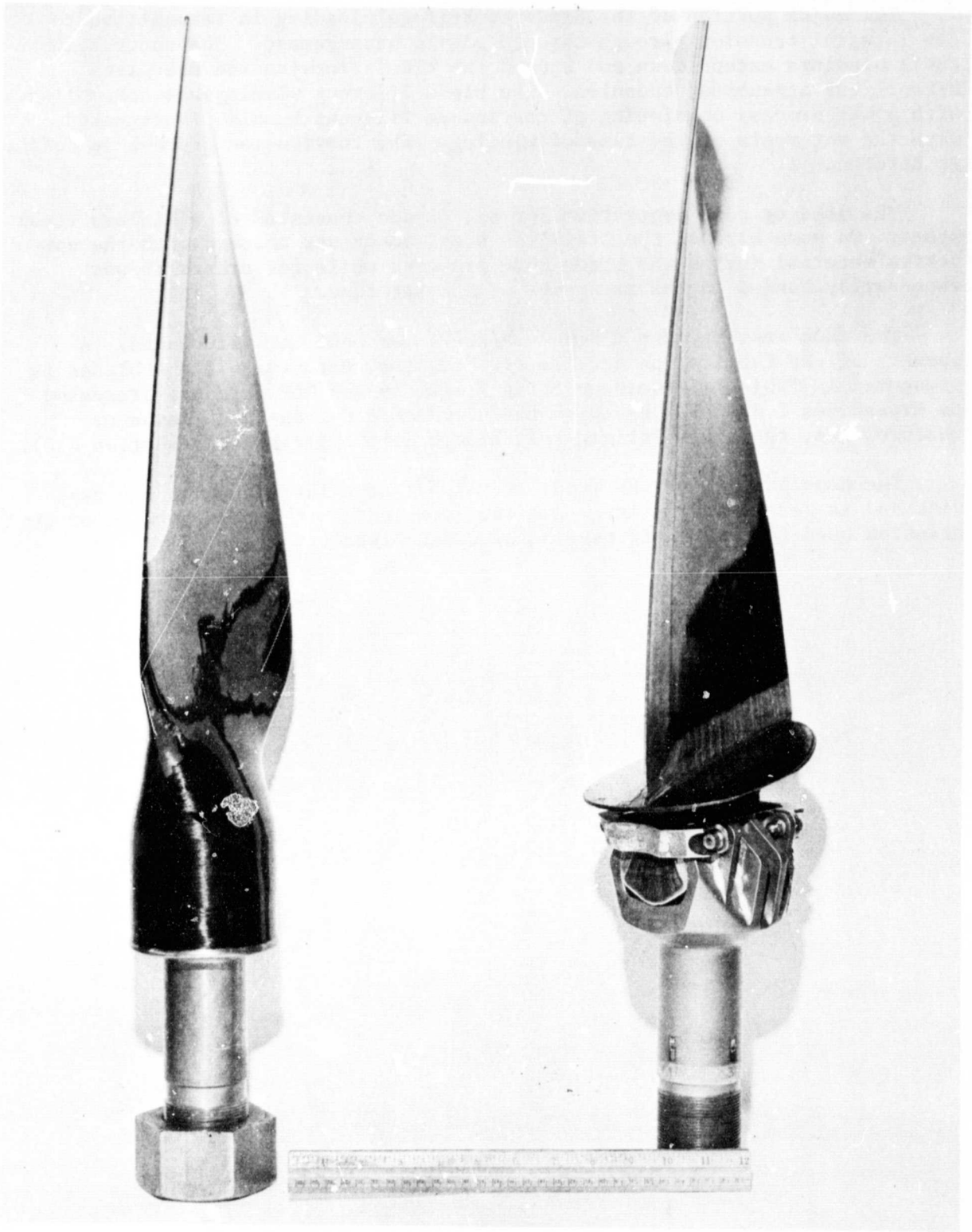

Figure 4. Test Blade and QCSEE Blade Viewed from Leading Edge Concave Side. Concave Side.

The major portion of the blade centrifugal loading is transmitted to the integral trunnion through the pin/clevis arrangement. The outer helical shell windings extend down and around the clevis forming the one-piece airfoil and attachment trunnion. The blade filament winding was accomplished with a wet process consisting of continuous filament bundles impregnated with the wet resin at the time of winding. The fabrication process is defined in Reference 1.

The leading edge protection for all blades consisted of stainless steel sheet. On some blades, the stainless steel sheet was cocured with the composite material during the blade cure process, while for others it was secondarily bonded to the composite at a later time.

The same resin system (APCO 2434/2347) was used for all blades. A summary of the fabrication details and frequency data for all the blades is presented in Table 1. The supporting frequency and NDE data are presented in Appendices I and II. Based on the ultrasonic C-scans and frequency measurements, the six whirligig test blades were selected (see Section 4.0).

The post portion of the steel trunnion that extends through the test disk and is retained by a large nut was identical to the post portion of the trunnion used for whirligig testing of QCSEE blades.

Table 1. Fiber Science QCSEE-Type Blade Fabrication Details.

	Blade S/N							
	4	5	6	7	8	10	11	12
Fiber								
T300	---	x	x	x	---	x	x	x
Carbolon Z-2-1	x	---	---	---	---	x (Shell)		---
Carbolon Z-3	---	---	---	---	---	x (Spar)		---
S-Glass	---	---	---	x	x	---	x	x
Spar %	---	---	---	20	20	---	10	10
Shell %	---	---	---	20	20	---	20	20
Resin								
APCO 2434/2347	x	x	x	x	x	x	x	x
Leading Edge								
Concured	---	---	---	x	x	x	x	x
Secondary Bond	---	x	x	---	---	---	---	---
LeRC Bond	x	---	---	---	---	---	---	---
NDE Inspection								
C-Scan LeRC	x	x	x	x	x	---	---	x
C-Scan GE	x	x	x	x	x	x	x	x
Infrared Scan LeRC	x	---	x	---	x	---	---	---
Bench Frequencies								
First Flex LeRC, cps	80	90	87	76	76	76	79	79
GE, cps	78	90	88	78	80	80	82	82
Second Flex LeRC, cps	210	218	210	200	195	210	185	205
GE, cps	248	242	244	240	244	---	240	246
First Torsion LeRC, cps	285	315	300	280	275	270	270	280
GE, cps	274	318	316	282	290	282	290	286
Selected Whirligig Impact Blades	x	x	x	---	x	x	x	---

3.0 WHIRLIGIG IMPACT TESTING

3.1 FACILITY SETUP

The test rig (whirligig) used for this effort was developed to closely simulate impact conditions that occur in turbofan engines. The rig consists of a horizontal spindle shaft, electric motor, gearbox, shrouding, and a belljar (Figure 5). The electric motor is a constant-speed, 700 kw (1000 hp) motor with a dynamic, variable-speed-output, magnetic clutch. Power is transmitted through a gearbox and a horizontal spindle shaft to the rotor. Shrouding is provided around the rotor to reduce air turbulence, thus reducing heat generation and power requirements. An environmental chamber (belljar), Figures 6 and 7, is soft-mounted to the facility shroud to provide a helium atmosphere to reduce the power requirement, to provide a housing for the injection mechanism, and to enable high-speed movies to be taken of the impact sequence.

The soft-mounted vehicle setup used is shown in Figure 8 and is basically a standard fan package with some additions and changes. The structure consists of a fan frame with the No. 1 and No. 2 bearings and sump systems, the stage 2 stator case, and slave stage 1 shrouding. The entire vehicle is soft-mounted and supported by spring-type hangers and shock absorbers. The rotor is constructed from a fan stub shaft with a slave stage 2 disk (ring) and stage 1 spacer. The QCSEE titanium whirligig disk fits directly into this setup. The rotor is driven by a Bendix flexible diaphragm coupling and slave adapting shaft. The extremely high rotor vibrations resulting from loss of significant portions of a blade during the impact test are dampened out by the spring and shock absorber mounting. The flexible drive coupling prevents damage of the facility drive spindle and bearings that result from large fan rotor displacements.

When impacting a full stage of blades, the timing between bird and blade is not critical, since the bird will always hit a blade. However, when trying to impact a single blade with a single bird fired in the axial direction, greater accuracy is required than can be attained with a gas gun. For example, when the QCSEE fan is running at 3255 rpm, one revolution of the rotor requires only 18 milliseconds. In order to impact a single blade at any point along the chord with a starling having a velocity of 76.2 m/s (250 ft/sec), it is necessary to have a timing accuracy of ±1.3 millisecond. To obtain repeatable strikes, a bird slice of ±0.03 kg would require an accuracy of ±0.06 millisecond. This precise timing is not attainable with existing ballistic facilities capable of shooting large birds. Thus, it was necessary to devise a mechanical injection mechanism which would have the repeatability required for impact testing.

An injection mechanism designed for this purpose and used for this testing has been in operation at General Electric for approximately five years and has been used successfully in the testing of numerous composite blades.

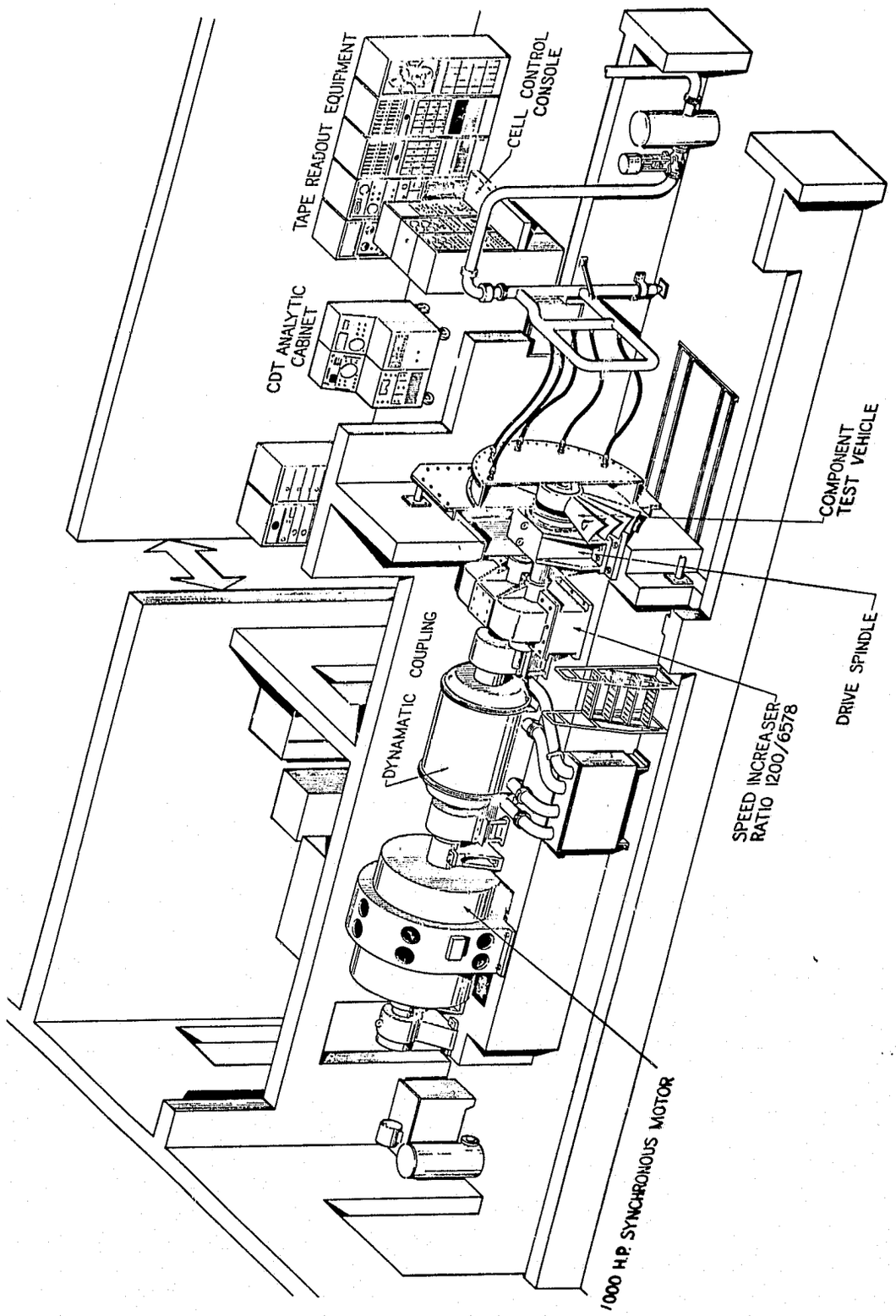

Figure 5. Whirligig Test Facility.

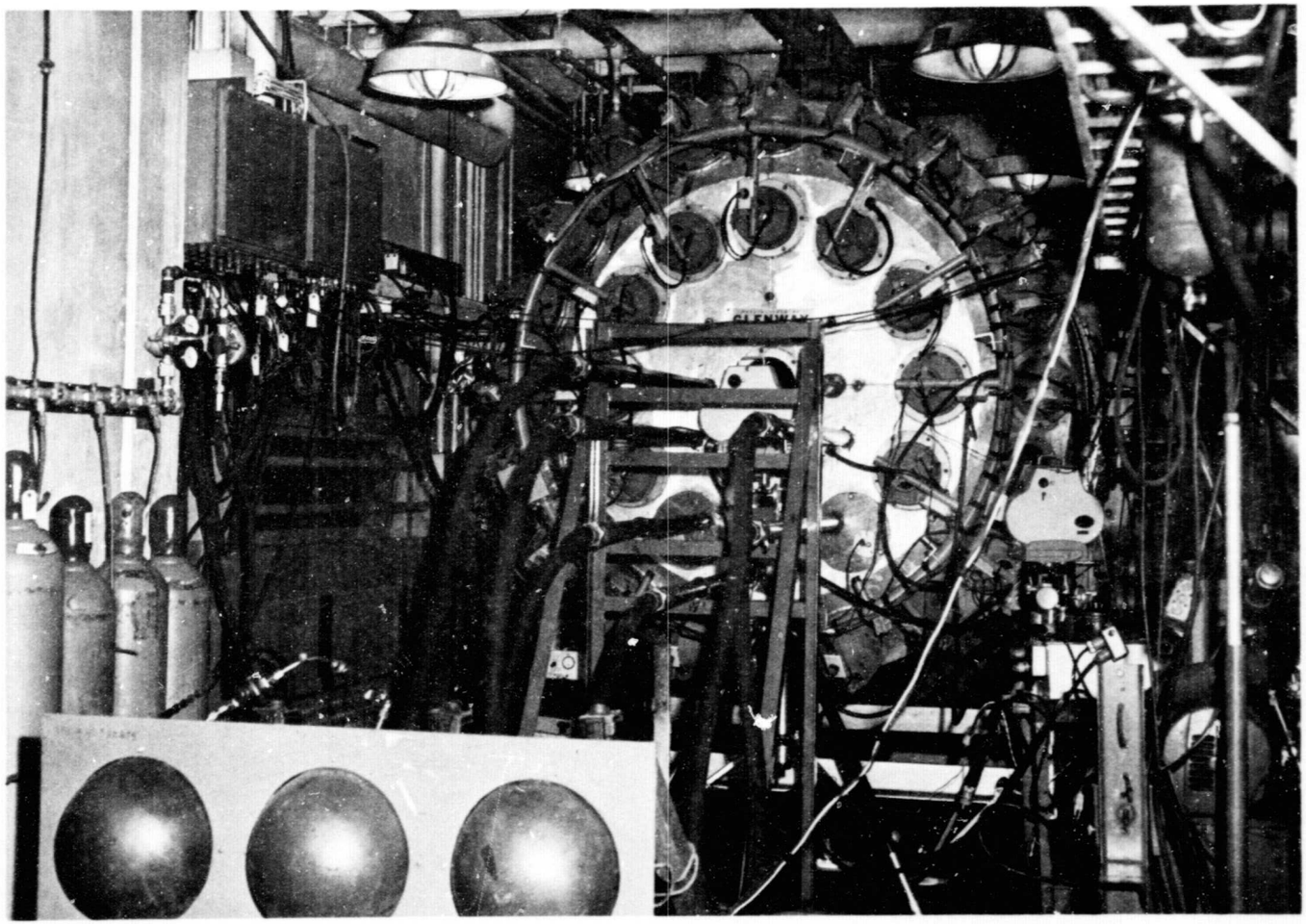

Figure 6. Whirligig Facility with Bell Jar, Projectile Guns, and High Speed Photography.

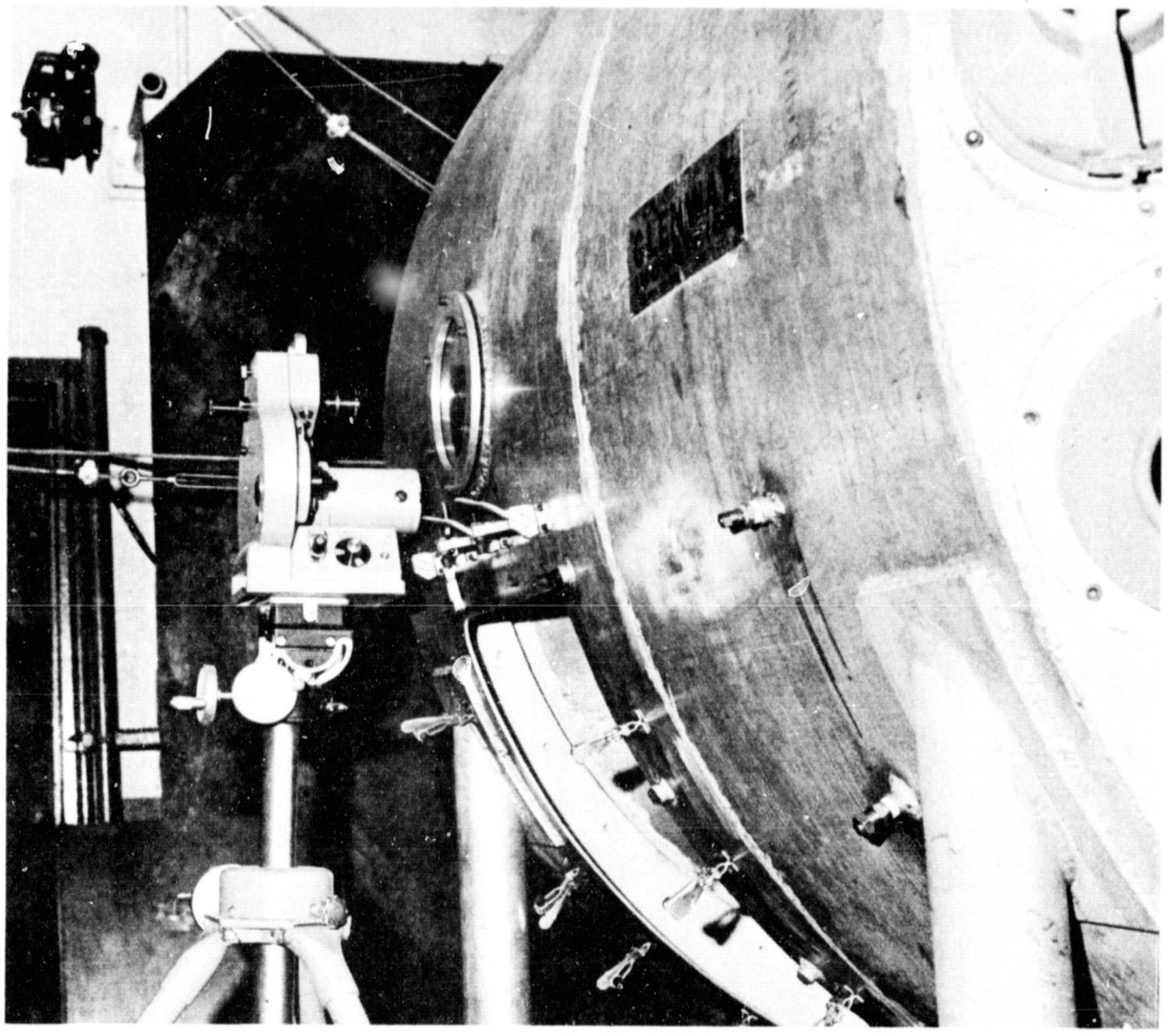

Figure 7. Whirligig Impact Facility.

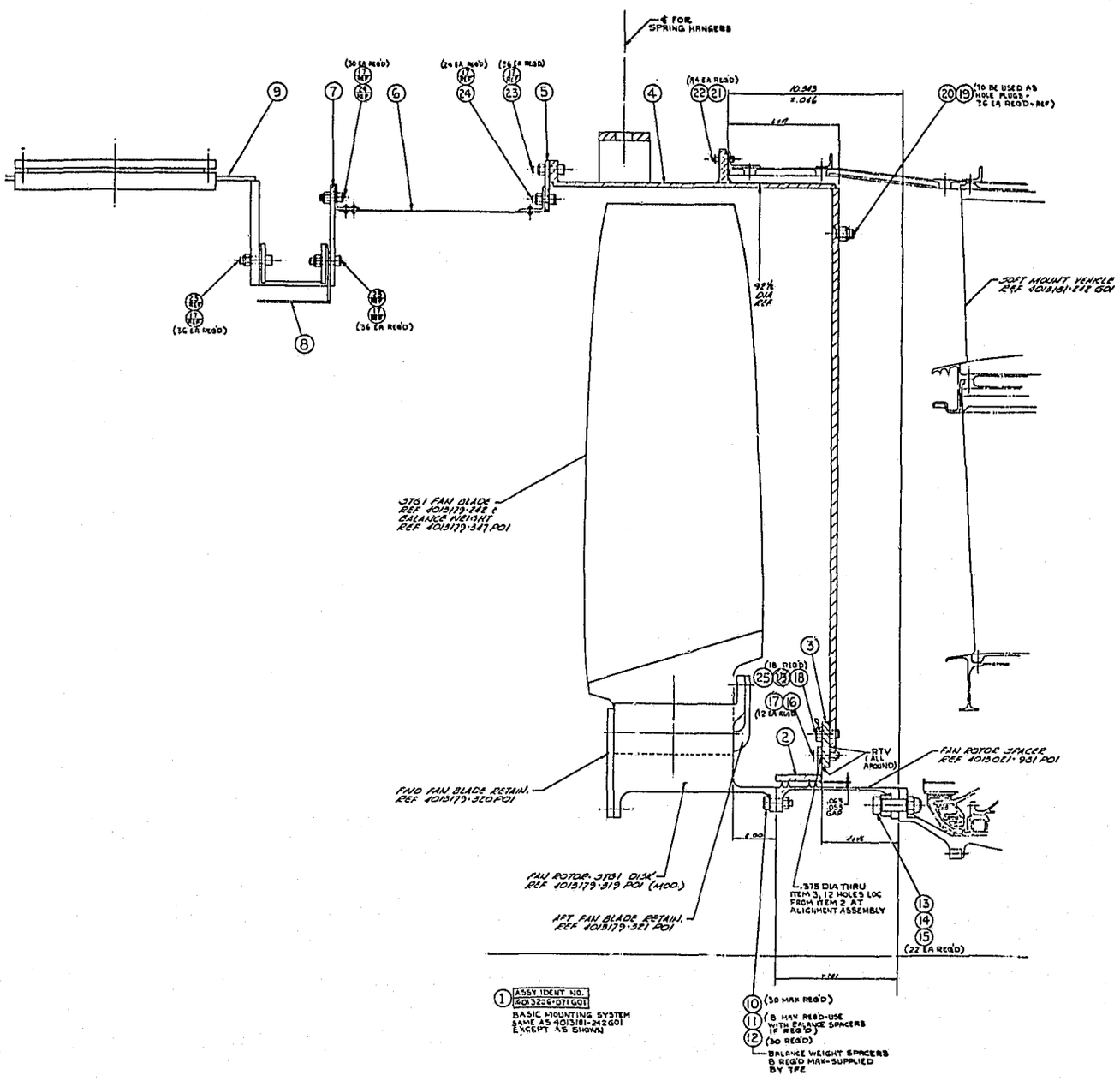

Figure 8. QCSEE Whirligig Impact Test Setup.

The injector mechanism shown in Figures 9 and 10 consists of two spring systems: the primary, which injects the real or simulated bird into the path of the rotating blade, and the secondary, which retracts the remaining carcass after impact. The entire mechanism is mounted on an adjustable-height stand which protrudes through the belljar and is securely fastened to the cell floor.

A simulated (RTV silicone rubber) bird or an actual bird is mounted in a cylindrical holder, Figure 11, on the front of the ram. The ram is mounted through two ball bushings which are supported by a pillow block. Two springs, one on either side of the ball bushings, move the primary system. The springs initially are loaded by manual cocking and are held in the loaded position by an explosive bolt. When the explosive bolt is fired, the springs actuate the ram forward and inject the bird into the path of the blade. To avoid the possibility of the bird striking the fan blades more than once, the secondary spring system, when actuated, moves the entire primary system out of the way of the rotor.

Firing of the explosive bolts is controlled by an electronic firing circuit. When the rotor reaches a predetermined speed, the photo floodlights and high speed cameras are actuated. When the cameras reach top speed, they close a circuit which allows a 1 per rev signal to trigger the explosive bolt in the primary spring system. The bolts for the secondary spring system are fired after a 15-millisecond delay.

There are 36 photoflood lamps of 1000 watts each that provide lighting for Hycam high speed movie cameras which have a framing rate of 10,000 frames per second. The quality of the individual frames is adequate to permit assessment of both primary and secondary damage.

3.2 FOREIGN OBJECTS USED

Simulated RTV birds were used to test four of the blades, while real starlings were used to test the other two blades.

The RTV foreign objects simulated a 0.907 kg (2 lb) bird and were made of silicone form material (RTV). They had a 12.7 cm (5 in.) diameter, solid-cylindrical shape so that a nominal 3.8 cm (1.5 in.) slice would provide a nominal 0.37 kg (13 oz) bird slice. The specific ingredients of the mixture and preparation technique are given below:

A. Base Mix

4000 g RTV560
350 g SF96-(50) silicon fluid
50 g Al silicate fibers (Johns Manville)

Mix three hours in a Sigma blade mixer and remove.

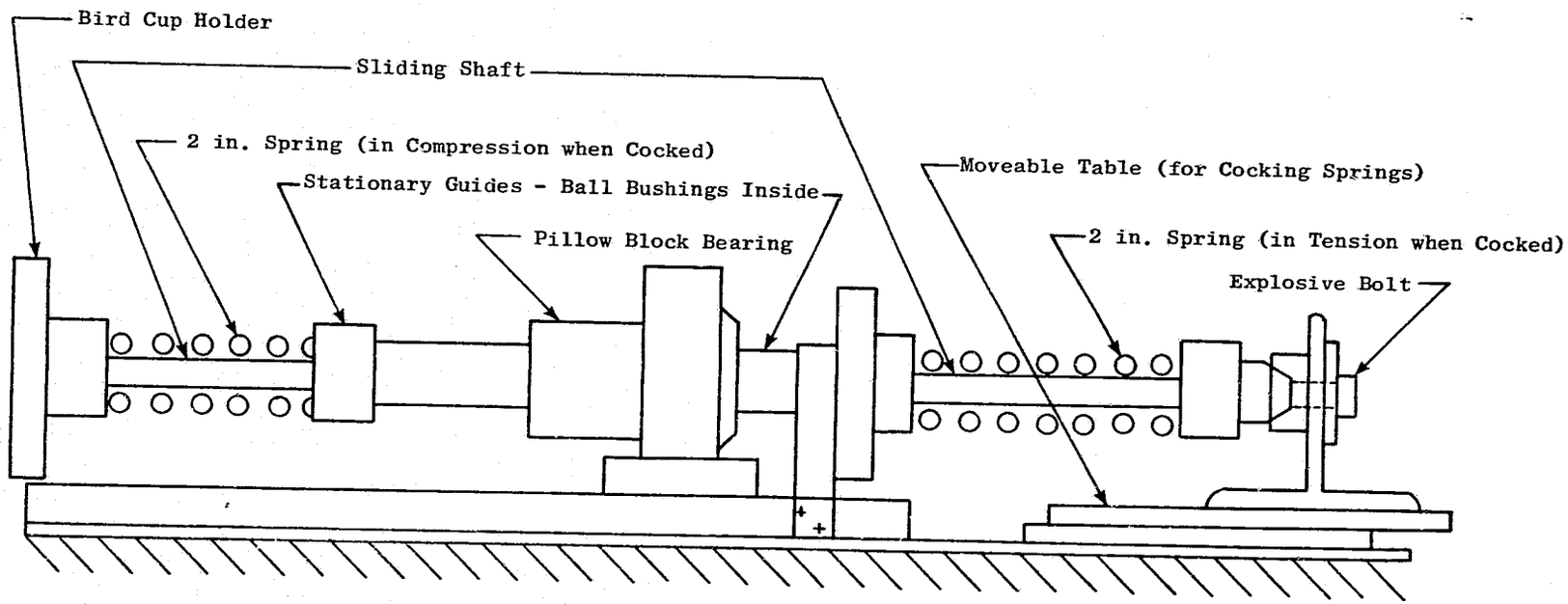

Figure 9. Bird Injecting Mechanism.

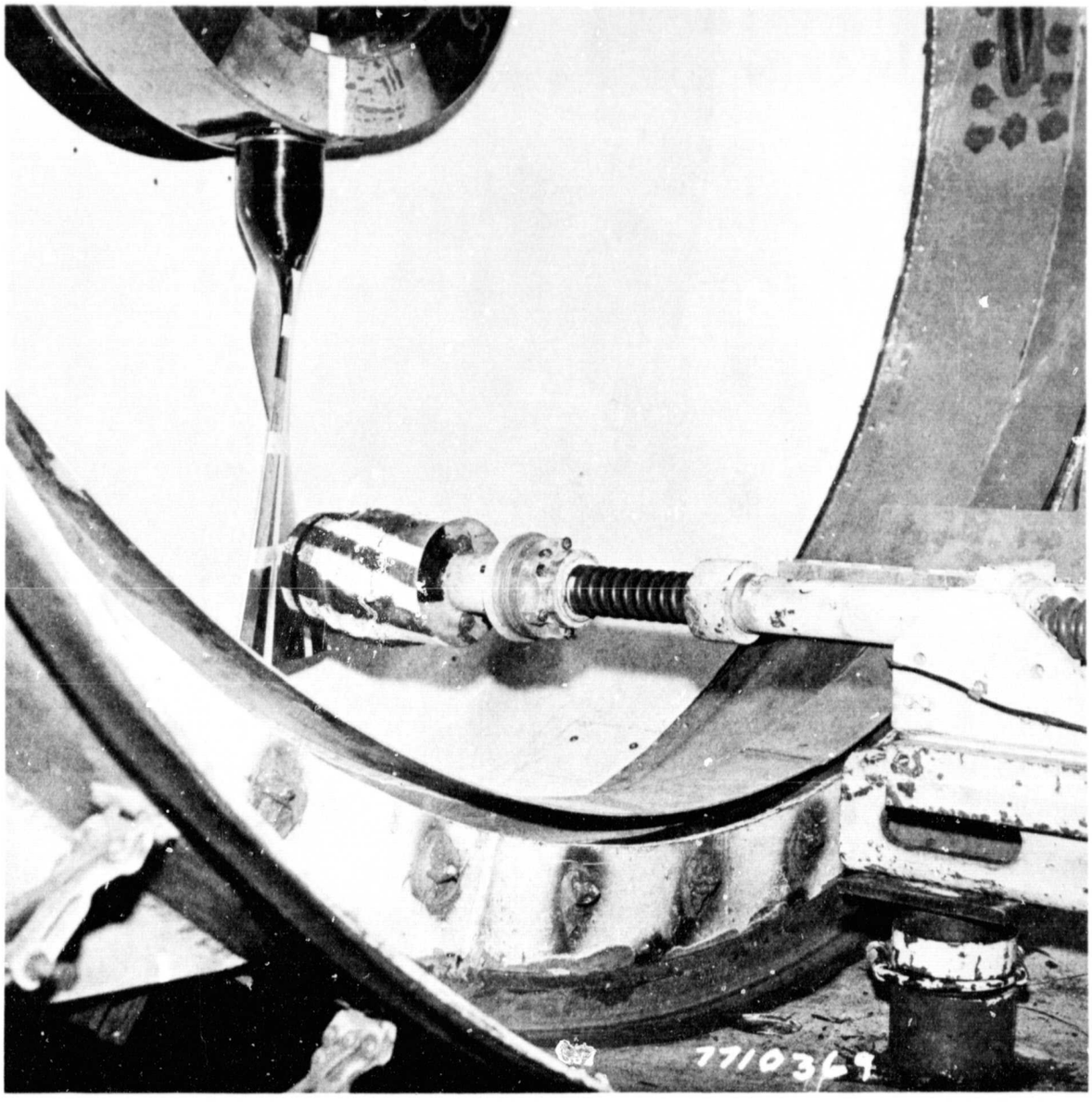

Figure 10. Foreign Object Injection Mechanism.

Figure 11. Simulated (RTV) Bird Used for Whirligig Impact Test, Showing Slice.

B. Foaming Agent

To foam the above base mix, use:

100 g base mix
30 g RTV921 blowing agent
0.5 g T-12 catalyst
4 drops Nucure 28

Mix three to four minutes in a propeller mixer, pour in mold, and cure for 16 hours at 344.4 K (160° F).

Figure 12 shows a typical RTV simulated bird and a styrofoam starling carrier after testing.

The starlings used for the remaining two tests consisted of a real starling, weighing ~0.113 kg (~4 oz), mounted on a foam post as shown in Figure 13. Upon impact, the blade slices the starling away from the foam post and simulates the condition of a full bite of a starling.

3.3 TEST CONDITIONS

The basic test conditions initially planned for all six tests were as follows:

- Flight condition: takeoff
- Simulated aircraft velocity: 48.8 m/s (160 ft/sec)
- Span impact location: 80%
- Whirligig rotor speed: 3255 rpm
- Simulated incidence angle: 33°
- Relative velocity: 271 m/s (890 ft/sec)
- Bird size: 0.907 kg (2 lb)
- Slice size: 0.37 kg (13 oz)

For test, the blade is positioned to allow simulating of an impact at the 80% span location of the blade during aircraft take-off conditions. Because the bird does not have an axial velocity in the test setup used, the bird-to-blade relative velocity is equal to the blade tangential velocity at the point of impact. The correct incidence angle, therefore, was obtained by positioning the blade in the disk using an adapter plate that orients the blade such that the angle between the direction of blade rotation and the blade chord line, at the impact radius, is equal to the bird-to-blade incidence angle. The spin rig chamber temperatures were monitored so that the blade temperature did not exceed 180° F at impact.

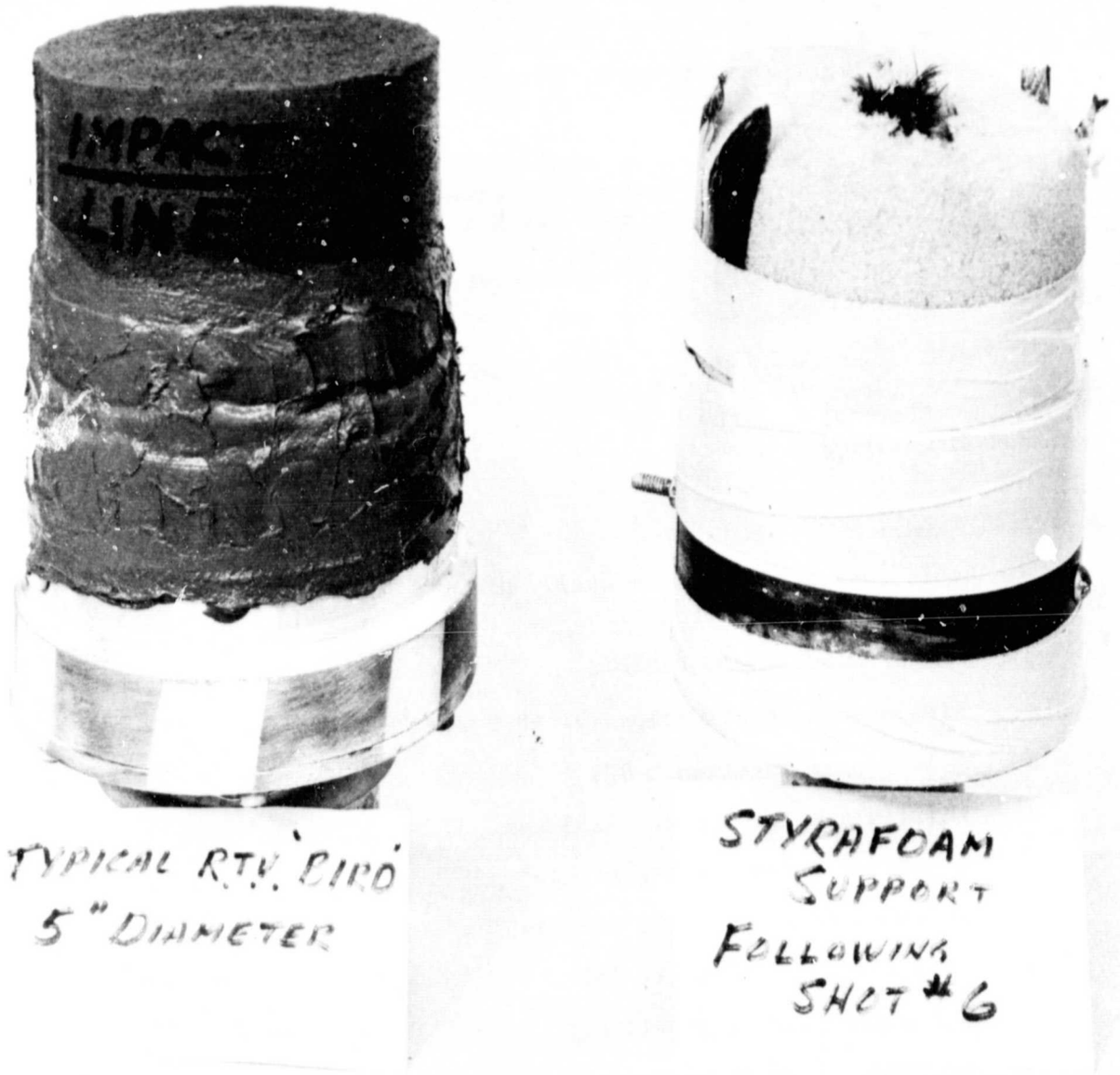

Figure 12. Typical RTV Simulated Bird Before Test and Remains of Starling Projectile Following Test.

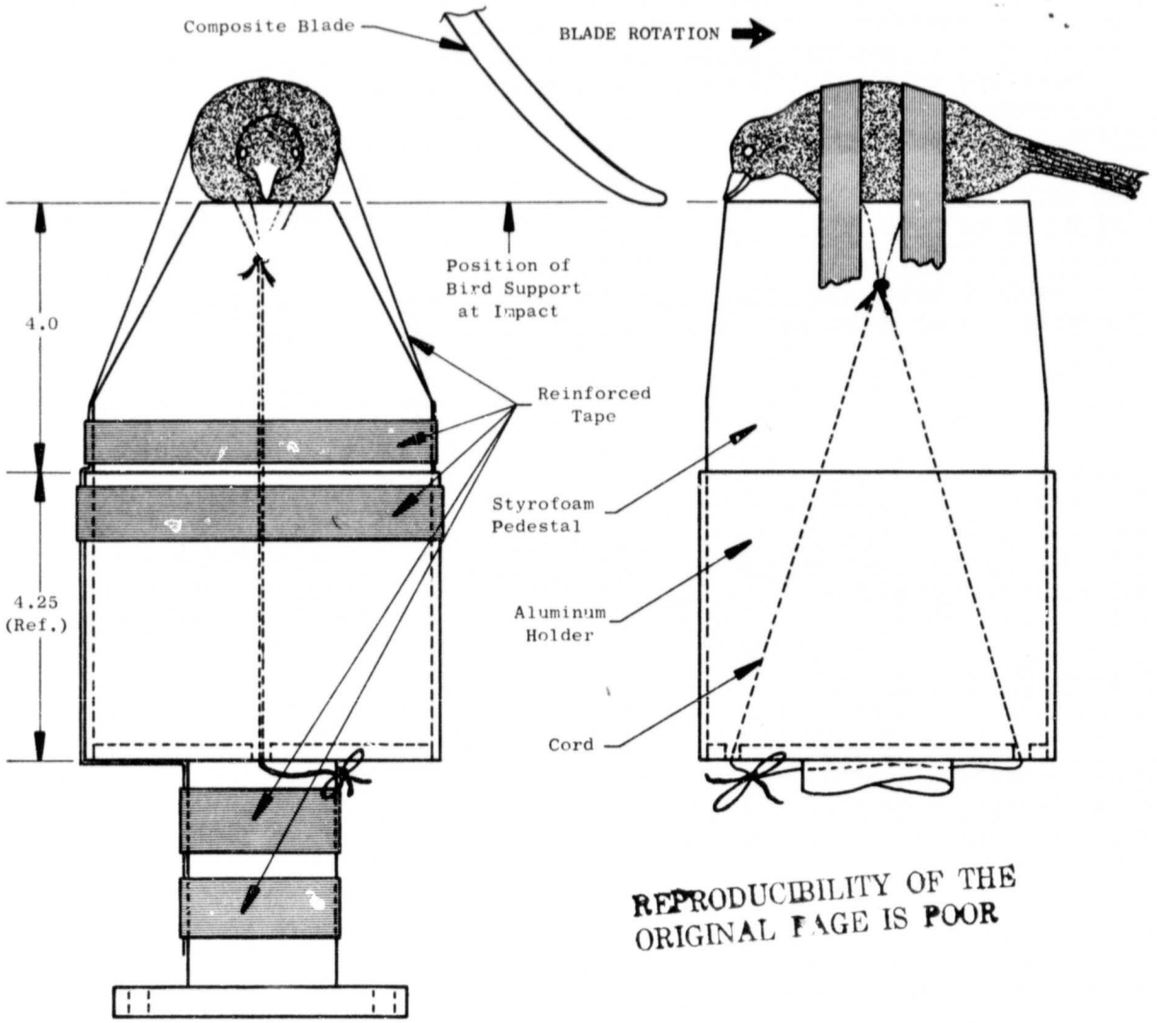

Figure 13. Typical Starling Injection Arrangement.

During the actual testing of the first three blades, the blades were damaged extensively. The test plan, therefore, was modified to include testing of the remaining blades with different incidence angles/bird size. A comparison of the initially planned tests and the actual test parameters shows that the only item that varied significantly from the plan was the slice weight. In each of the RTV bird tests, the leading edge impacted the bird at the planned target area for the desired slice but the leading edge dug into the RTV as the blade failed and took bites ranging from 0.39 kg (13.8 oz) to 0.50 (17.6 oz).

Table 2 lists the actual test conditions for the six tests as well as the slice total momentum, normal momentum, and normal energy.

In summary, the first four blades were tested by injecting a 12.7 cm (5 in.) diameter RTV "bird" into the path of the blade, rotating at 3255 rpm; the last two blades were tested by injecting a 11.3 kg (4 oz) starling into the path of the blade. Test numbers 1, 2, and 3 had the blade angle set at 33° at the 80% span impact location while, for Test No. 4, the blade angle was set at 23°. For Test No. 5 (starling test), the blade angle was set at 33°, for Test No. 6, the second starling test, the angle was set at 23°. All test conditions were reviewed and approved by NASA prior to testing.

3.4 TEST RESULTS

All tests, except that of blade S/N 4 (Test No. 6), which was tested with a starling at 23° incidence, resulted in the loss of the stainless steel leading edge and suffered severe breakage and delamination of the airfoil. Damage to blade S/N 4 for Test No. 6 consisted of bending of the stainless steel leading edge protection and delamination in the airfoil outer span but no weight loss. The results of the testing (including weight loss and extent of delamination) are summarized in Table 3. Photos of all blades after impact testing are presented in Appendix III. The results of ultrasonic and frequency inspections are discussed in Section 4.0.

The results of earlier testing of QCSEE blades, Reference 3, are also summarized in Table 3 for comparison purposes. Figure 14 shows blade materials loss versus impact normal energy for the SPAR-SHELL blades and the QCSEE all-composite blades tested. The supplied blades had levels of damage less than the original QCSEE design and generally greater than the blades from the NASA-sponsored impact improvement program (Reference 3). At high energy levels the weight loss for the blades was very similar to that of the improved QCSEE blades, while at the lower energy levels the weight loss was greater. For corresponding energy levels, the SPAR-SHELL blades had generally greater airfoil delamination than the improved QCSEE blades. A positive result of the testing was that none of the blades failed at the root and a new type blade attachment technique was demonstrated.

Table 2. Summary of Test Conditions.

Blade S/N	Test	% Span	Incidence Angle (degrees)	Slice Weight (oz.)	Speed, rpm	Total Momentum (lb-sec)	Normal Momentum (lb-sec)	Normal Energy (ft-lb)
6	1	80	33	17.6	3256	30.67	16.70	4085
8	2	80	33	13.5	3260	23.56	12.83	3141
10	3	80	33	14.9	3256	25.97	14.14	3458
11	4	80	23	14.0	3256	24.40	9.53	1672
5	5	80	33	3.6	3256	6.27	3.41	835
4	6	80	23	4.4	3250	7.65	2.99	524

Table 3. Summary of Test Results and Comparative QCSEE Test Results.

Type Blade	Blade S/N	% Span	Incidence Angle (degrees)	Slice Weight (oz.)	Speed (rpm)	Normal Energy (ft-lb)	Blade Weight Loss (lbs)	% Airfoil Area Delamination
SPAR-SHELL	6	80	33	17.6	3256	4085	1.55	95
Filament-Wound	8	80	33	13.5	3260	3141	1.02	99
	10	80	33	14.9	3256	3458	1.27	90
	11	80	23	14.0	3256	1672	1.12	98
	5	80	33	3.6	3256	835	.66	80
	4	80	23	4.4	3250	524	0	80
Preliminary QCSEE	QP005	75	33	8.0	3260	1759	.37	89
(Ref NAS3-18021)	QP011	75	33	13.0	3260	2859	4.09	100
	PQP010	75	23	8.5	3200	931	0	74
Improved QCSEE	PQP003	75	33	2.9	3320	661	0	10
	PQP003	75	33	17.0	3320	3877	1.38	81
(Ref. NAS3-17836)	PQP004	75	33	12.8	3320	2919	.80	68
	PQP005	75	33	8.2	3320	1870	.75	94
	PQP006	75	33	13.0	3320	2964	1.34	66

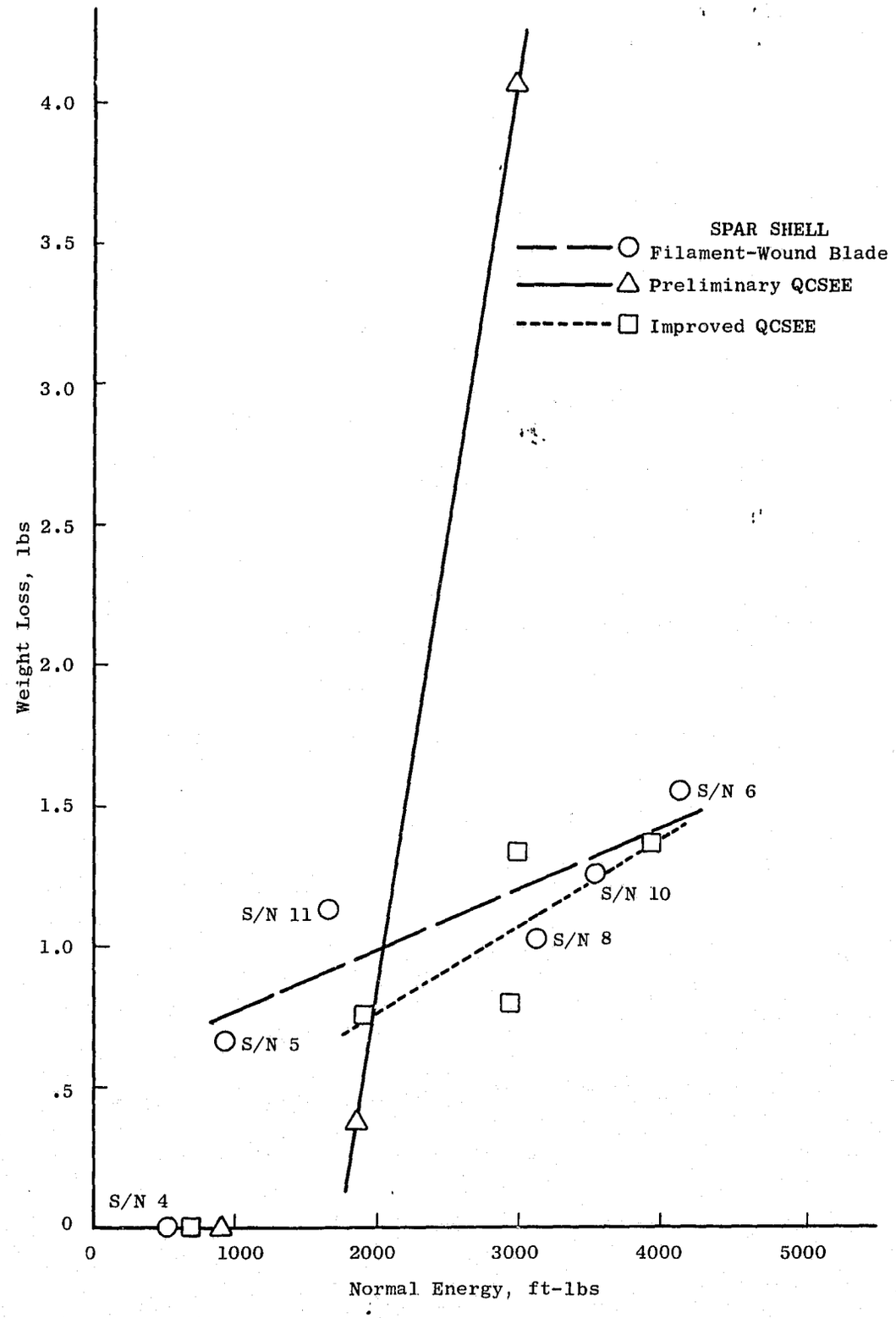

Figure 14. Blade Weight Loss for 80% Span Whirligig Impact Tests.

4.0 NONDESTRUCTIVE BLADE DAMAGE EVALUATION

4.1 NONDESTRUCTIVE TEST METHODS

The nondestructive test equipment used for the program consisted of a Sperry 621 immerscope, associated electronics, and mechanical fixturing. The NDE test setup, shown in Figure 15, basically uses a measurement of sound attenuation due to both absorption and scattering. The through-transmission approach (as opposed to pure pulse-echo or reflection-plate, pulse-echo/transmission approaches) provides for a more efficient energy transfer with a minimal influence of test equipment configuration or material/component shape. The scanner contour follows the airfoil with a master/slave servomechanism. The attenuation values used are referenced to the specific blade configuration.

High-resolution scanning (75 lines per inch for 15,000 units of data per square inch), combined with 10 shades of gray (5% to 95% on the oscilloscope) recording on dry facsimile paper, provides an "attenugraph" image which is illustrated in Figure 16. These pictures have been of particular value in comparisons of before- and after-impact tests. Defects detected by this inspection include delaminations, FOD protection-to-airfoil unbond, dry tip, porosity, and internal wrinkles.

For frequency determination, each blade is root-mounted on a table and electromagnetically excited into free-resonant vibration. An appropriately mounted detector provides the frequency count signal. Frequency values are obtained for first flexure, second flexure, and first torsional whole-body vibration modes as well as higher modes as desired. The values provide a measure of quality as well as assuring the accomplishment of the design vibration envelope.

4.2 NDE RESULTS

Eight blades received from NASA were subjected to through-transmission ultrasonic C-scan inspections. Bench frequencies and nodal lines also were determined for the eight blades. Of these eight blades, six were subsequently impact tested and were reinspected. Blades S/N 5, 6, 8, 10, and 11 had severe airfoil breakage and could only be manually ultrasonically scanned to determine airfoil regions that had not been damaged. Blade S/N 4 was partially delaminated and was posttest ultrasonically and frequency inspected in the same manner as the pretest inspections. The C-scans and hand-scanning results for all blades before and after testing are presented in Appendix IV. All frequency results are given in Appendix II.

The eight blades were each inspected using two signal intensity levels (gain settings of 50 × .1 and 50 × 1) to assist in distinguishing between regions of porosity and delaminations. The C-scans in Appendix IV are for the 50 × 1 setting. The lower setting of 50 × .1 generally shows all areas of

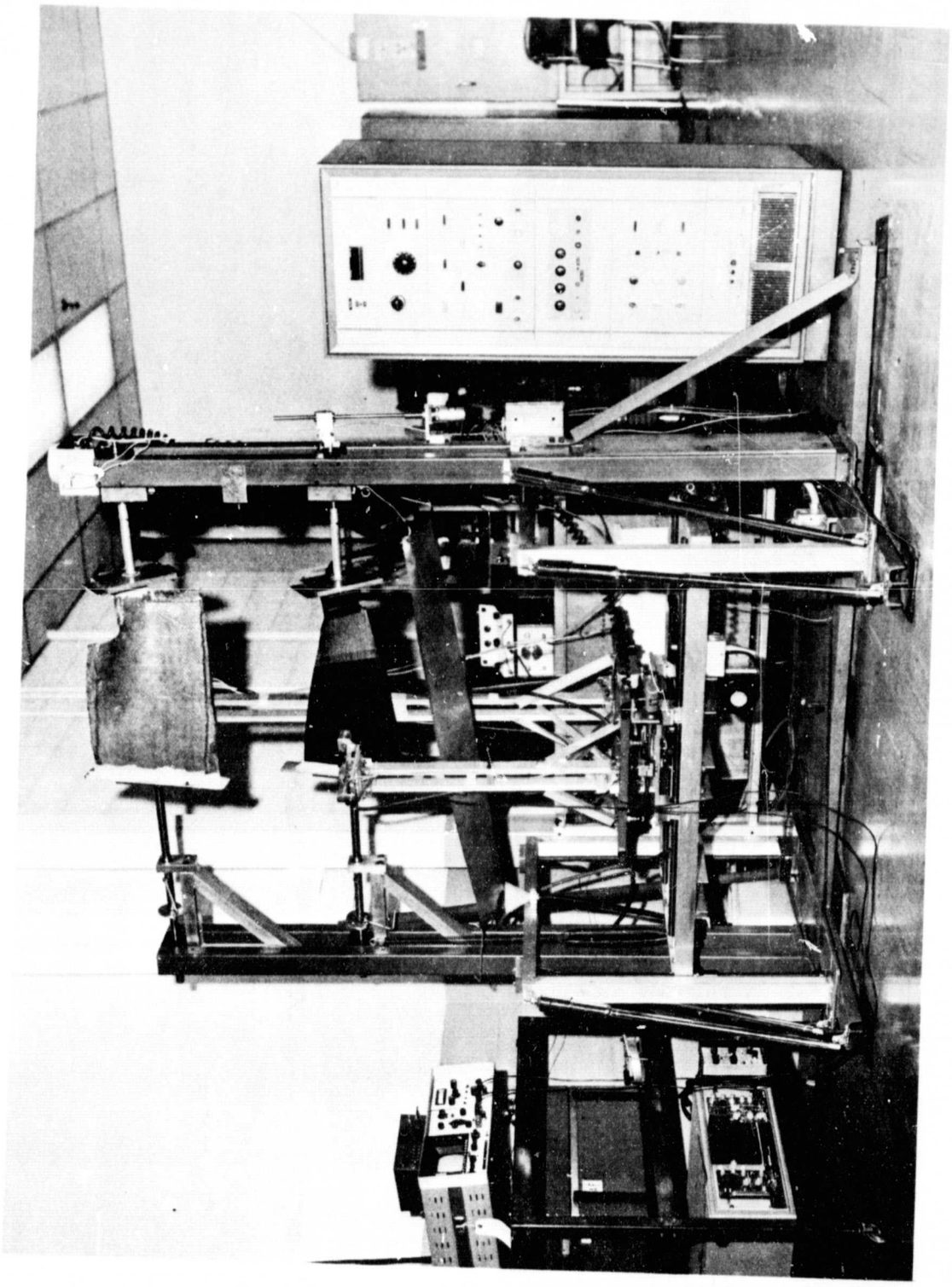

Figure 15. QCSEE Blade and Follower Mounted in Ultrasonic C-Scan Equipment.

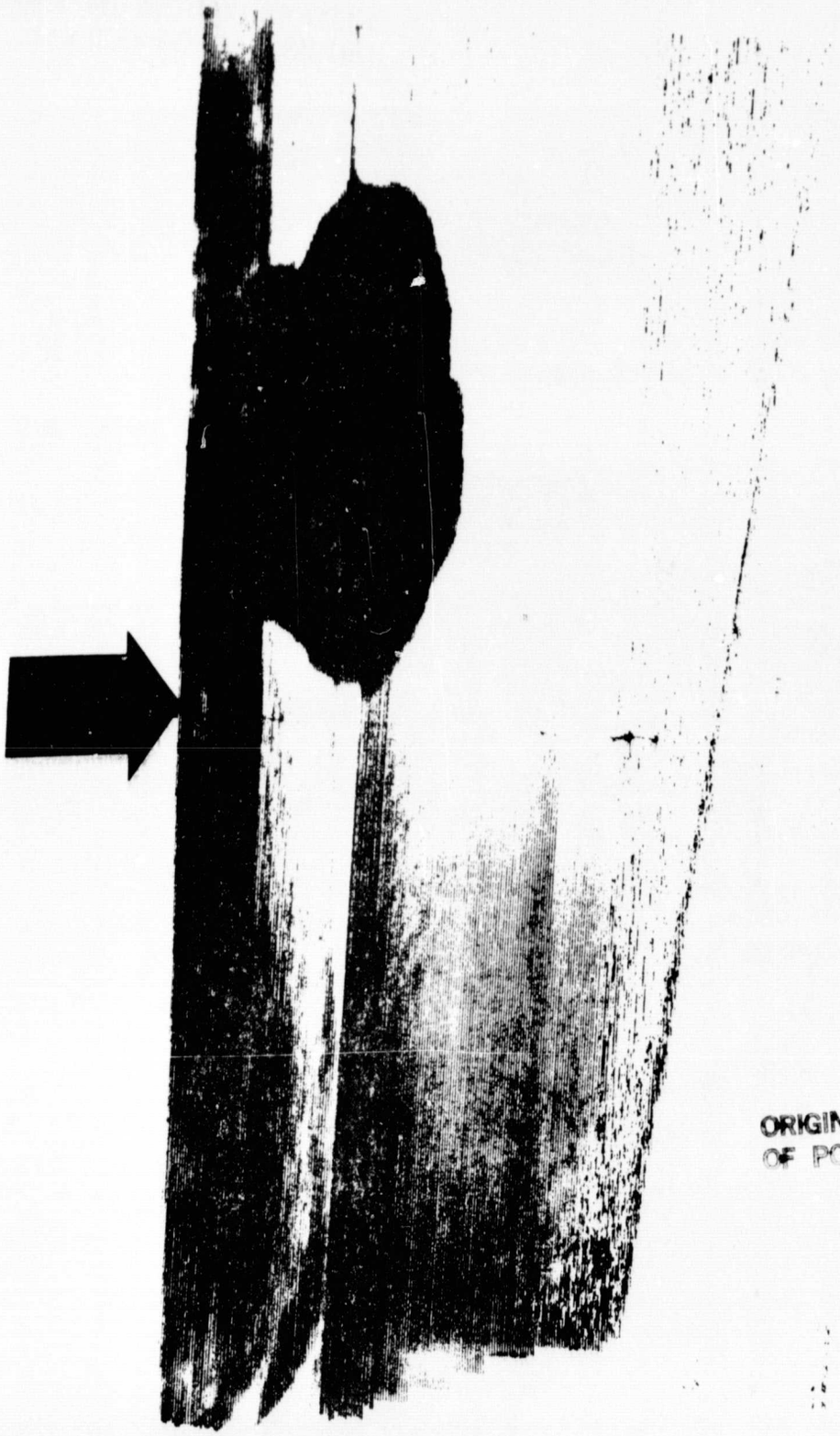

Figure 16. Typical Airfoil Postimpact Test Through-Transmission, Ultrasonic C-Scan.

porosity but does not permit distinguishing delaminations from porosity. The higher setting of 50 × 1 generally indicates only regions of very high porosity and delaminations. Dark areas with very sharp boundaries are indicative of delaminations. Sharp changes in section thickness also can cause dark regions and prevent clear interpretation in such areas. Because of the sharp changes in section thickness at the blade's root transition, meaningful scans were restricted to the airfoil regions.

A review of the scans indicates that only several of the blades are relatively free of porosity and several have indications of quite high porosity and even possibly some delamination in the lower airfoil region. Several blades show unbond in the leading edge protection.

Based on the pretest C-scans, the blades were listed in order from "most-sound" to "least-sound" as follows:

S/N 6, 5, 8, 10, 11, 7, 4, 12

Blades S/N 4, 5, 6, 8, 10, and 11 were selected for test based on these results and to select at least one blade of each design combination for testing.

The posttest C-scan of S/N 4 shows that approximately 80% of the airfoil was delaminated by the impact. The posttest hand-scan results of blades S/N, 5, 6, 8, 10, and 11 show that 80 to 99% of the airfoils was either delaminated or had surface material pulled away. The regions on each airfoil that are not damaged are marked on each blade and can be seen in the photographs in Appendix IV.

The posttest frequency measurements on blade S/N 4 show that the first flexural frequency was reduced by approximately 7% and the higher modes by somewhat higher amounts. First torsional frequency could not be established.

5.0 CONCLUSIONS

1. Six blades were successfully impact tested in the whirligig facility and subjected to pretest and posttest inspections in fullfillment of contract requirements.

2. The tested blades had levels of damage less than for the original QCSEE blades tested.

3. At high energy levels, the weight loss for the tested blades was very similar to that of improved QCSEE blades from program NAS3-17836; while, at the lower energy levels (starling range), the tested blades had considerably more damage.

4. For corresponding energy levels, the SPAR-SHELL blades generally had greater airfoil delamination than did the improved QCSEE blades.

5. None of the blades failed in the root. This demonstrated capability for the new type attachment technique employed.

6.0 RECOMMENDATIONS

1. It is expected that improved FOD capabilities for such filament-wound blades could result from a more uniform distribution and mixing of the blade core and shell plies.

2. The leading edge protection should have a tapered thickness from the leading edge aft for best results.

3. Future development blades should have airfoils which more completely simulate those of operational blades so that the results of testing are more applicable to actual blade design.

7.0 REFERENCES

1. "Filament-Winding Fabrication of QCSEE Configuration Fan Blades," NASA CR-135332.

2. "Quiet Clean Short Haul Experimental UTW Composite Fan Blade Preliminary Design Test Report," NASA CR-134846.

3. "Fiber Composite Fan Blade Impact Improvement Program Final Report," NASA CR-135078.

APPENDIX I
BLADE FREQUENCY VERSUS AMPLITUDE AS GENERATED AT LeRC

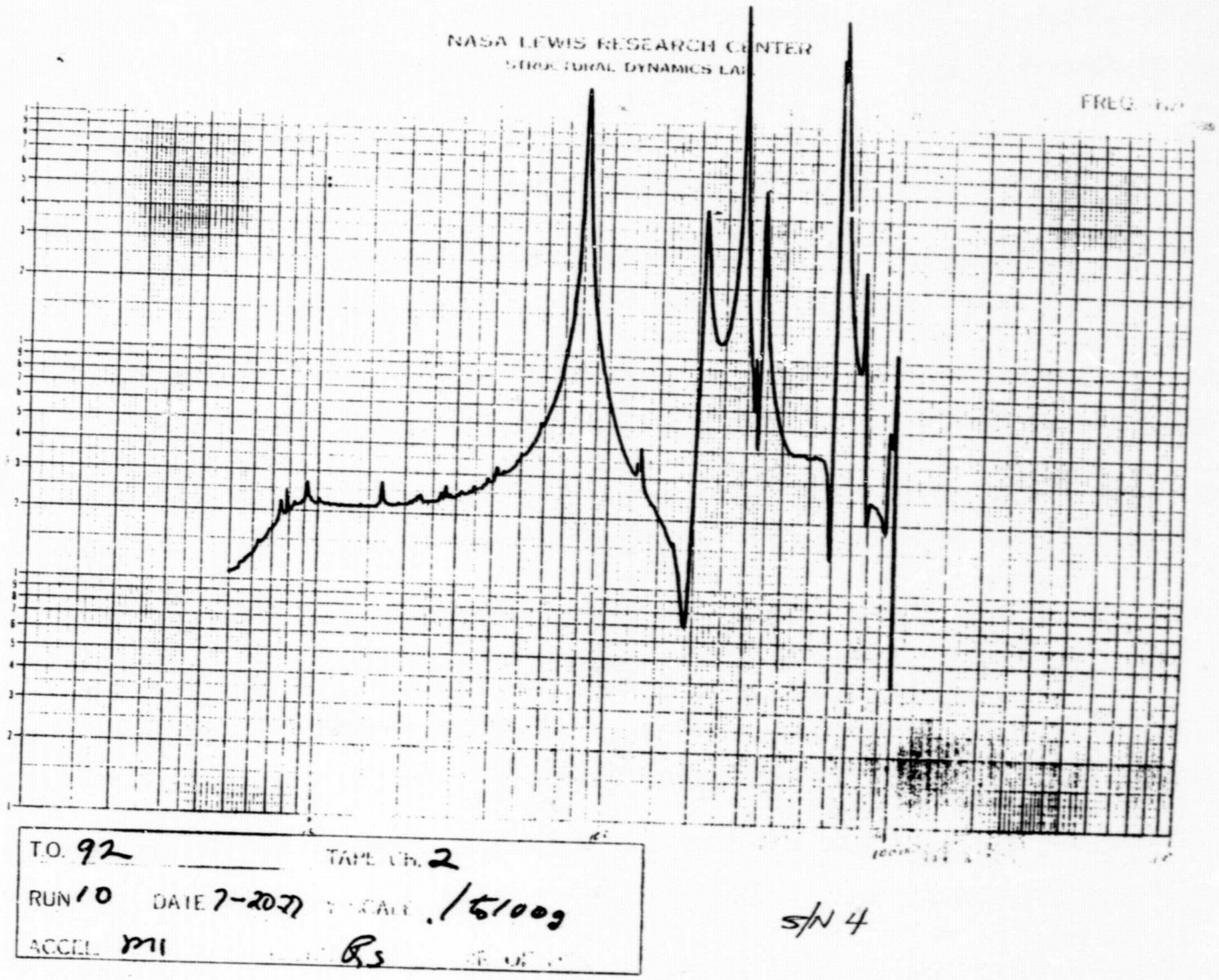

Figure 17. Frequency Response of As-Received Blade S/N 4.

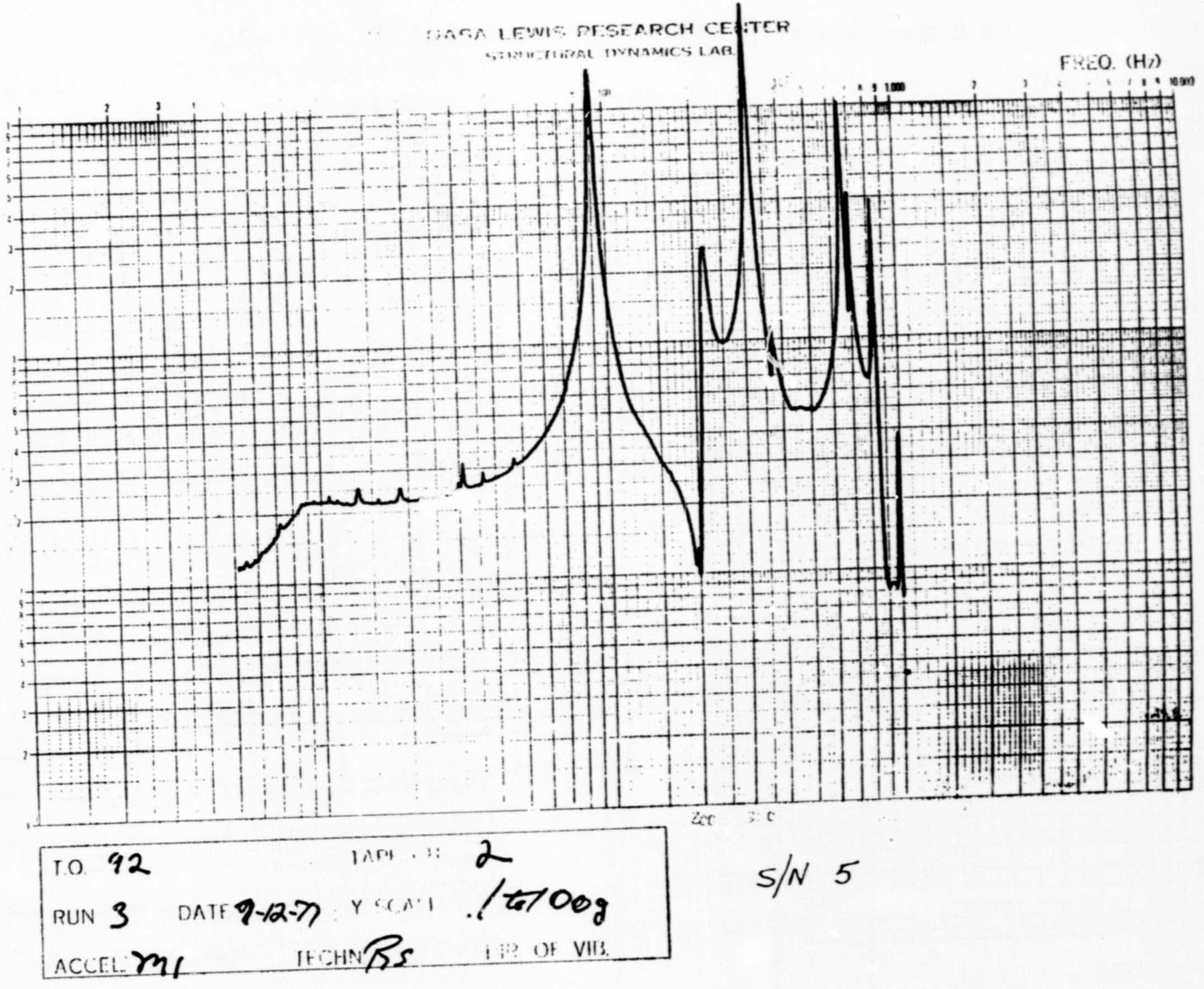

Figure 18. Frequency Response of As-Received Blade S/N 5.

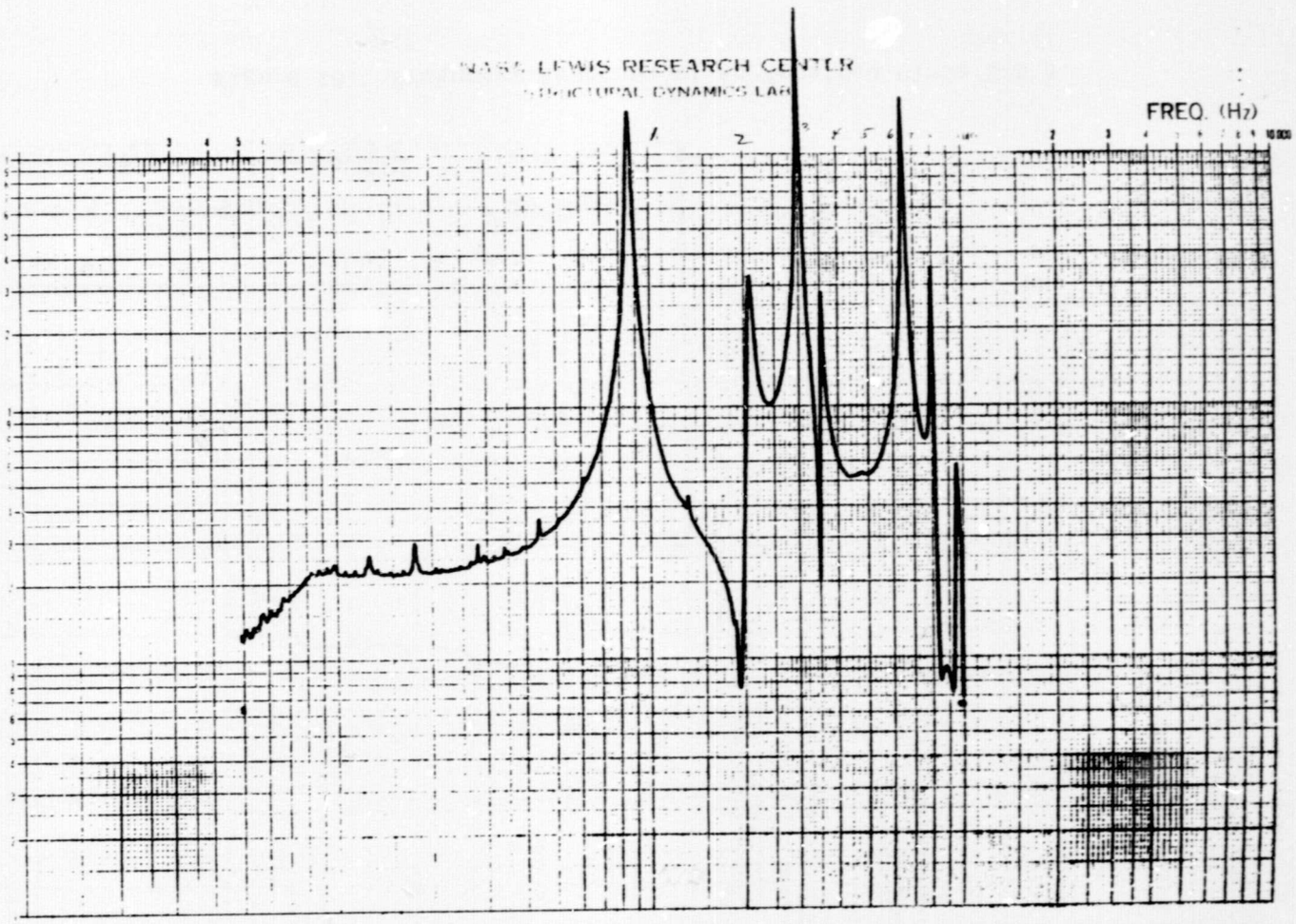

Figure 19. Frequency Response of As-Received Blade S/N 6.

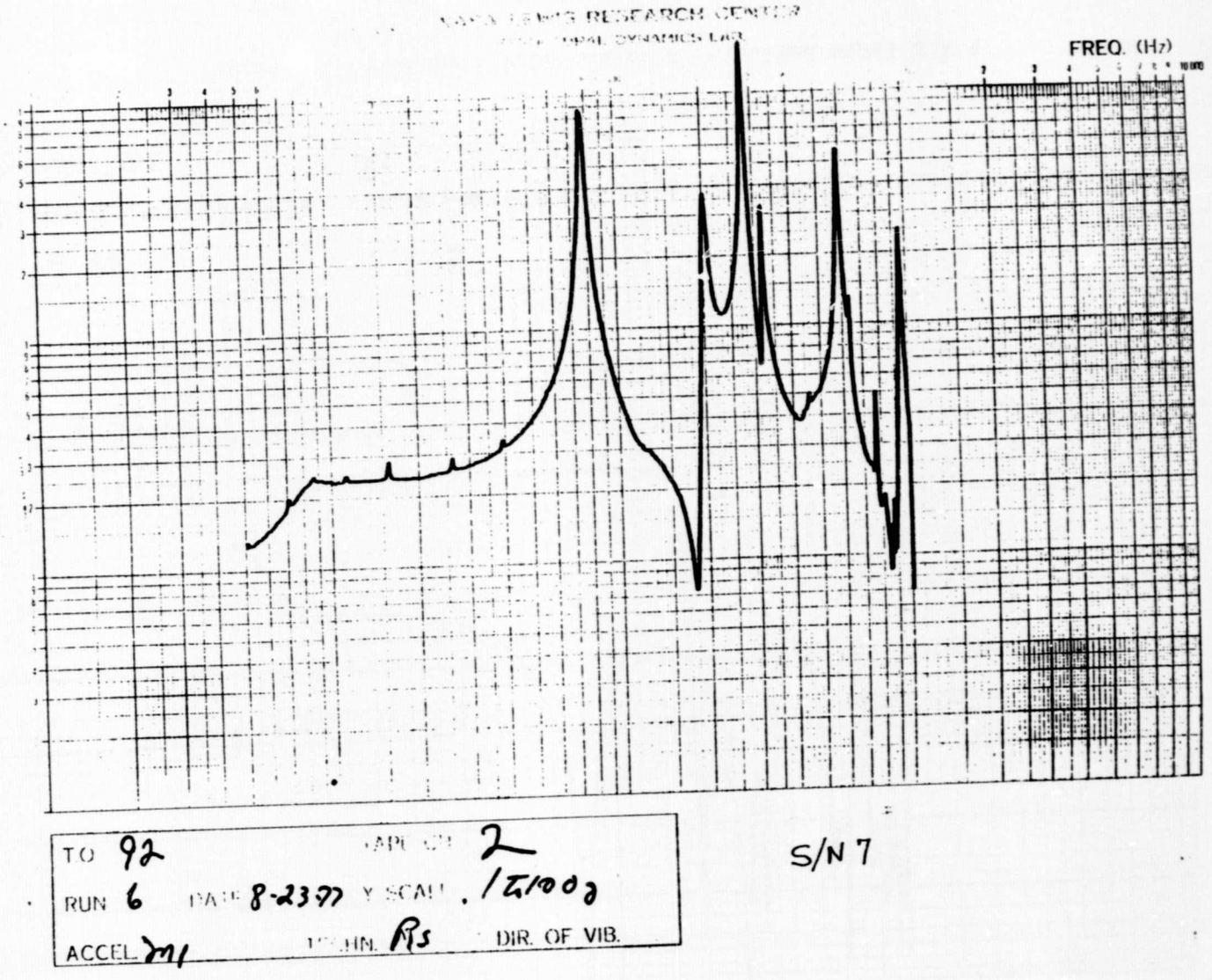

Figure 20. Frequency Response of As-Received Blade S/N 7.

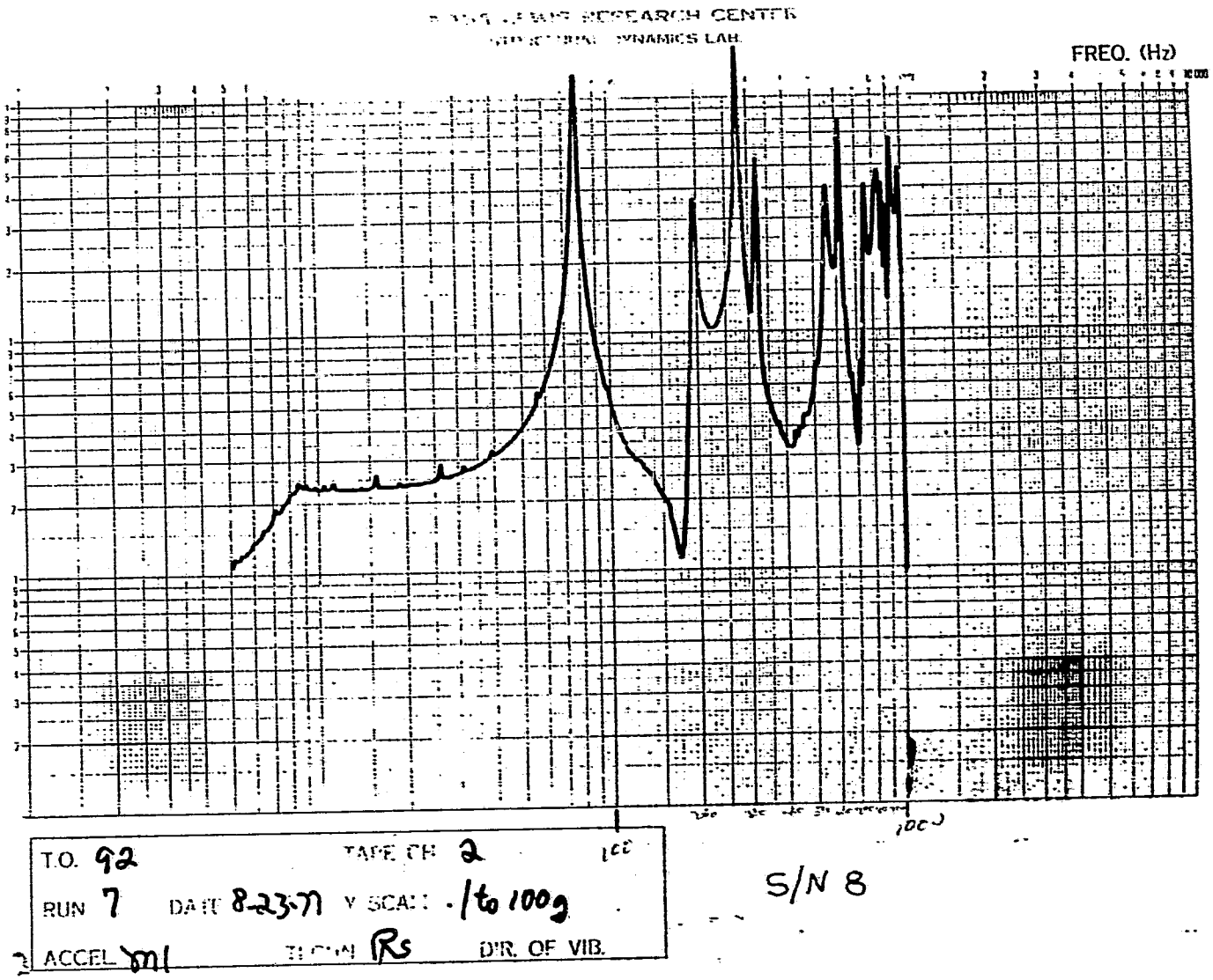

Figure 21. Frequency Response of As-Received Blade S/N 8.

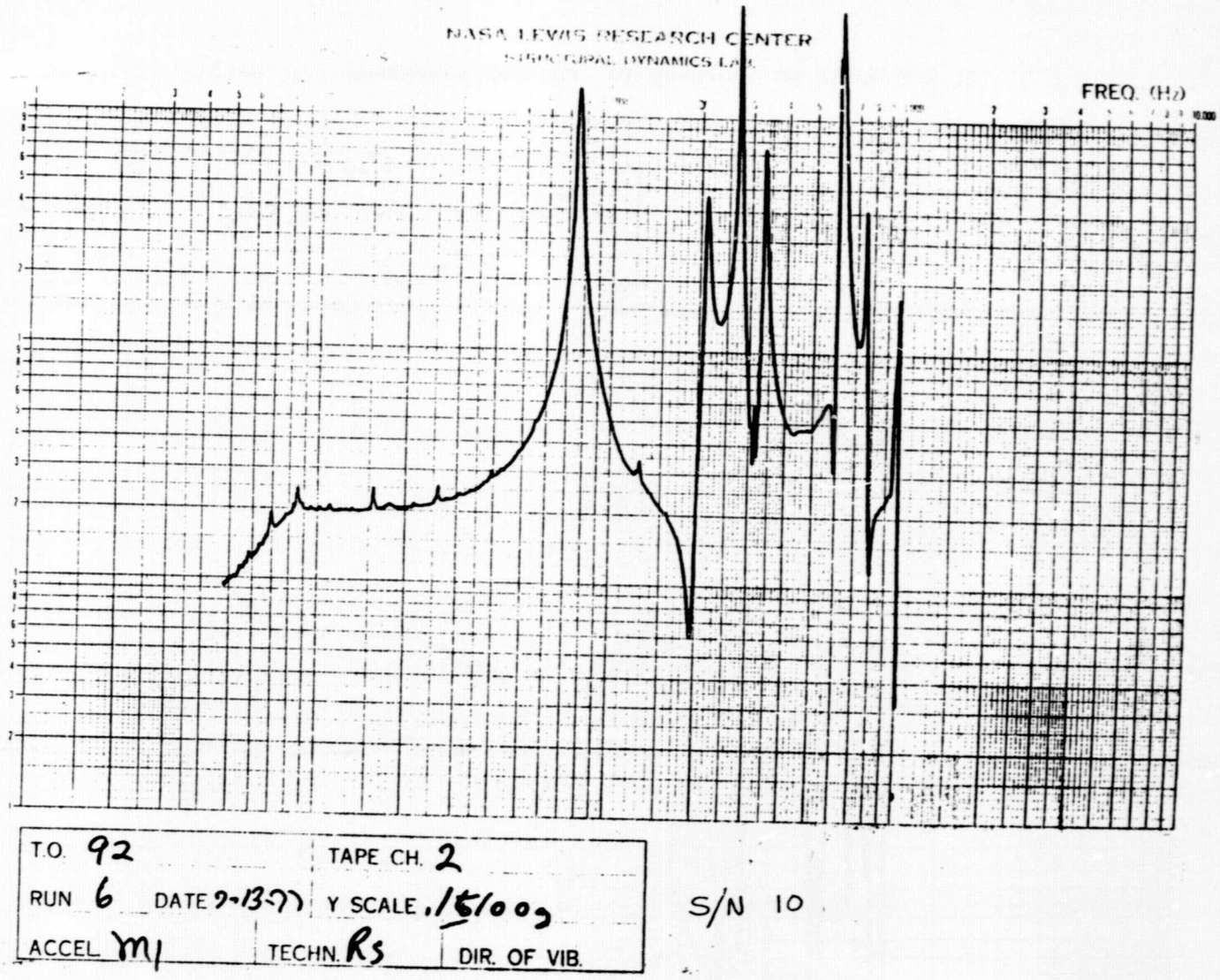

Figure 22. Frequency Response of As-Received Blade S/N 10.

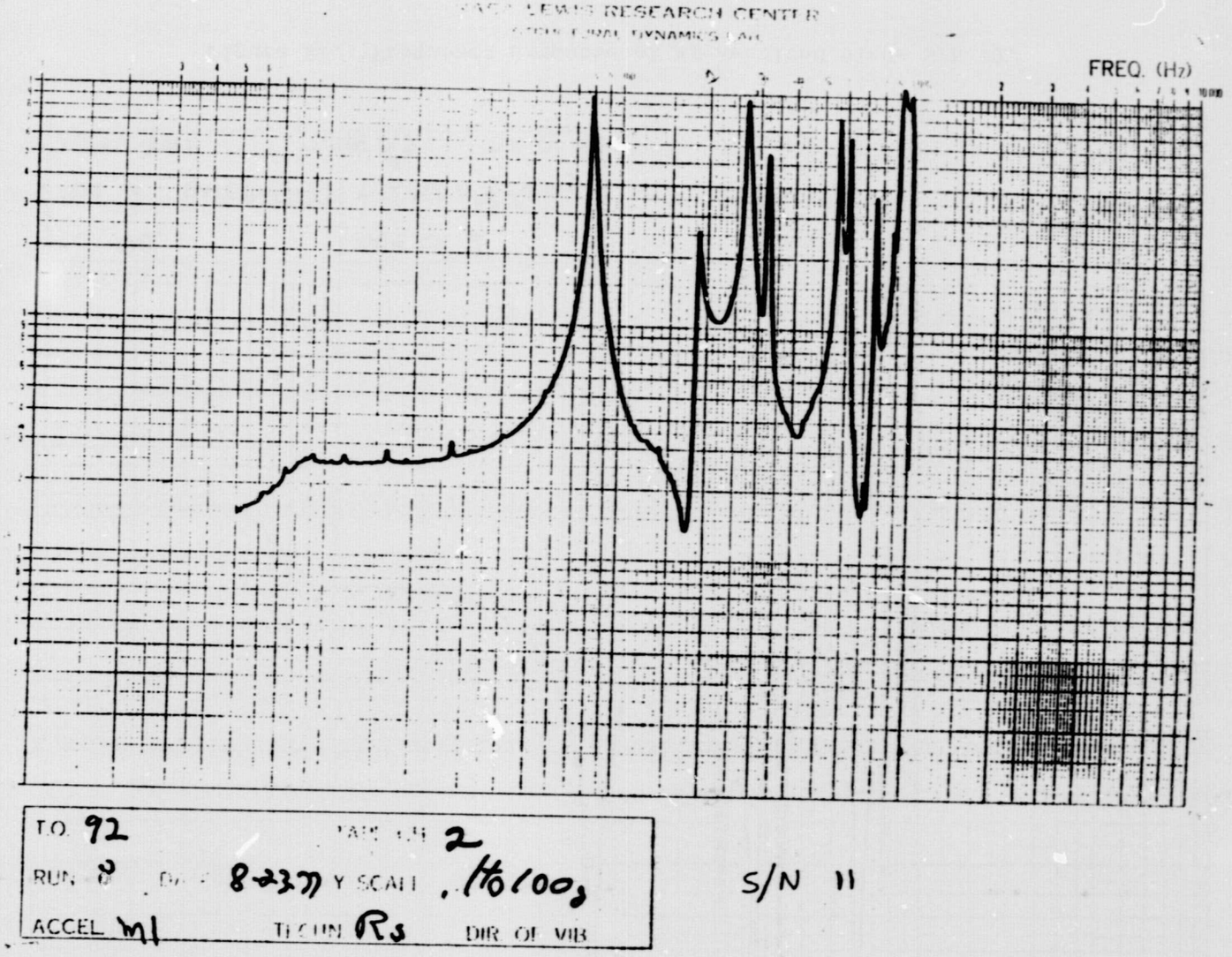

Figure 23. Frequency Response of As-Received Blade S/N 11.

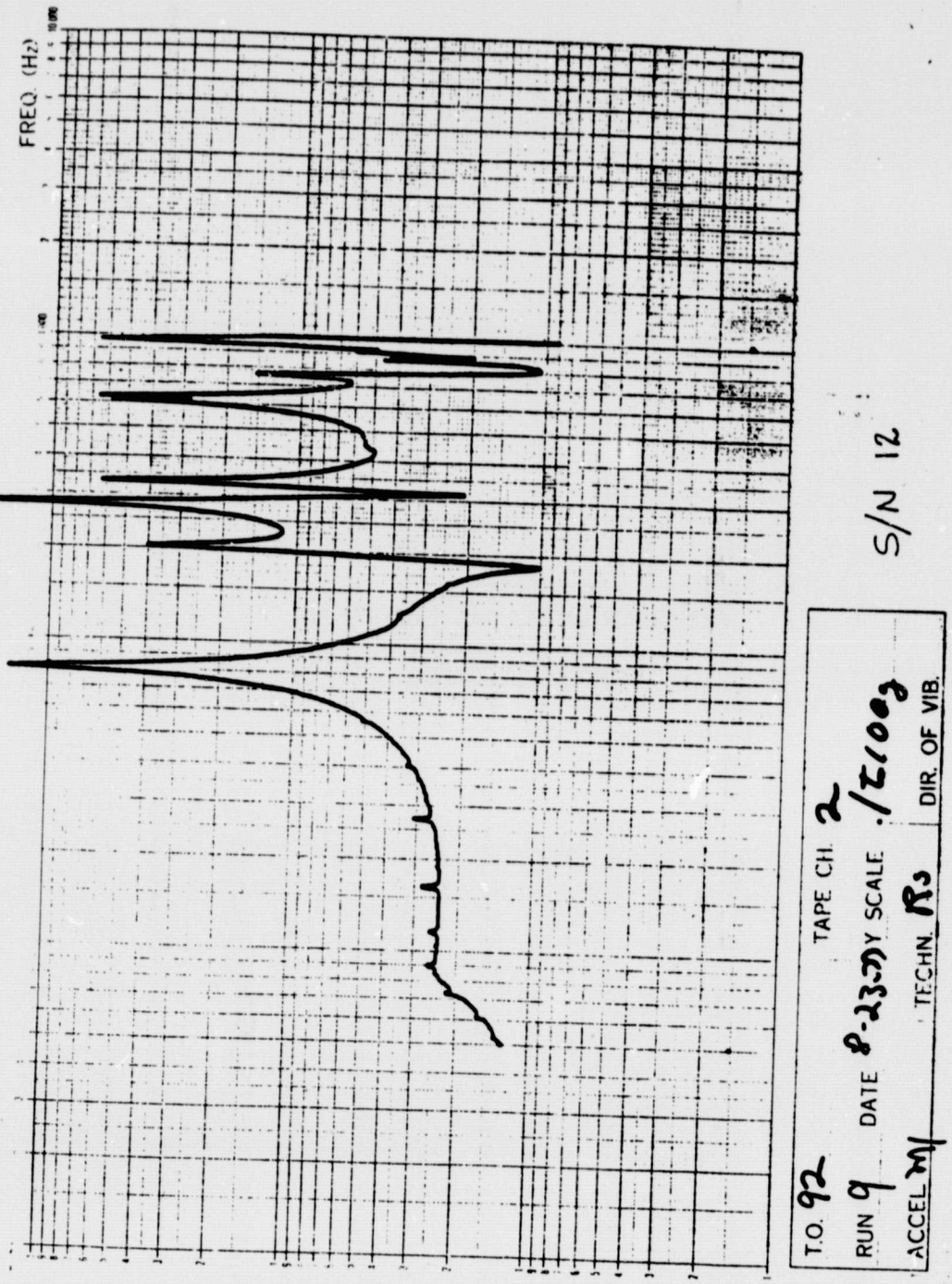

Figure 24. Frequency Response of As-Received Blade S/N 12.

APPENDIX II
FREQUENCY AND NODAL LINES FOR TEST BLADES AS GENERATED BY GENERAL ELECTRIC

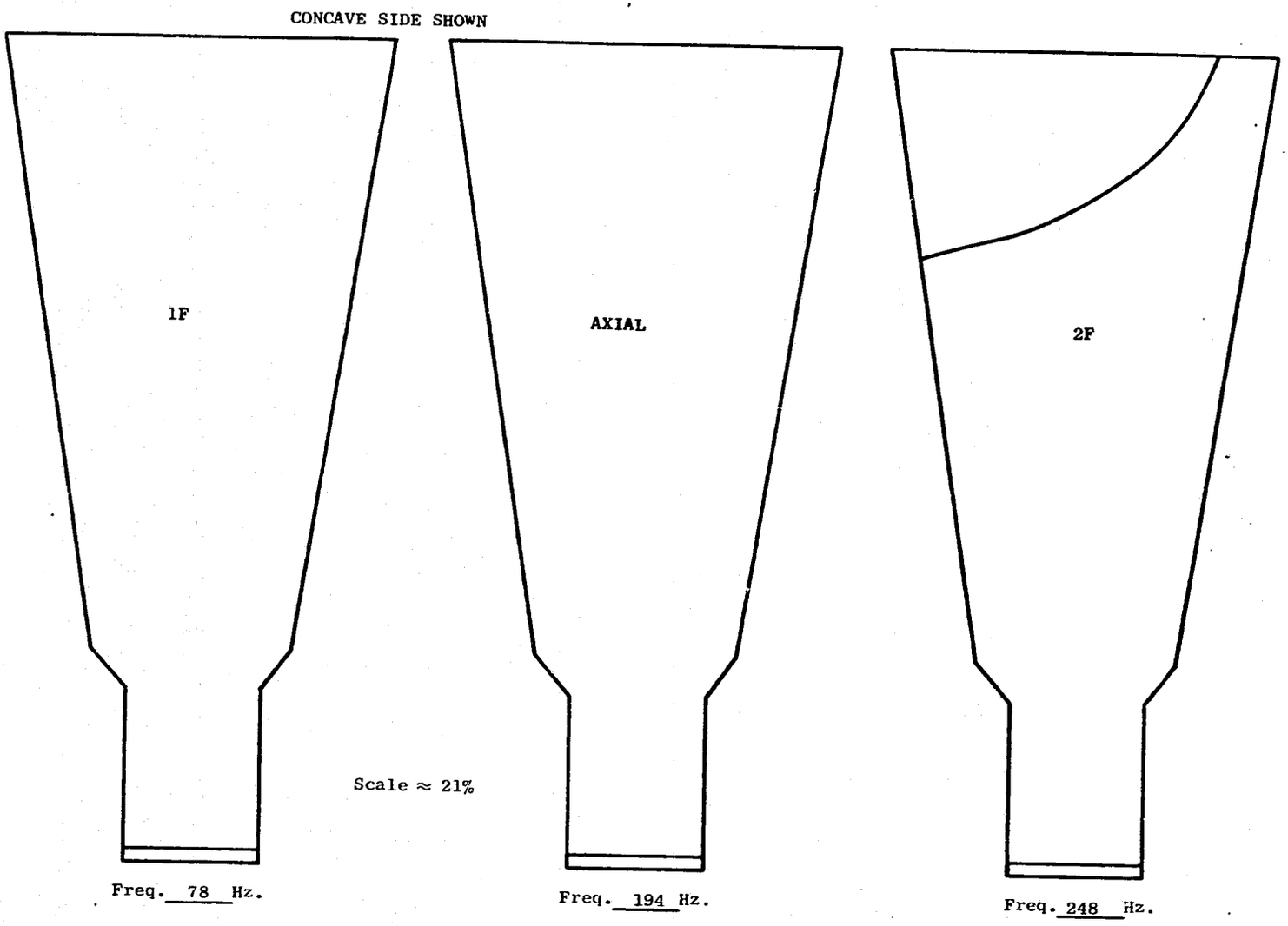

Figure 25. Resonant Frequencies and Nodal Patterns, QCSEE Fiber-Wound Blade, S/N 4, Concave Side, 78 to 248 Hz.

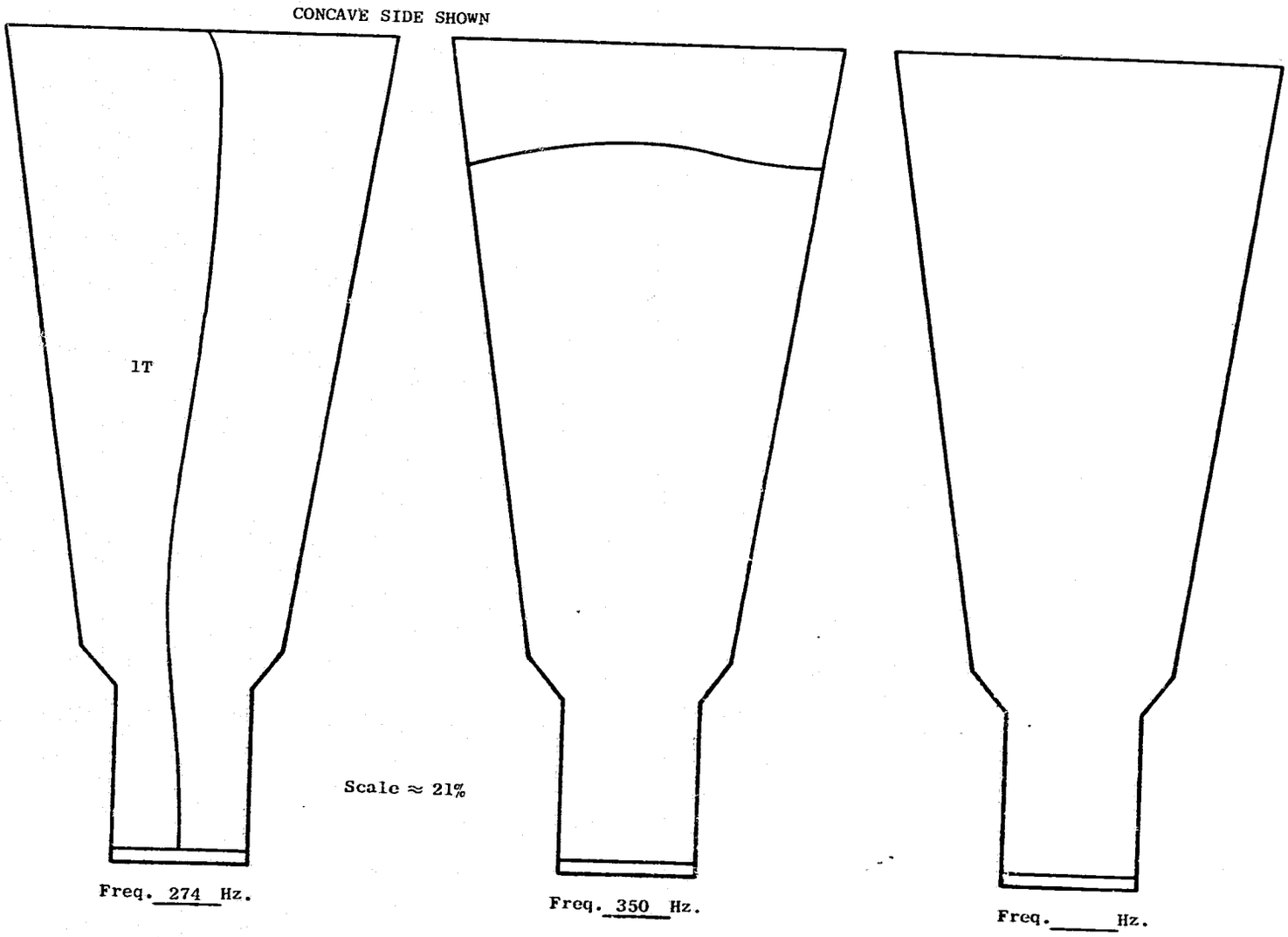

Figure 26. Resonant Frequencies and Nodal Patterns, QCSEE Fiber-Wound Blade, S/N 4, Concave Side, 274 and 350 Hz.

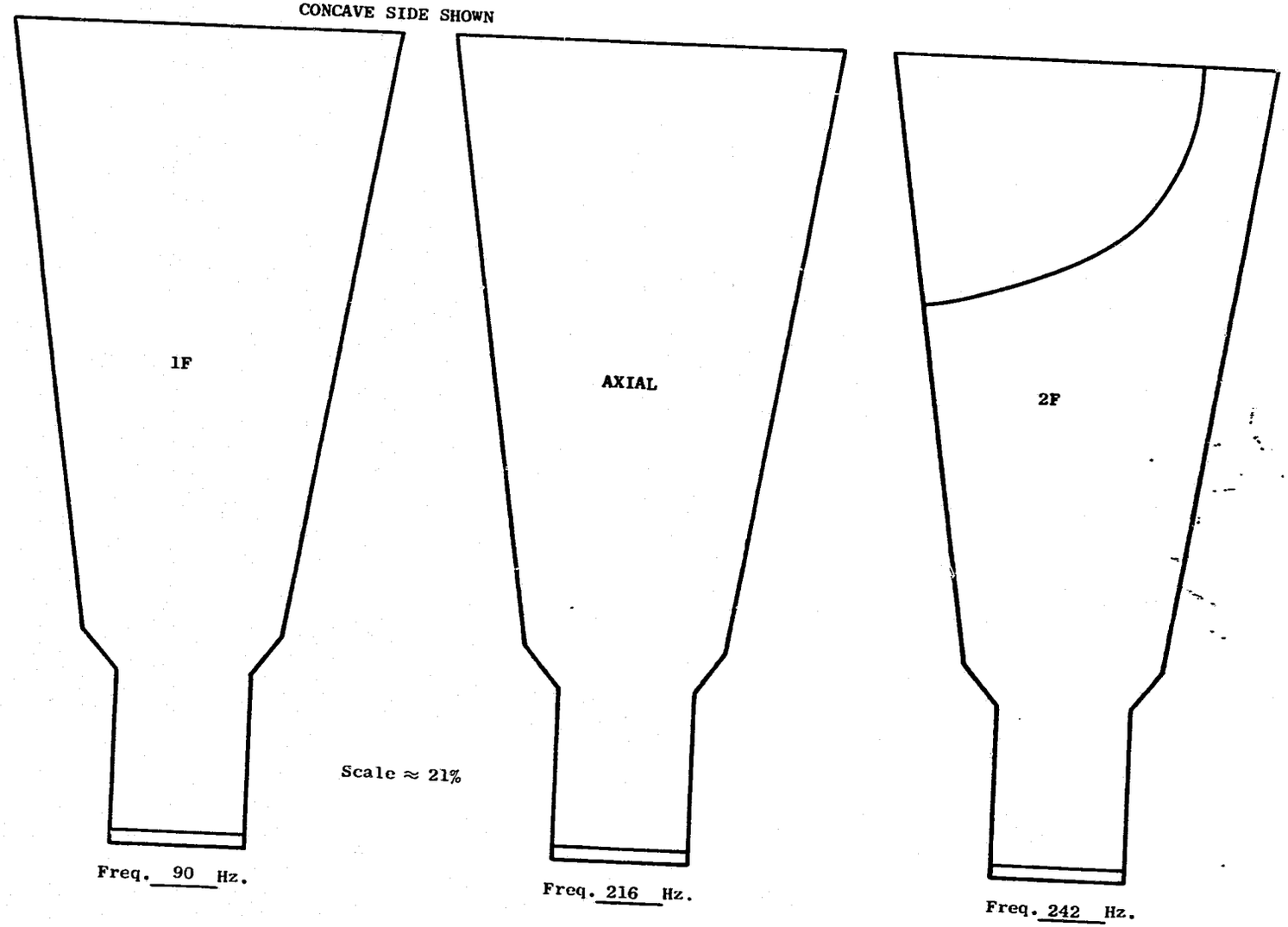

Figure 27. Resonant Frequencies and Nodal Patterns, QCSEE Fiber Wound Blade, S/N 5, Concave Side, 90 to 242 Hz.

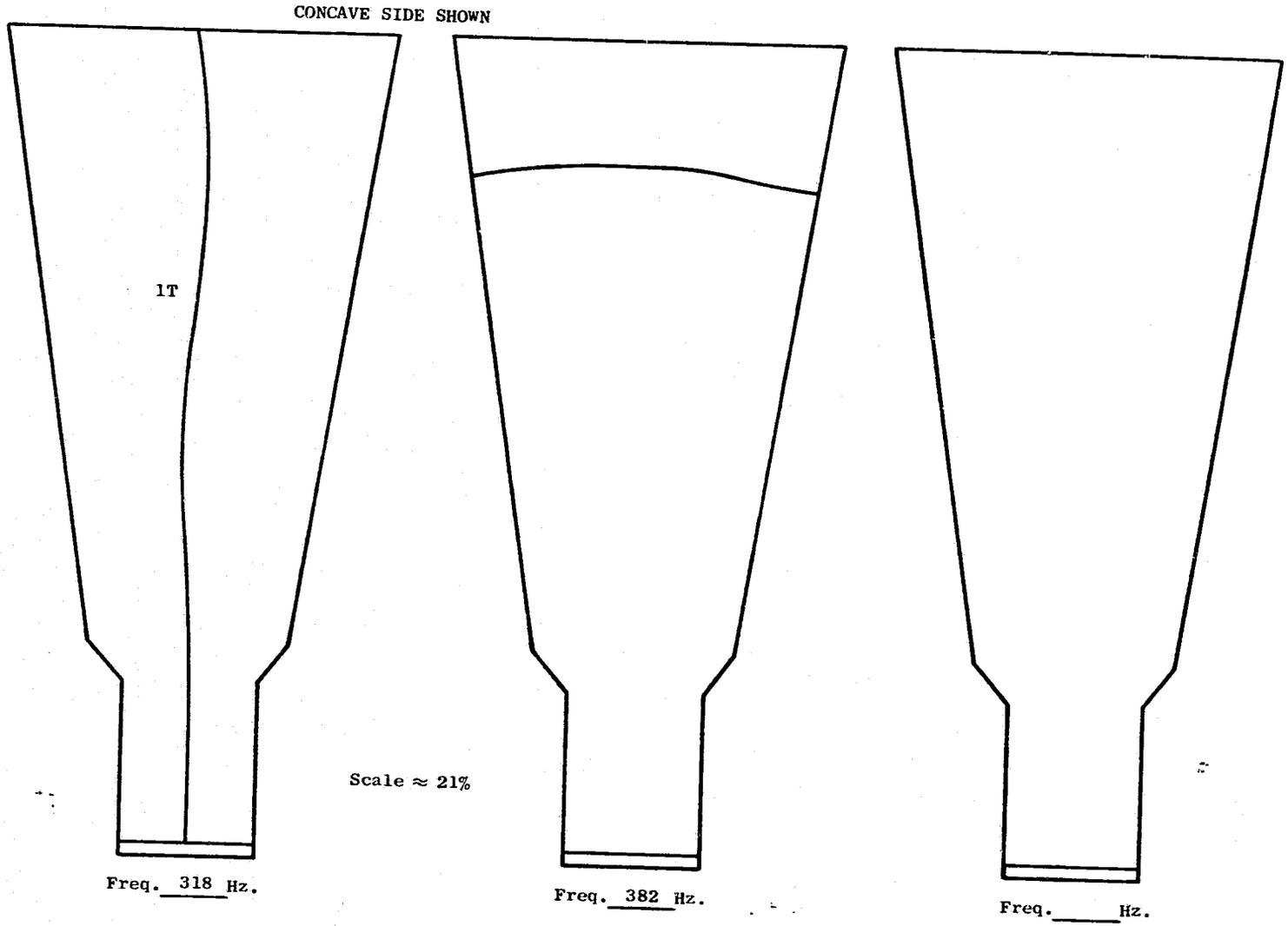

Figure 28. Resonant Frequencies and Nodal Patterns, QCSEE Fiber-Wound Blade, S/N 5, Concave Side, 318 and 382 Hz.

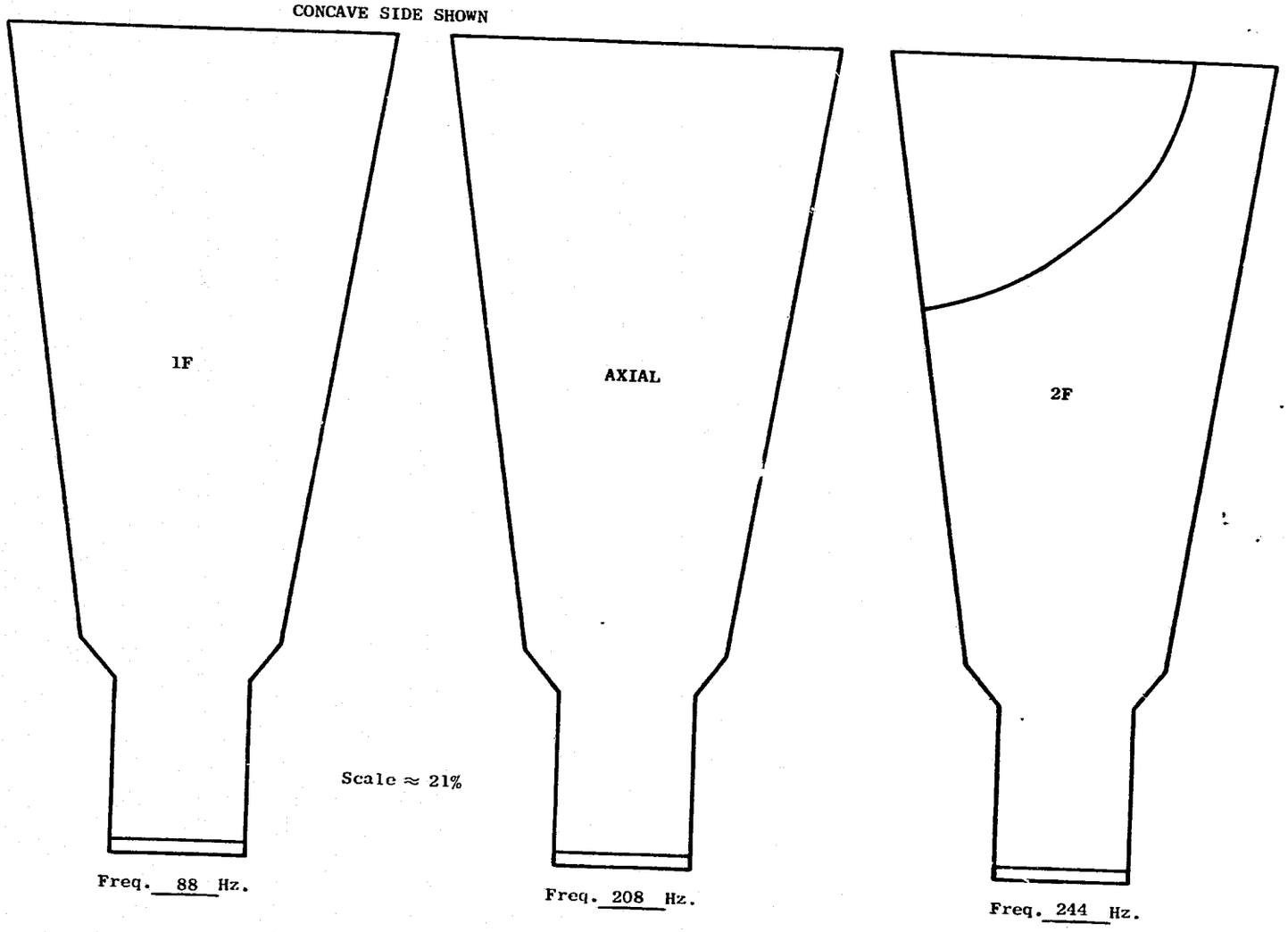

Figure 29. Resonant Frequencies and Nodal Patterns, QCSEE Fiber-Wound Blade, S/N 6, Concave Side, 88 to 244 Hz.

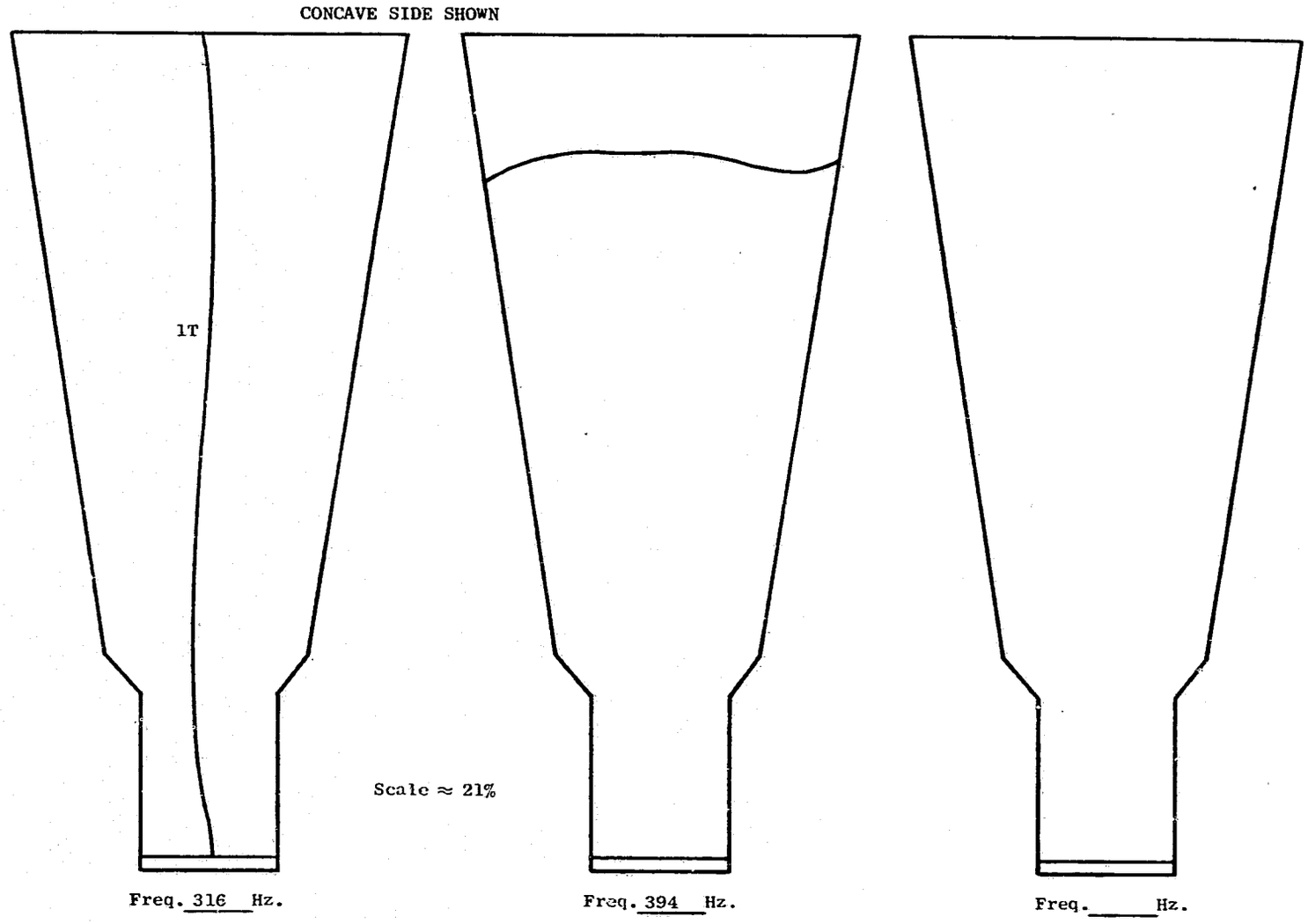

Figure 30. Resonant Frequencies and Nodal Patterns, QCSEE Fiber-Wound Blade, S/N 6, Concave Side, 316 and 394 Hz.

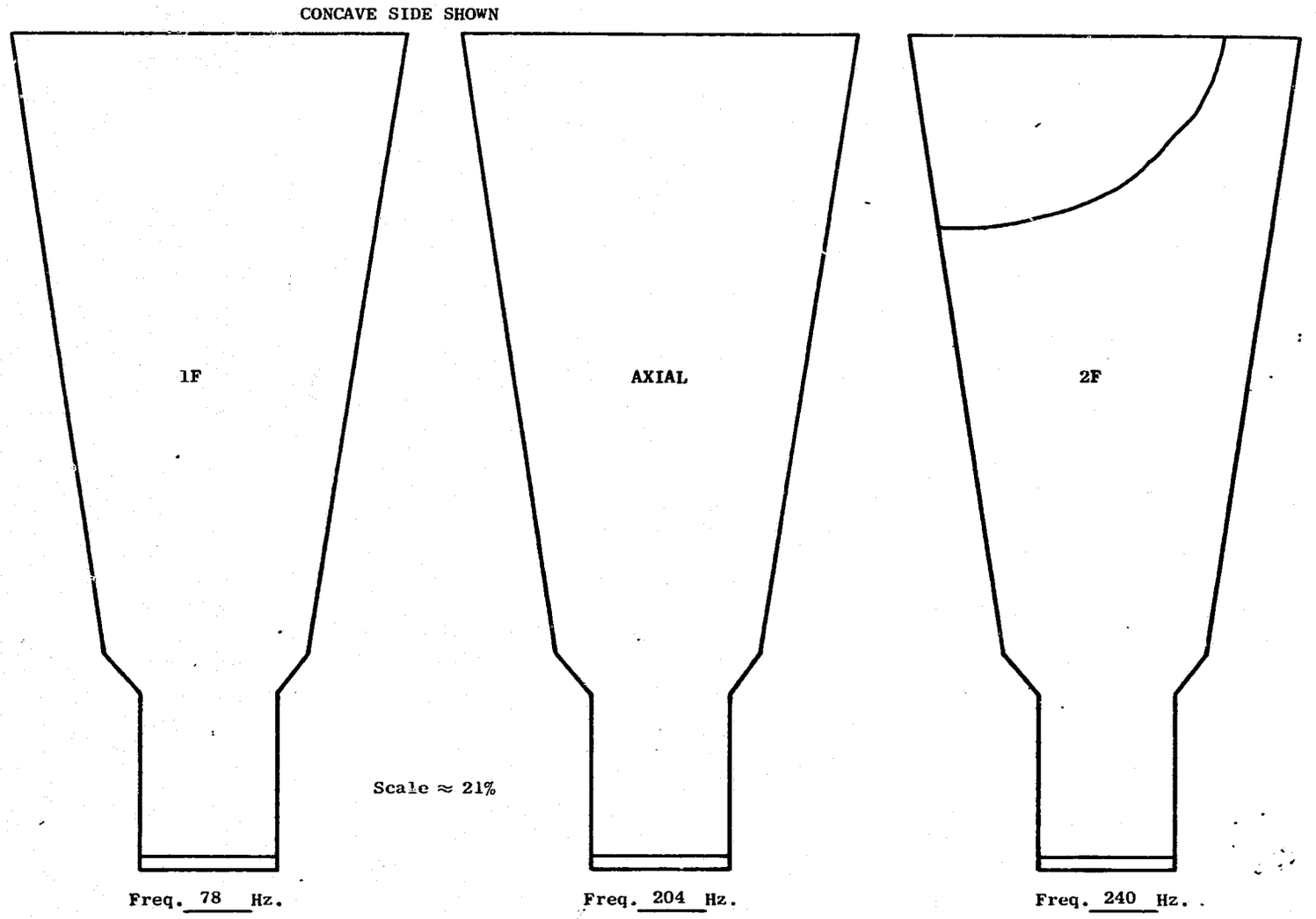

Figure 31. Resonant Frequencies and Nodal Patterns, QCSEE Fiber-Wound Blade, S/N 7, Concave Side, 78 to 240 Hz.

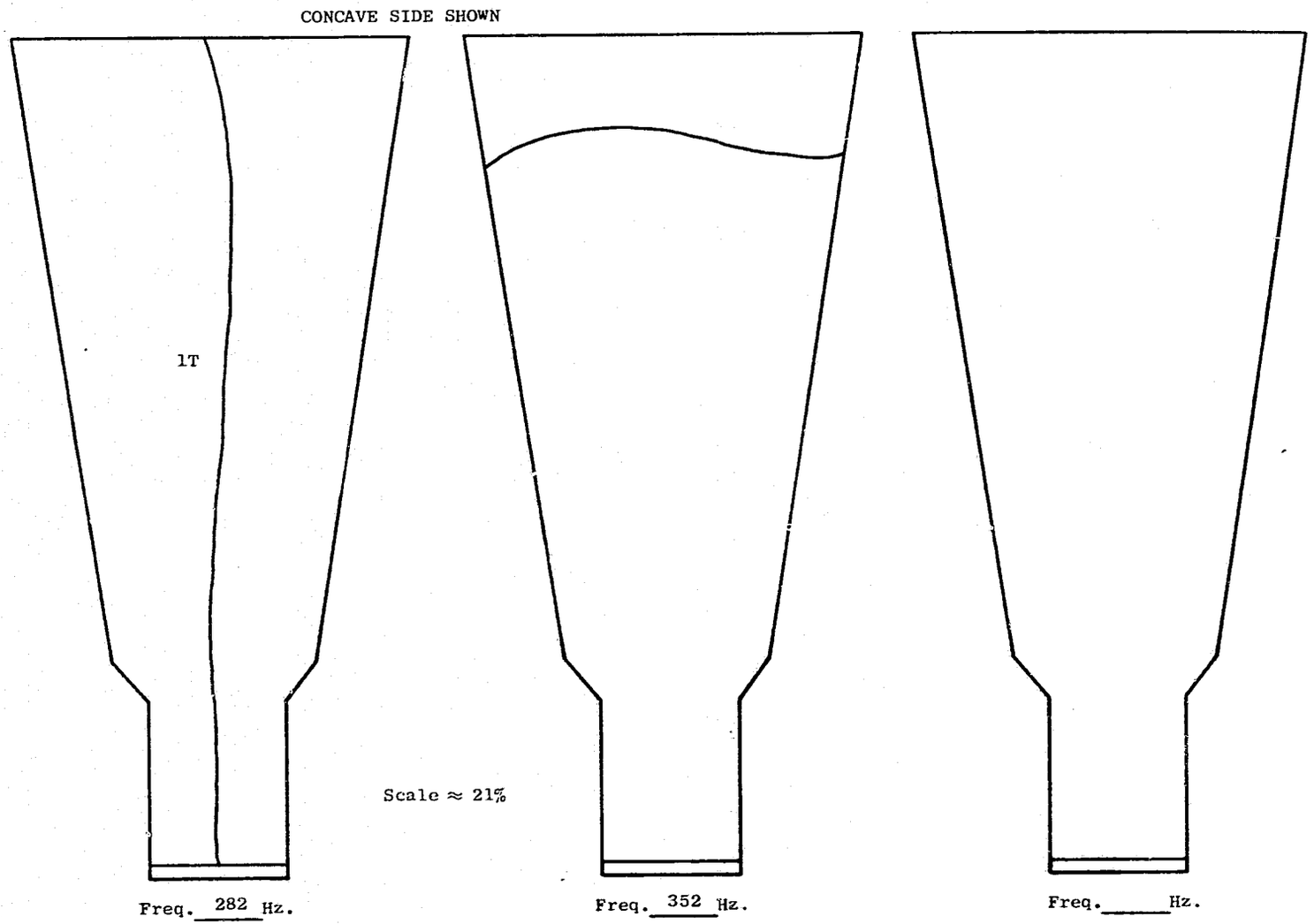

Figure 32. Resonant Frequencies and Nodal Patterns, QCSEE Fiber-Wound Blade, S/N 7, Concave Side, 282 and 352 Hz.

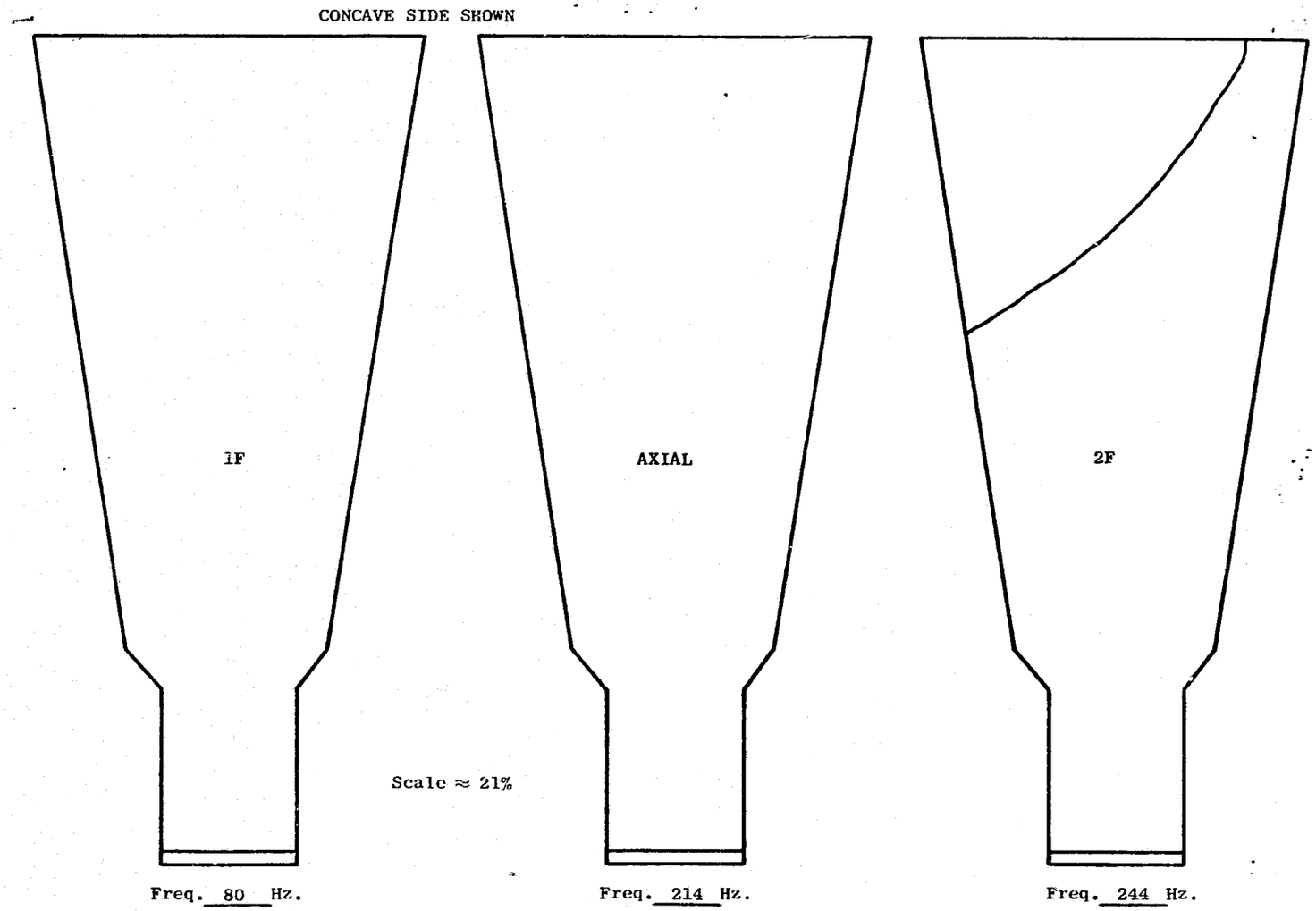

Figure 33. Resonant Frequencies and Nodal Patterns, QCSEE Fiber-Wound Blade, S/N 8, Concave Side, 80 to 244 Hz.

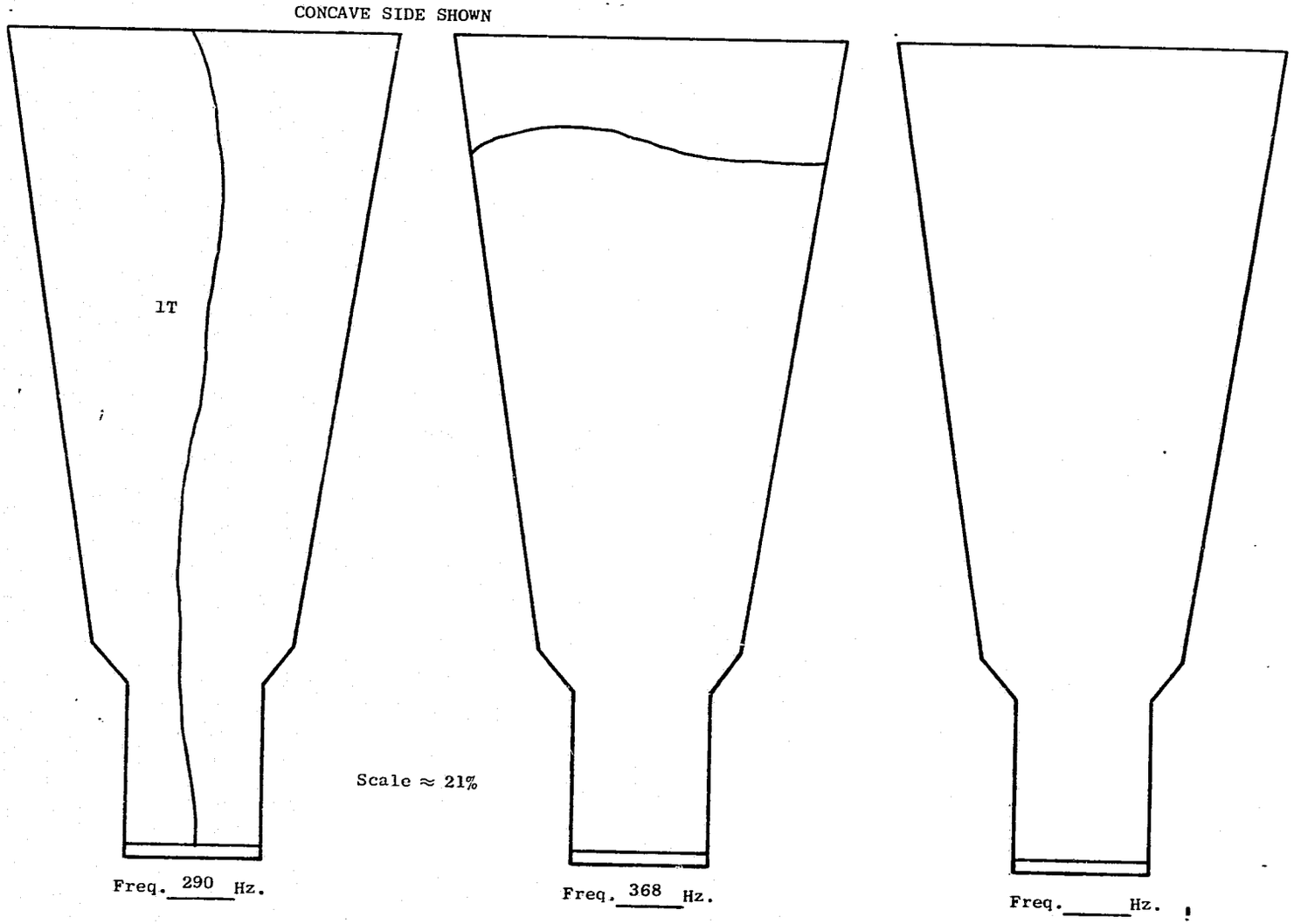

Figure 34. Resonant Frequencies and Nodal Patterns, QCSEE Fiber-Wound Blade, S/N 8, Concave Side, 290 and 368 Hz.

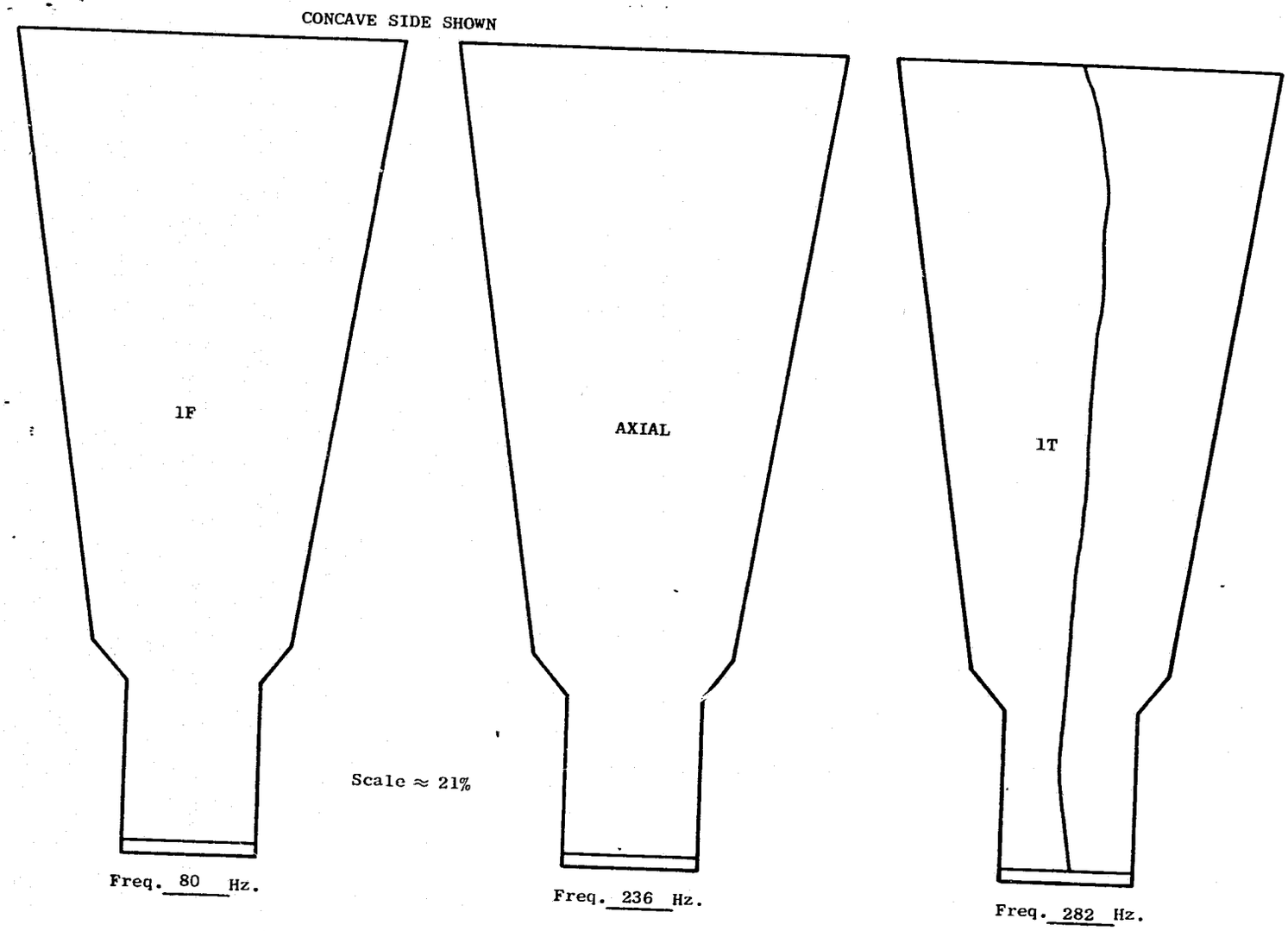

Figure 35. Resonant Frequencies and Nodal Patterns, QCSEE Fiber-Wound Blade, S/N 10, Concave Side, 80 to 282 Hz.

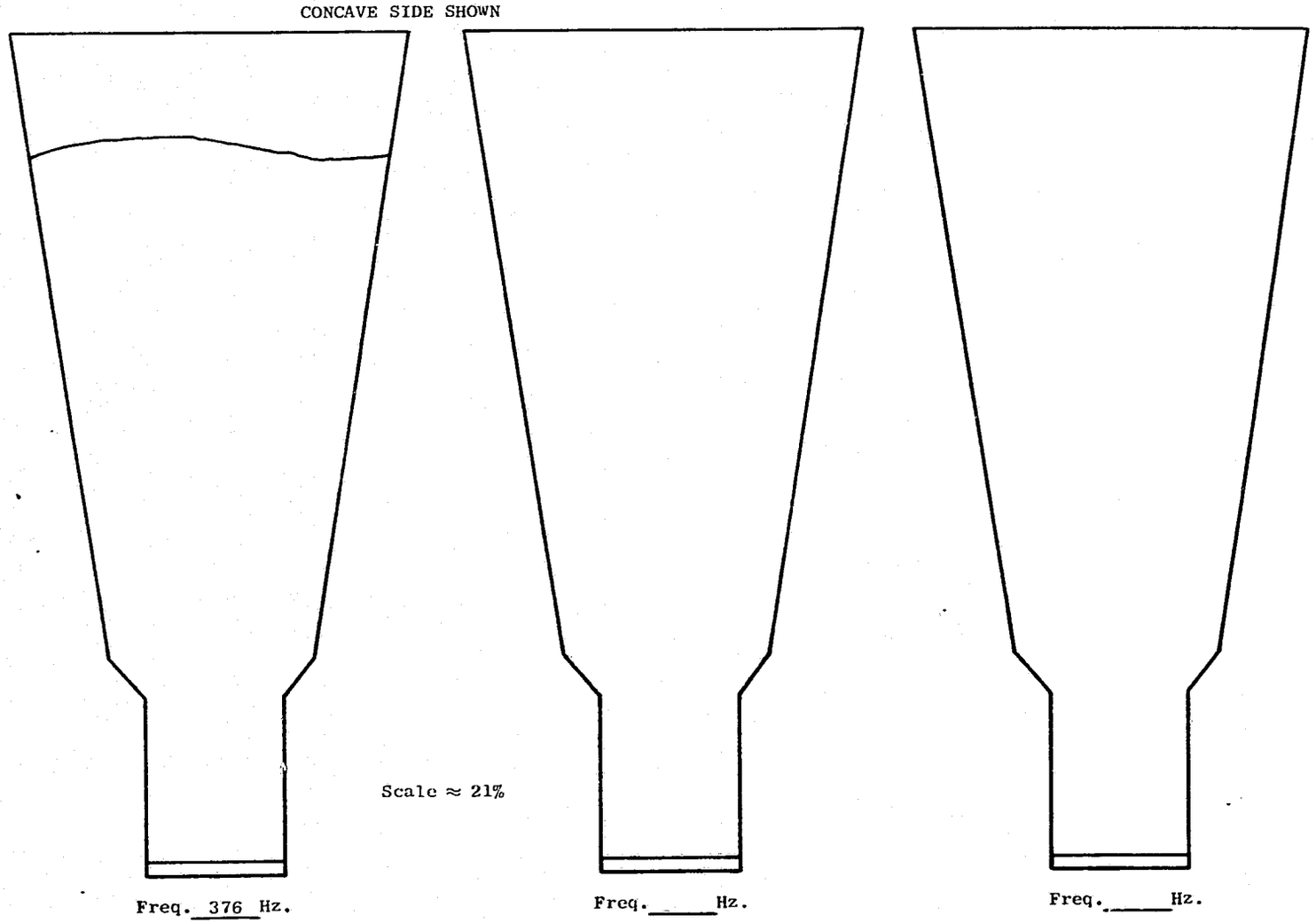

Figure 36. Resonant Frequencies and Nodal Patterns, QCSEE Fiber-Wound Blade, S/N 10, Concave Side, 376 Hz.

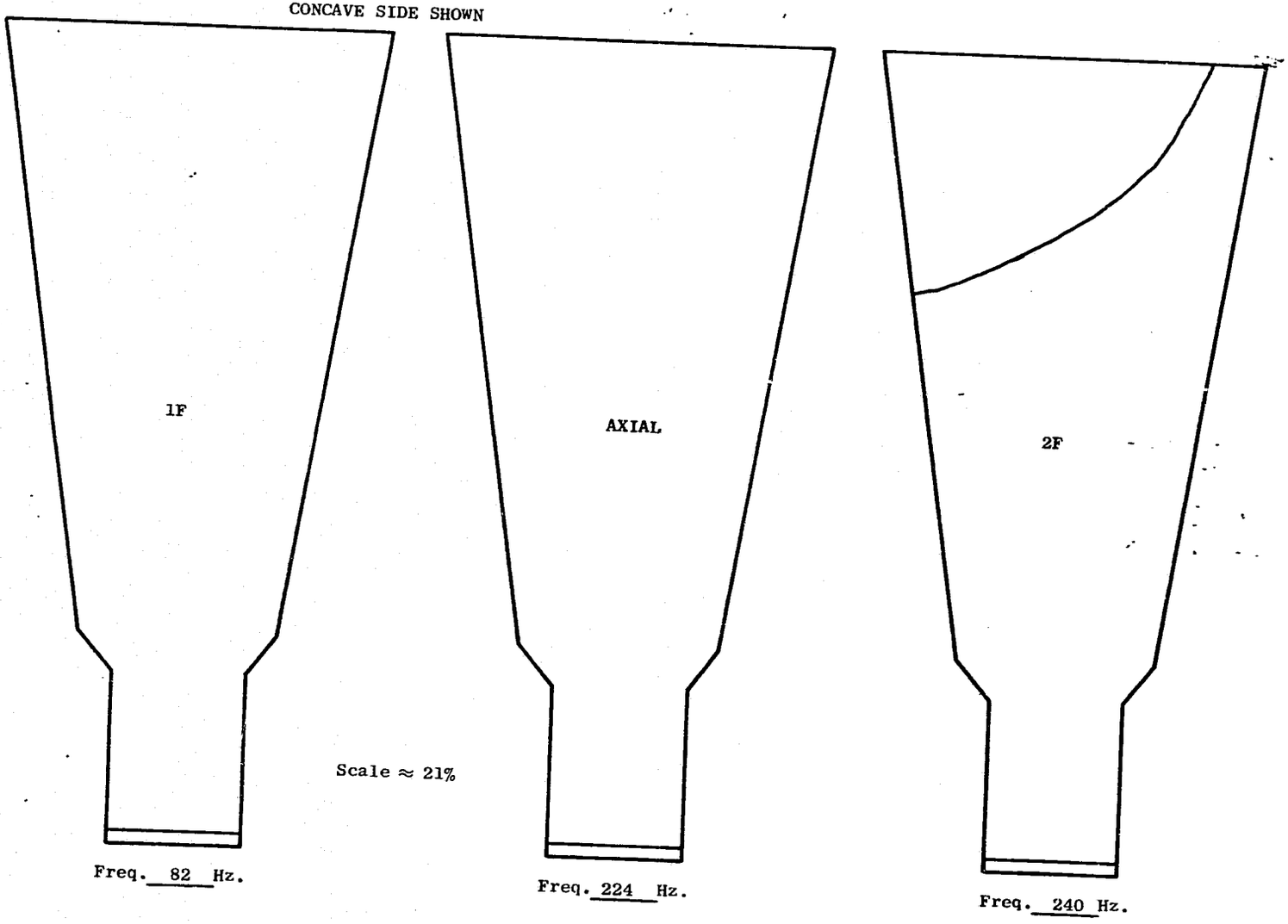

Figure 37. Resonant Frequencies and Nodal Patterns, QCSEE Fiber-Wound Blade, S/N 11, Concave Side, 82 to 240 Hz.

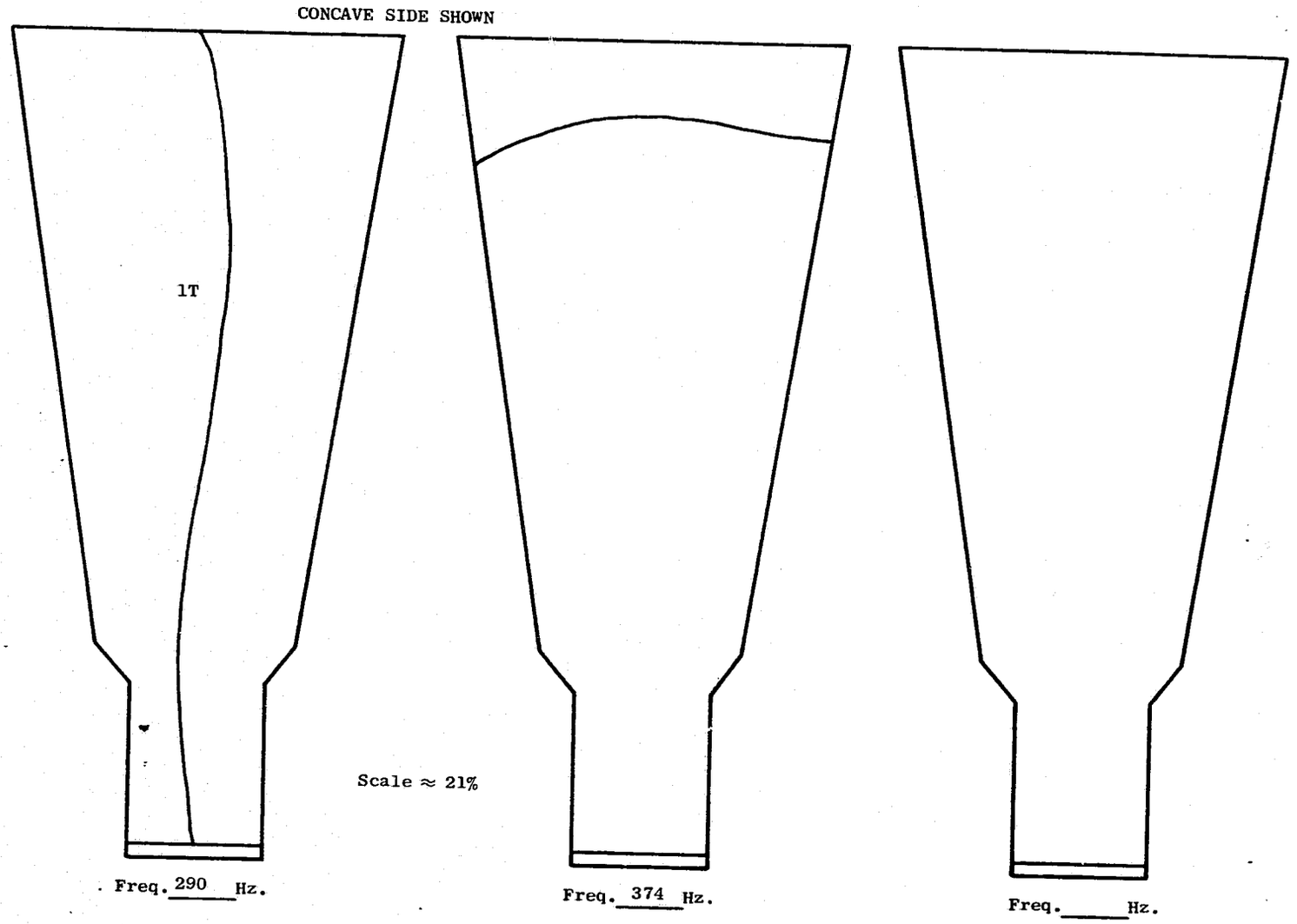

Figure 38. Resonant Frequencies and Nodal Patterns, QCSEE Fiber-Wound Blade, S/N 11, Concave Side, 290 and 374 Hz.

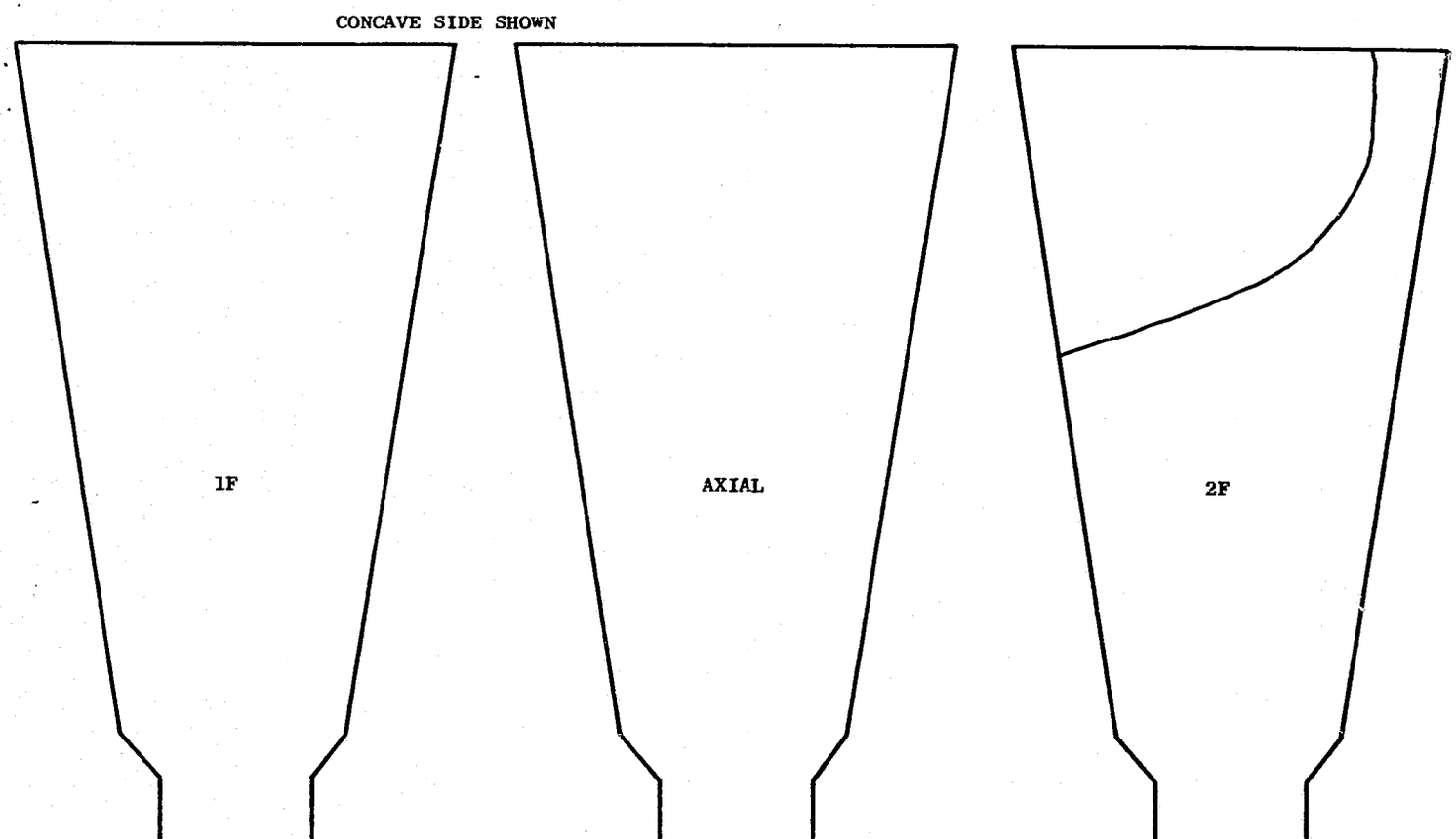

Figure 39. Resonant Frequencies and Nodal Patterns, QCSEE Fiber-Wound Blade, S/N 12, Concave Side, 82 to 246 Hz.

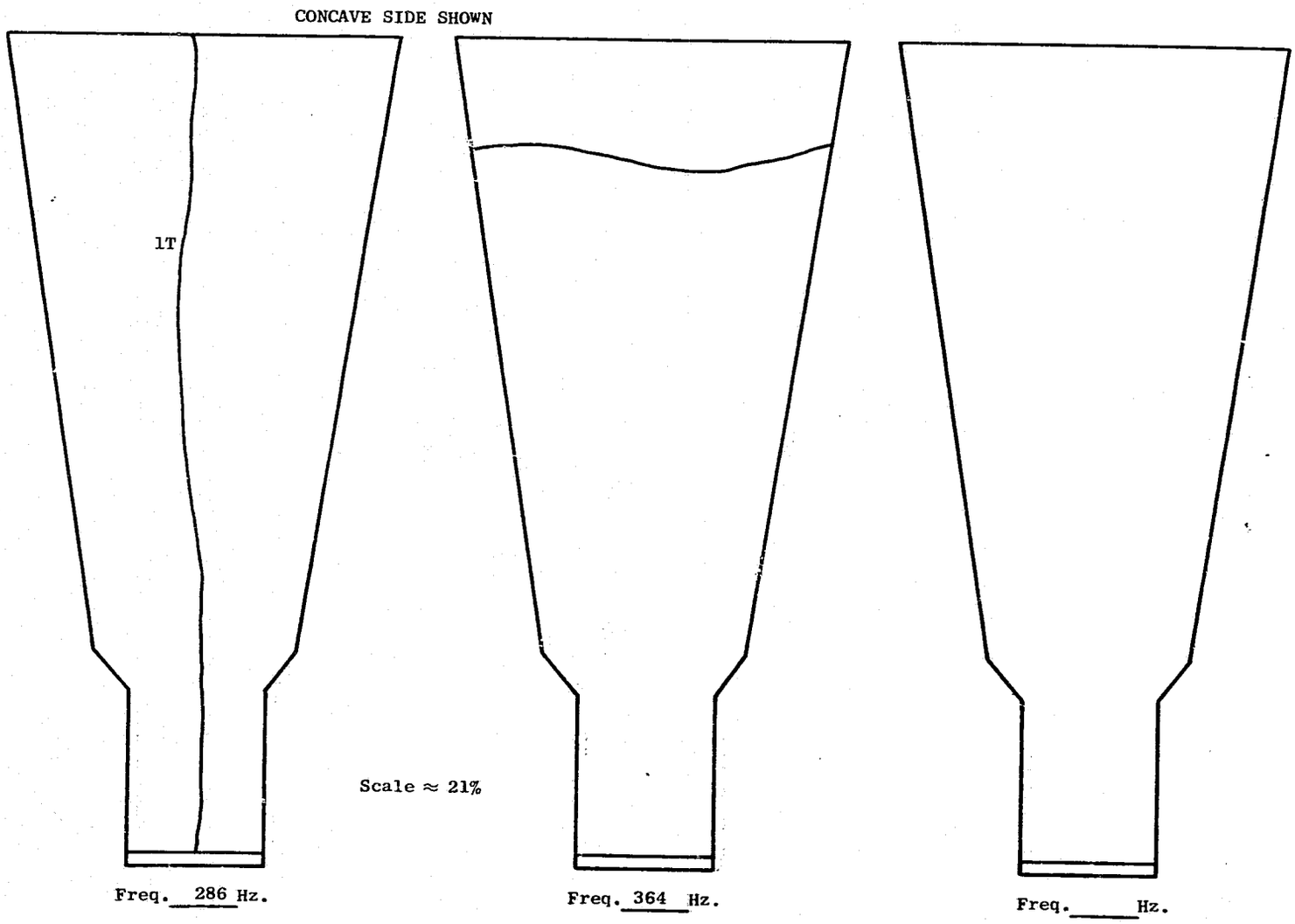

Figure 40. Resonant Frequencies and Nodal Patterns, QCSEE Fiber-Wound Blade, S/N 12, Concave Side, 286 and 364 Hz.

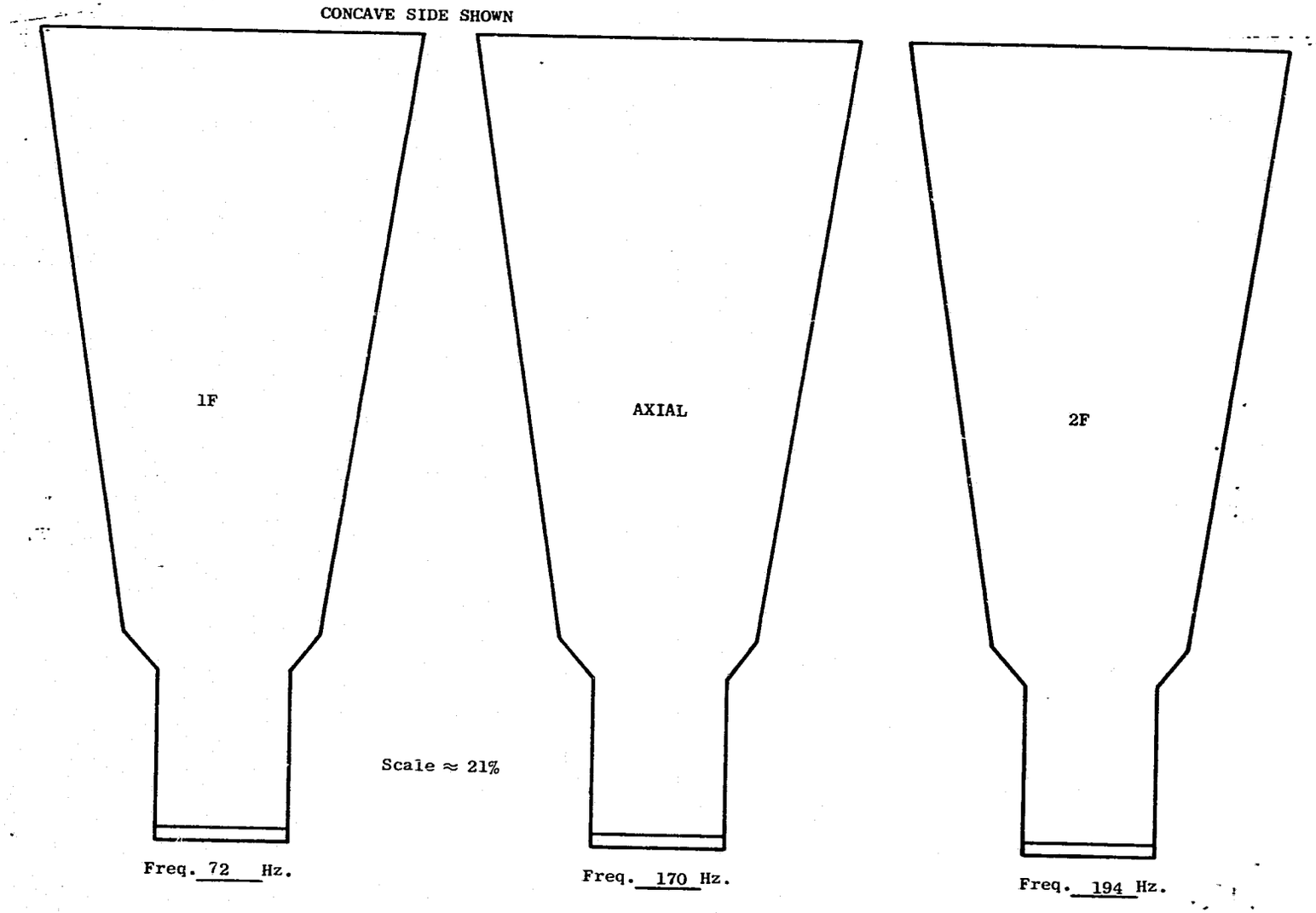

Figure 41. Resonant Frequencies and Nodal Patterns, QCSEE Fiber-Wound Blade S/N 4, Concave Side, 72 to 194 Hz after Bird Test.

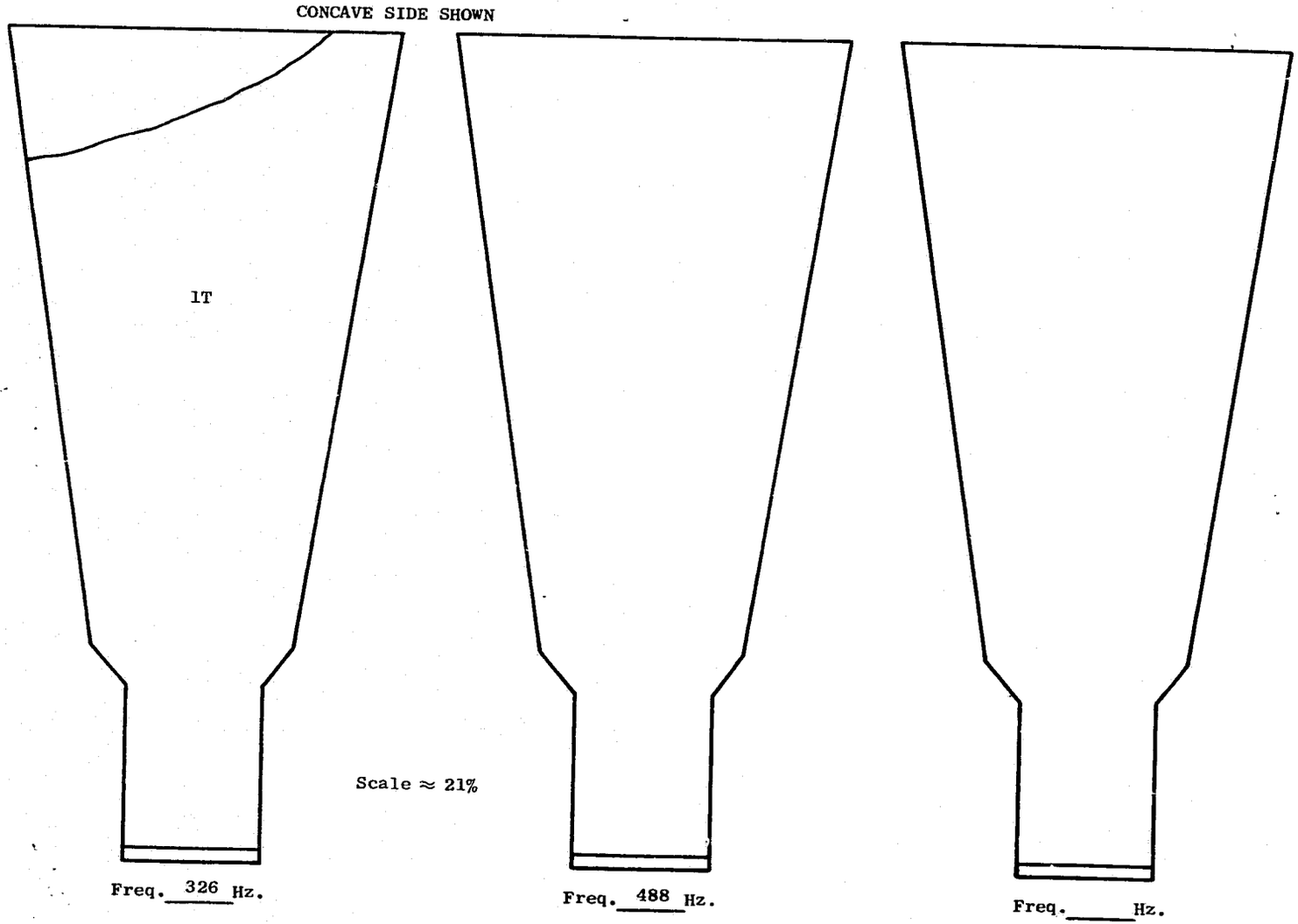

Figure 42. Resonant Frequencies and Nodal Patterns, QCSEE Fiber-Wound Blade S/N 4, Concave Side, 326 and 488 Hz after Bird Test.

APPENDIX III
PHOTOS OF TESTED BLADES

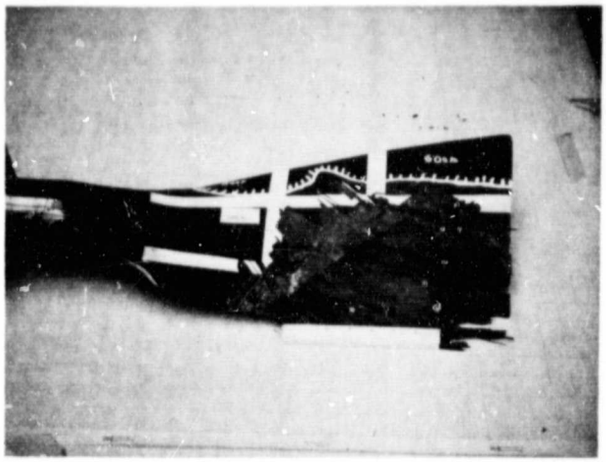

Blade S/N 5

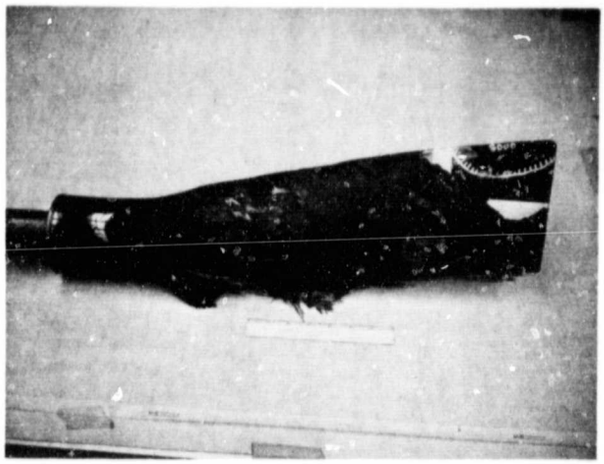

Blade S/N 6

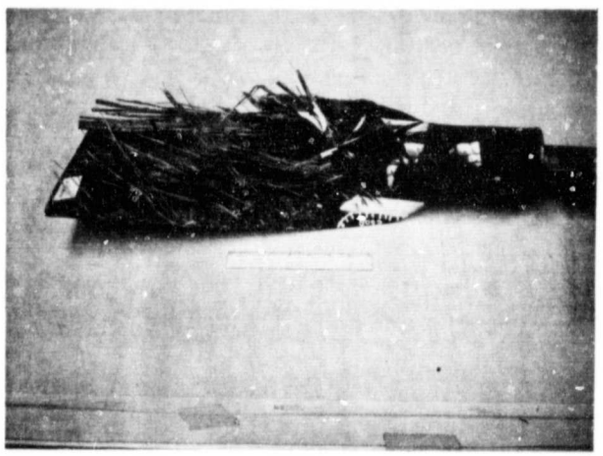

Blade S/N 8

Figure 43. Photographs Showing Undamaged Portions of Airfoils of Impacted Blades S/N 5, 6, and 8.

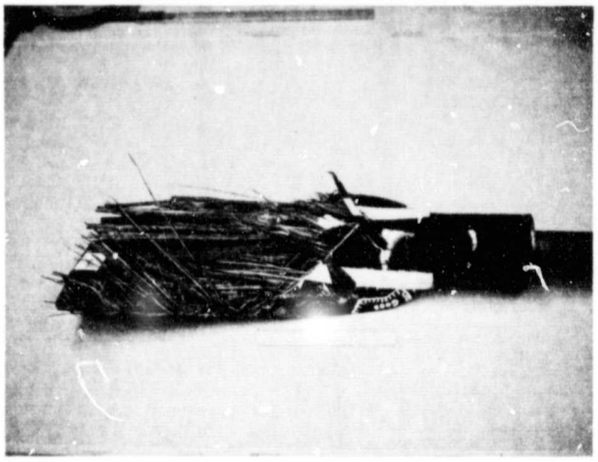

Blade S/N 10

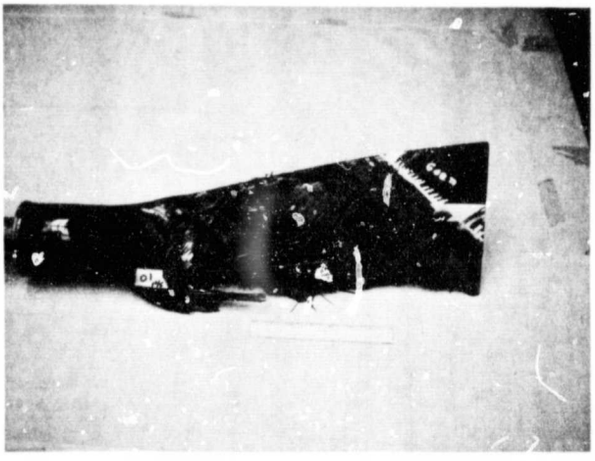

Blade S/N 11

Figure 44. Photographs Showing Undamaged Portions of Airfoils of Impacted Blades S/N 10 and 11.

Figure 45. QCSEE Fiber-Wound Composite Blades After Whirligig Impact Testing, Tip View.

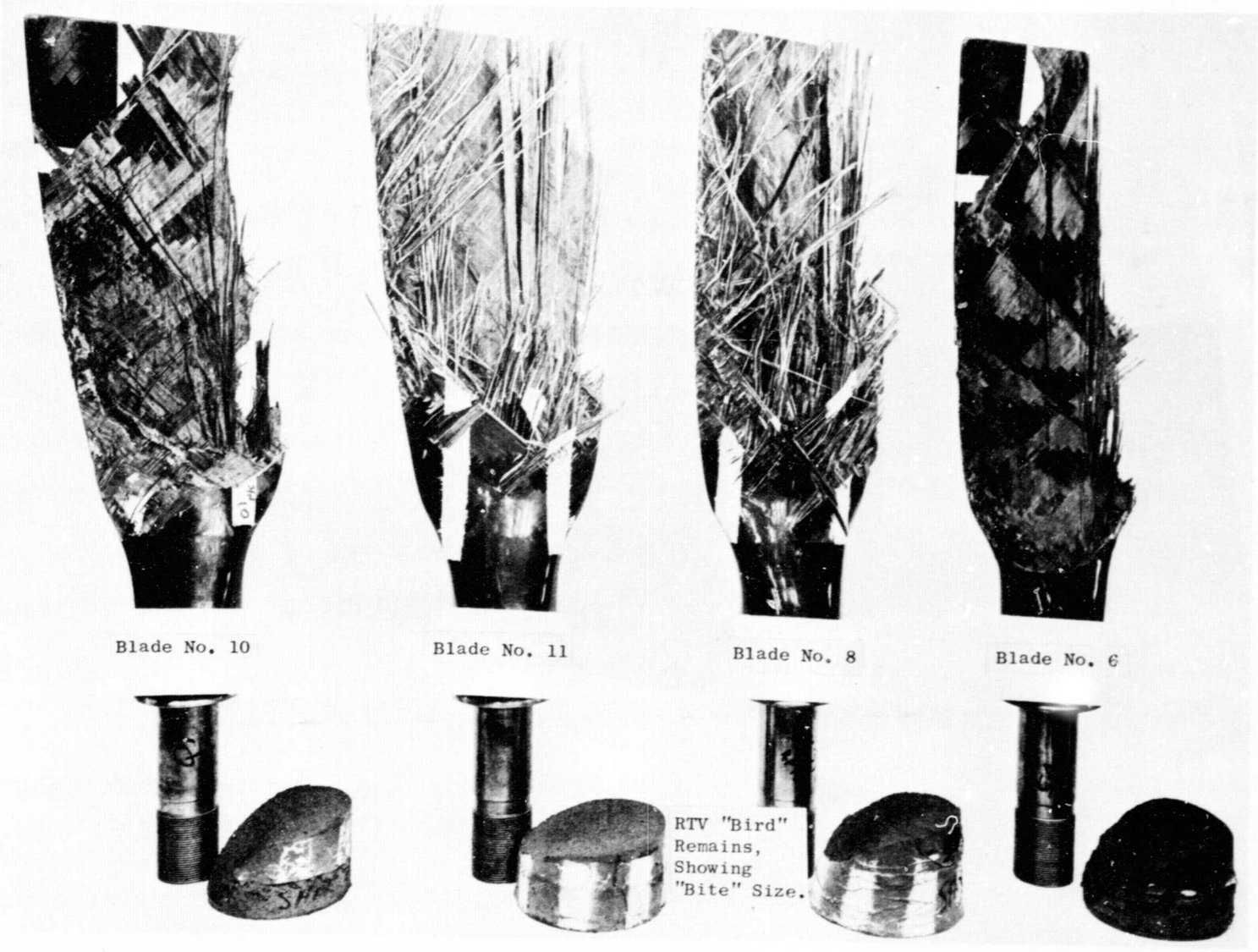

Figure 46. QCSEE Fiber-Wound Composite Blades After Whirligig Impact Testing, Front View.

Blade No. 4

Figure 47. QCSEE Fiber-Wound Composite Blade, Concave View After Impact, S/N 4.

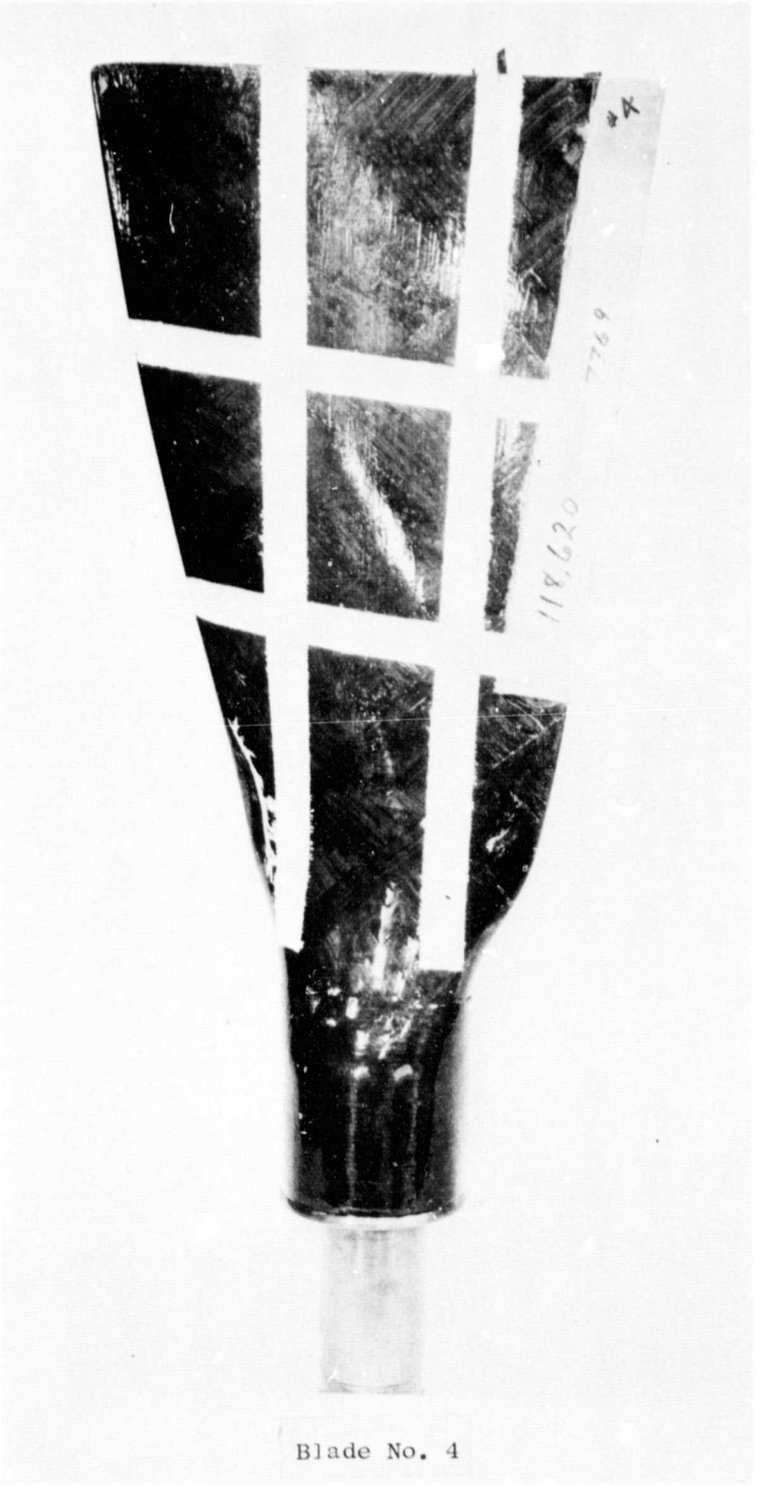

Figure 48. QCSEE Fiber-Wound Composite Blade, Convex View After Impact, S/N 4.

Blade No. 5

Figure 49. QCSEE Fiber-Wound Composite Blade, Concave View After Impact, S/N 5.

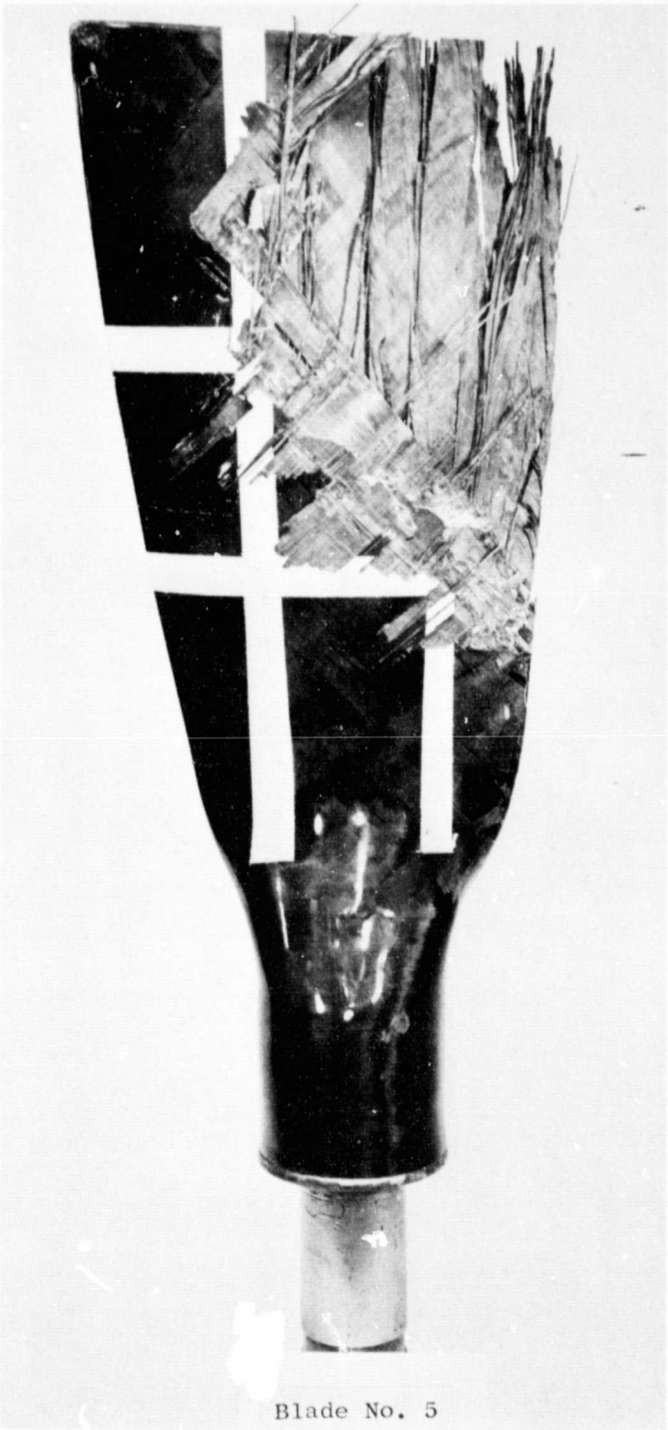

Figure 50. QCSEE Fiber-Wound Composite Blade, Convex View After Impact, S/N 5.

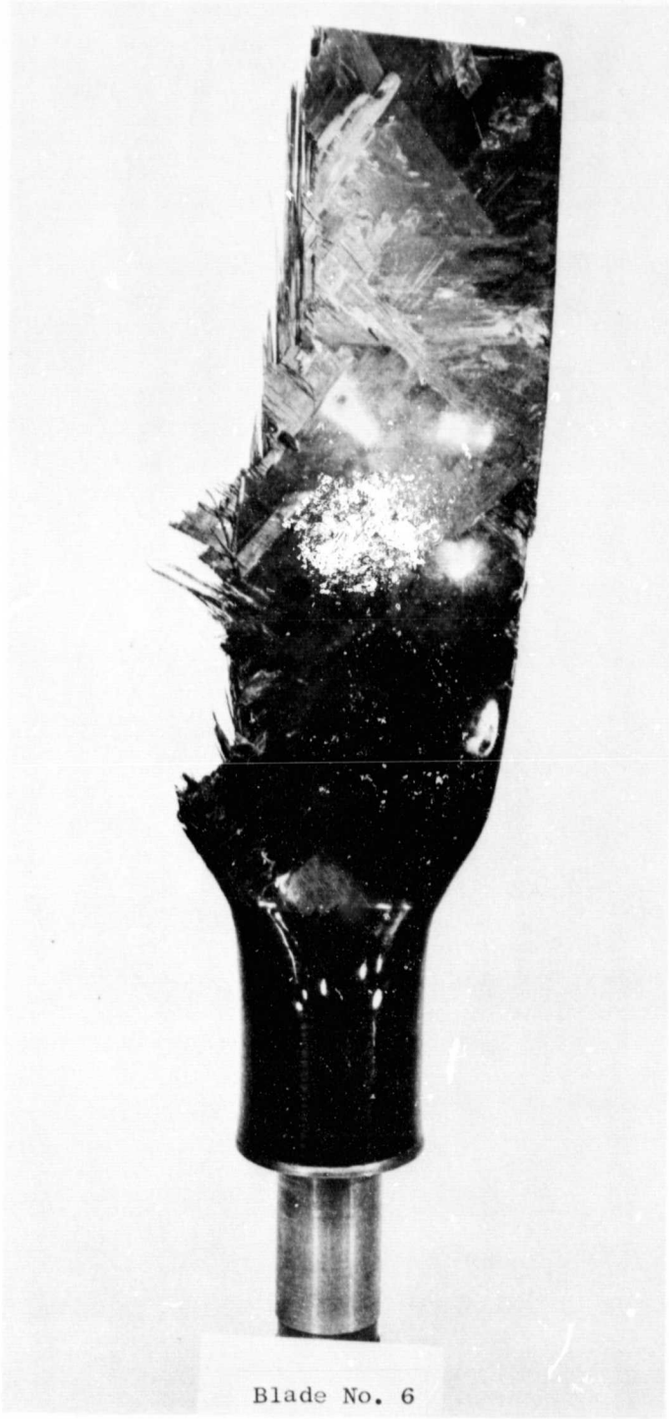

Figure 51. QCSEE Fiber-Wound Composite Blade, Concave View After Impact, S/N 6.

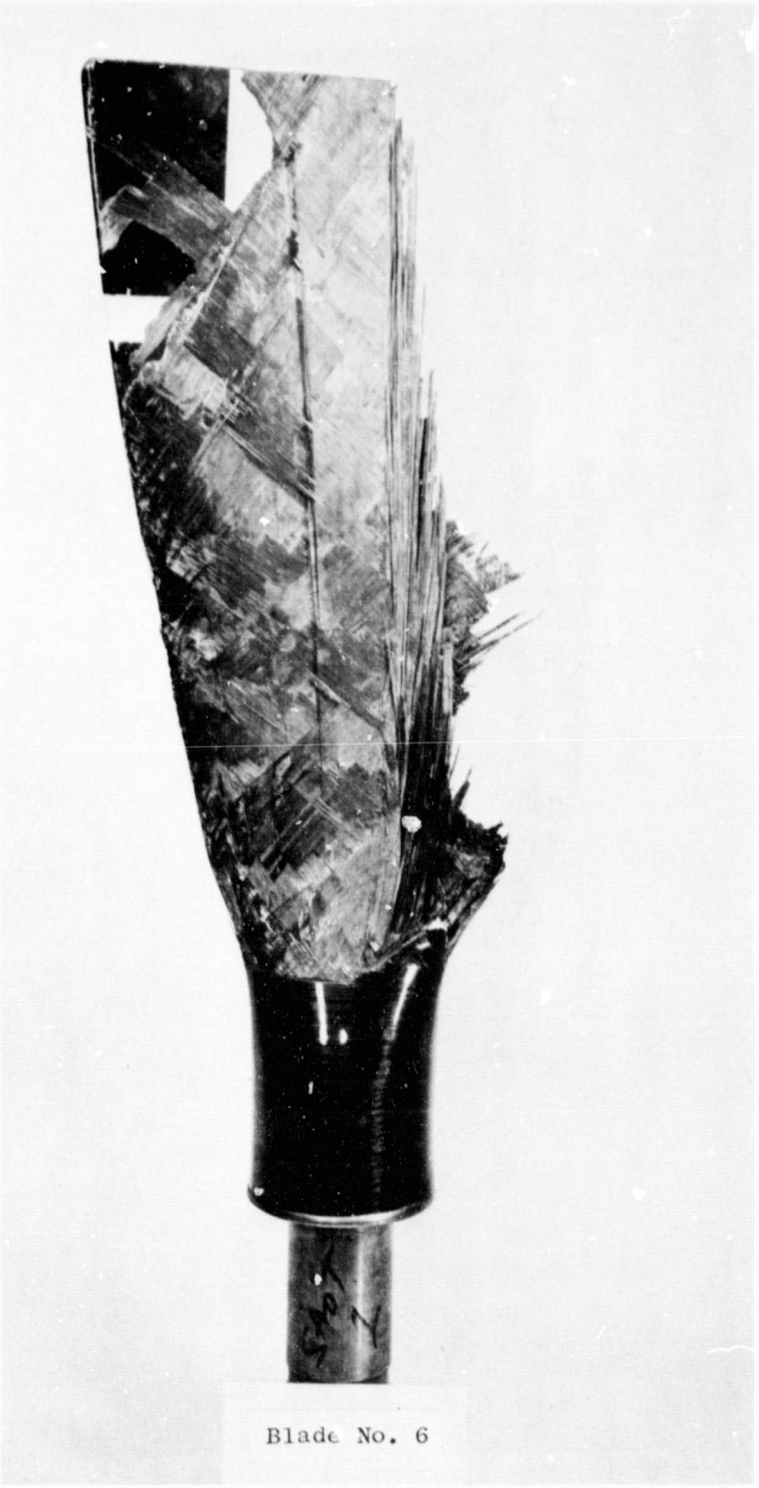

Figure 52. QCSEE Fiber-Wound Composite Blade, Convex View After Impact, S/N 6.

Blade No. 8

Figure 53. QCSEE Fiber-Wound Composite Blade, Concave View After Impact, S/N 8.

Figure 54. QCSEE Fiber-Wound Composite Blade, Convex View After Impact, S/N 8.

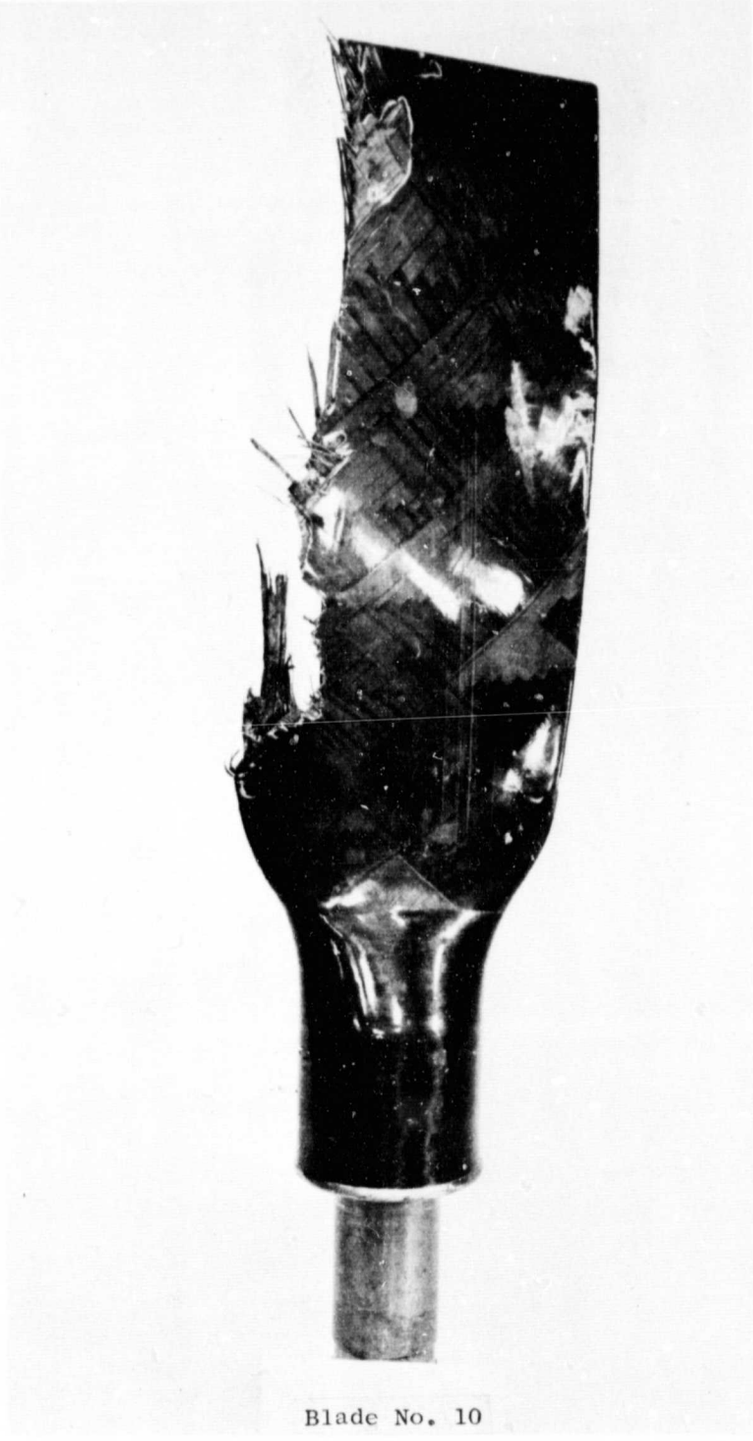

Blade No. 10

Figure 55. QCSEE Fiber-Wound Composite Blade, Concave View After Impact, S/N 10.

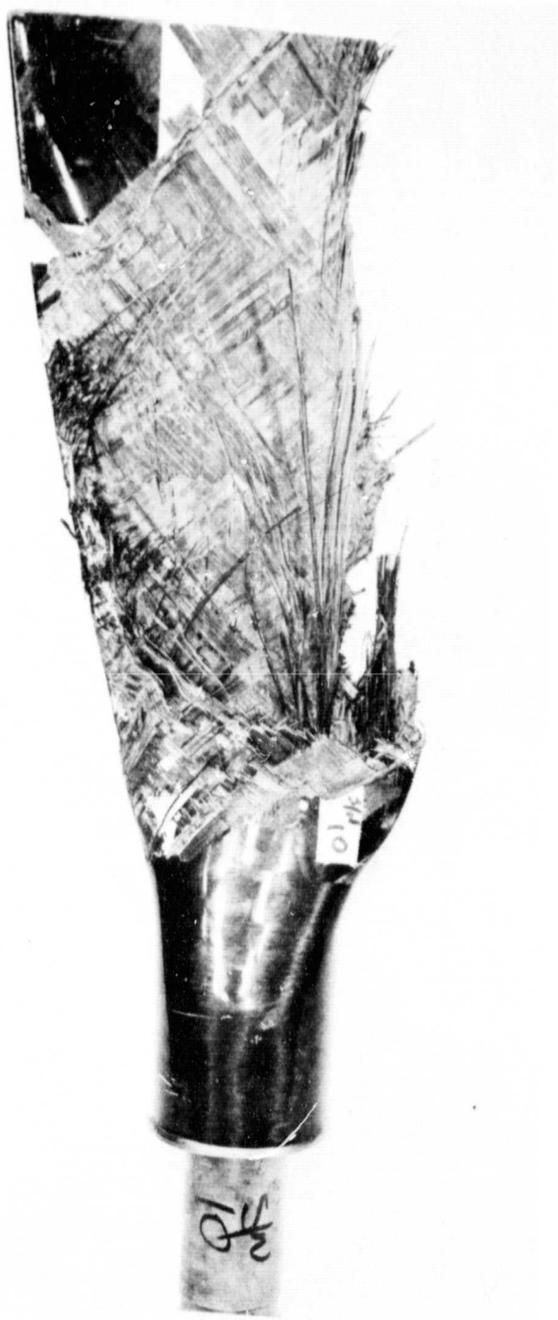

Blade No. 10

Figure 56. QCSEE Fiber-Wound Composite Blade, Convex View After Impact, S/N 10.

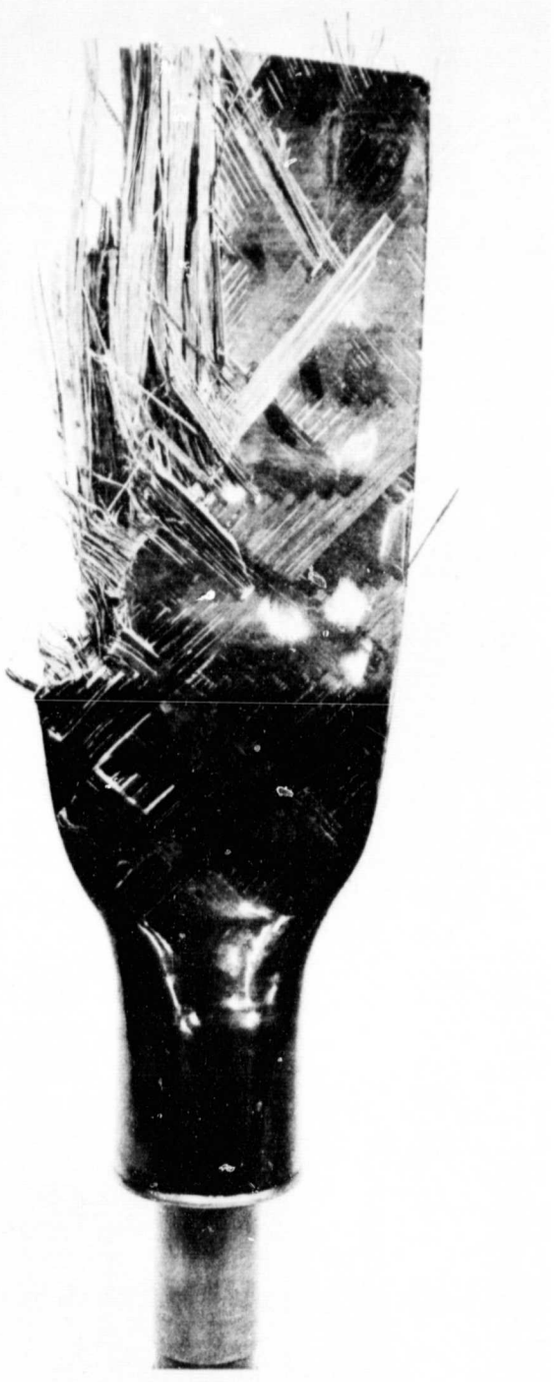

Blade No. 11

Figure 57. QCSEE Fiber-Wound Composite Blade, Concave View After Impact, S/N 11.

Figure 58. QCSEE Fiber-Wound Composite Blade, Convex View After Impact, S/N 11.

APPENDIX IV
GREY SCALE C-SCAN PLOTS OF TEST BLADES IN AS-RECEIVED AND POST-TEST CONDITION AS GENERATED BY GENERAL ELECTRIC

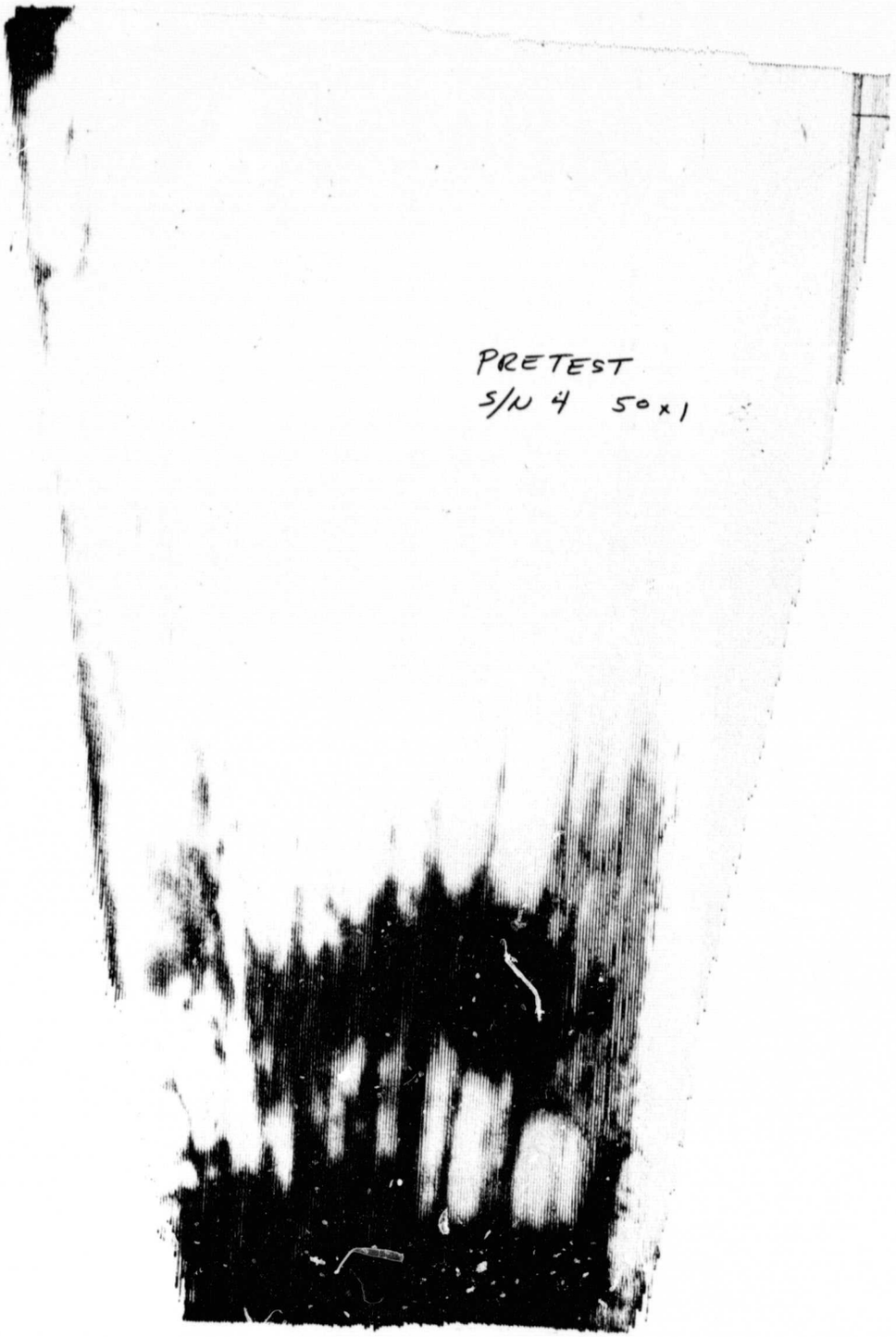

Figure 59. Ultrasonic C-Scan of As-Received Blade N 4.

Figure 60. Ultrasonic C-Scan of As-Received Blade S/N 5.

Figure 61. Ultrasonic C-Scan of As-Received Blade S/N 6.

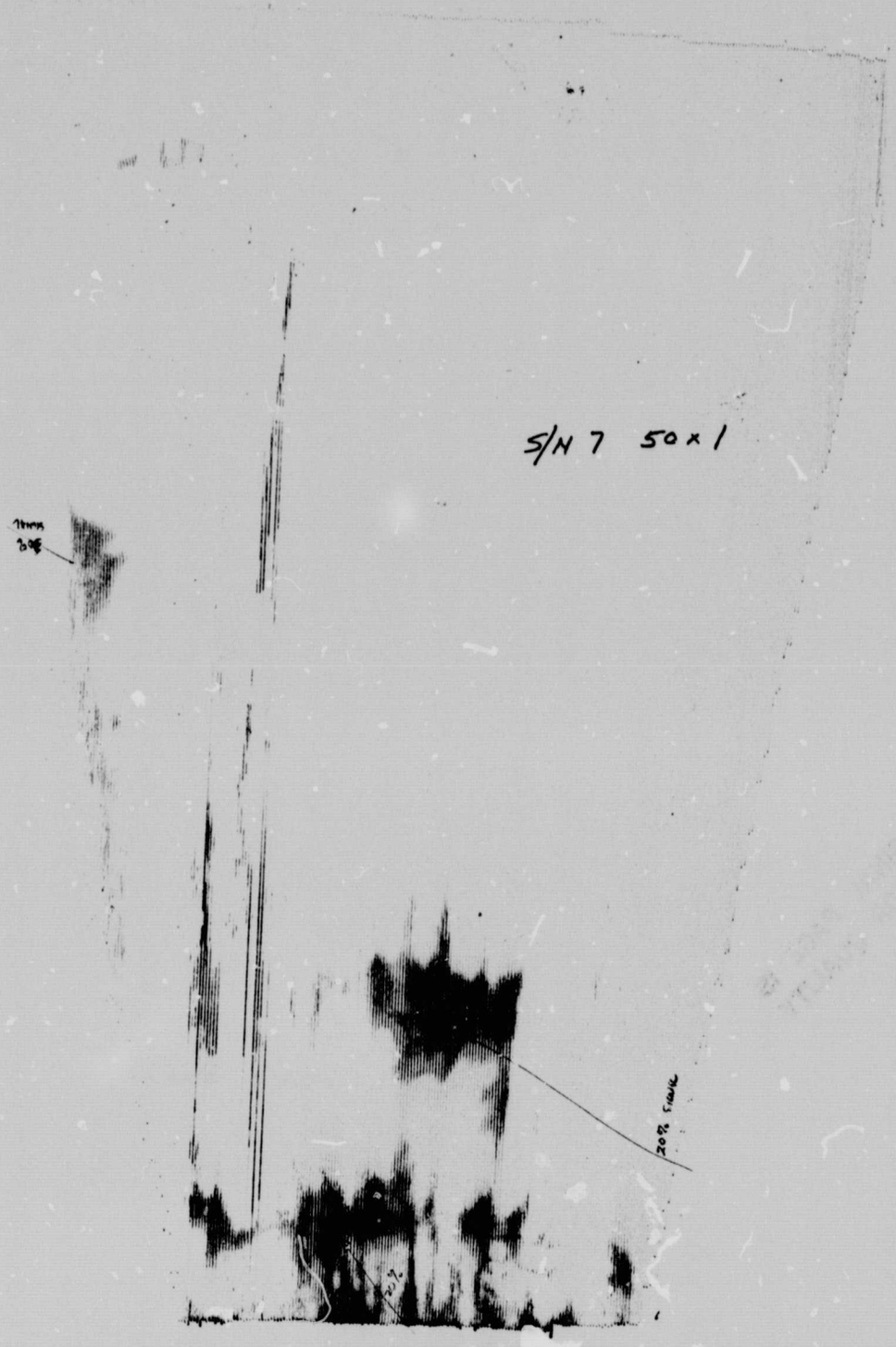

Figure 62. Ultrasonic C-Scan of As-Received Blade S/N 7.

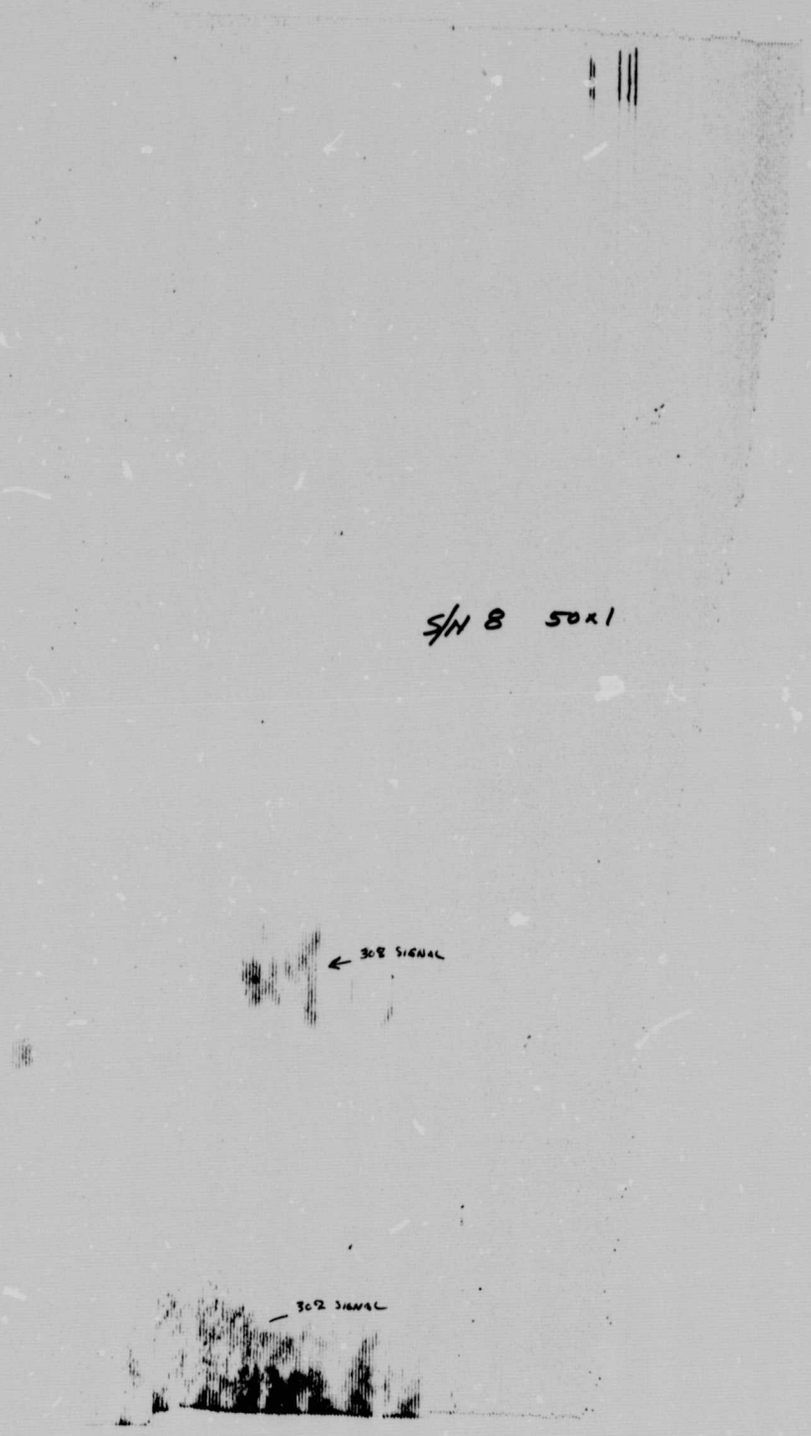

Figure 63. Ultrasonic C-Scan of As-Received Blade S/N 8.

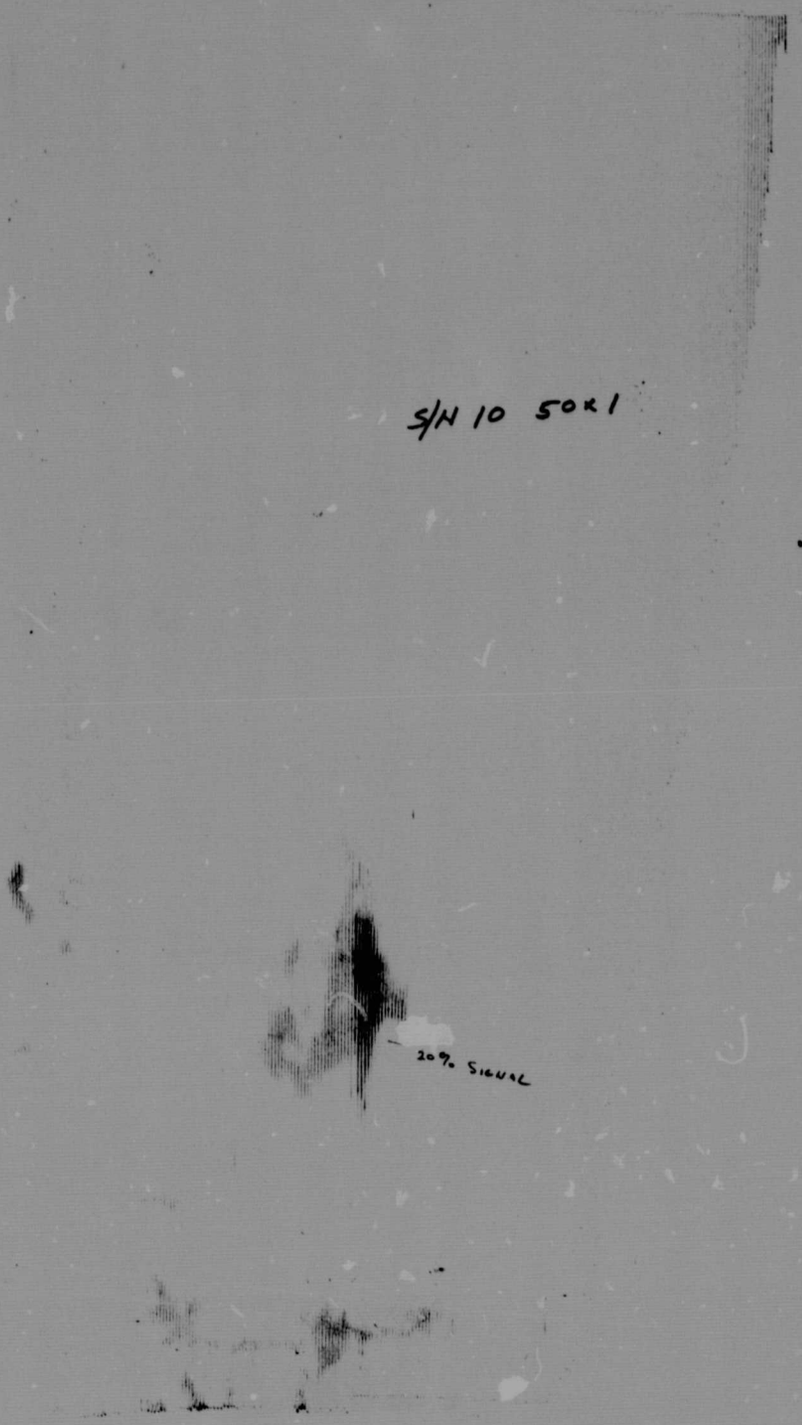

Figure 64. Ultrasonic C-Scan of As-Received Blade S/N 10.

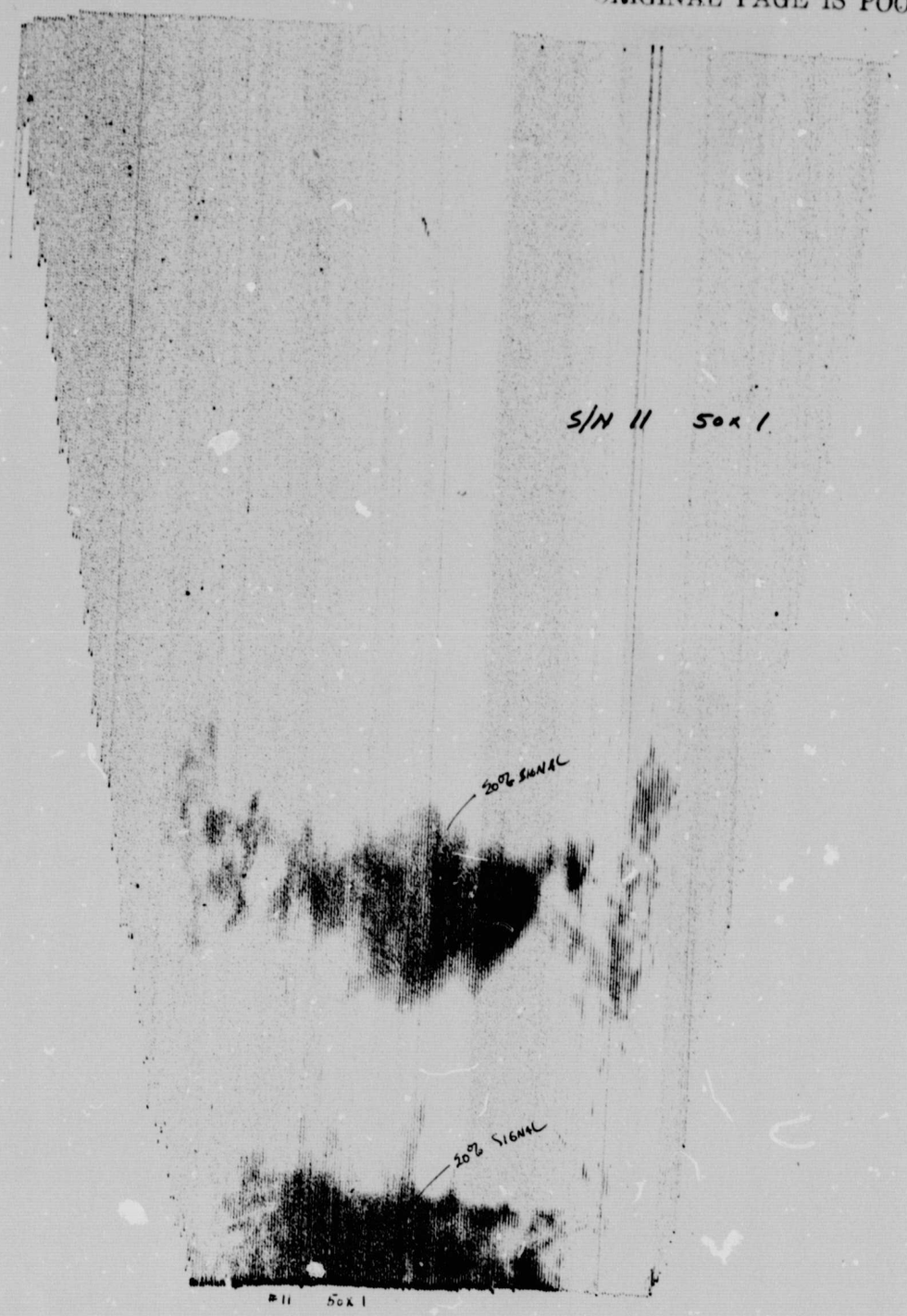

Figure 65. Ultrasonic C-Scan of As-Received Blade S/N 11.

Figure 66. Ultrasonic C-Scan of As-Received Blade S/N 12.

Figure 67. Ultrasonic C-Scan of Posttest Blade S/N 4.